The Feasibility of High Synthesis Gas Conversion over Ruthenium Promoted Iron-based Fischer Tropsch Catalyst

By

Ian Fraser

ND: Chemical Engineering (Cape Peninsula University of Technology)
BTech: Chemical Engineering (Cape Peninsula University of Technology)

Thesis submitted in fulfilment of the Requirement for the Degree of Masters of Engineering: Chemical Engineering, Faculty of Engineering, Cape Peninsula University of Technology.

Cape Town

2017

The Feasibility of High Synthesis Gas Conversion over Ruthenium Promoted Iron-based Fischer Tropsch Catalyst

---

By

Ian Fraser

Supervisors:

Ademola Rabiu, CPUT

Eric van Steen, UCT

Declaration

I, Ian Fraser, declare that the contents of this dissertation/thesis represent my own unaided work, and that the dissertation/thesis has not previously been submitted for academic examination towards any qualification. Furthermore, it represents my own opinions and not necessarily those of the Cape Peninsula University of Technology.

Signed: ……

Date: ……

Acknowledgements

There are many without whom this research project would not have been a success. Unfortunately it would be impossible for me to thank everyone by name, but I would like to extend my gratitude to any and all who contributed in any way to this work.

To my supervisor and co-supervisor, Mr. Ademola Rabiu and Prof. Eric van Steen, I would like to extend my gratitude to your support and guidance over the course of this project. Thank you to the Centre for Catalysis research at the University of Cape Town for allowing the use of their facilities and equipment for the completion of the experimental runs. In the same breath I would like to say thank you to Dr. Doreen Nabaho for your help, insights and advice in running my experiments, analysing- and making sense of the data. To Anna Peterson, thank you for your advice and help in the lab and to everyone else at the Centre for Catalysis research, thank you very much for making me feel welcome at your institution during my relatively short time with you.

A big thank you to Stephanie la Grange and everyone at the Analytical Chemistry Laboratory for all the analyses and re-analyses of my catalyst samples and Miranda Waldron at the Electron Microscopy unit for SEM-EDX.

Thank you to my long-time friend Mr. Riki Strydom for your unwavering friendship and support during this endeavour. Know that it is greatly appreciated. Mrs. Elizma Alberts, Mrs. Hannelene Small and Mr. Alwyn Bester, thank you very much for providing a much needed distraction from time to time, coffee breaks, as well as support to help me keep my sanity during these last years.

I would also like to extend my thanks to Prof. Dr.-Ing. Andreas Jess at the chair of Chemical Engineering at the University of Bayreuth for acting as my supervisor during my research stay in Germany. Though the data were not used in this work, the experience alone has been of immeasurable importance. Also, thank you to the rest of the staff and students at the chair for your welcoming attitude and willingness to help. On this note I would like to thank DAAD for funding the exchange.

Last, but not least, I would like to extend my gratitude and appreciation to my family who have supported me from day one financially, mentally and emotionally. Honestly, without you I would not have made it to where I am today. I am truly grateful beyond words.

I would like to acknowledge, with much gratitude, the financial support provided by the DAAD and NRF during my period of Master's degree study, without which neither the initiation nor the completion of this project would have been possible. Opinions expressed in this thesis and the conclusions arrived at, are those of the author, and are not necessarily to be attributed to DAAD or the National Research Foundation.

Summary

One of the very promising synthetic fuel production strategies is the Fischer-Tropsch process, founded on the Fischer-Tropsch Synthesis, which owes its discovery to the namesake researchers Franz Fischer and Hans Tropsch. The Fischer-Tropsch Synthesis (FTS) converts via complex polymerisation reaction a mixture of CO and H_2 over transition metal catalysts to a complex mixture of hydrocarbons and oxygen containing compounds with water as major by-product. The mixture of CO and H_2 (termed syngas) may be obtained by partial oxidation of carbon containing base feedstocks such as coal, biomass or natural gas via gasification or reforming. The Fischer-Tropsch (FT) process thus presents the opportunity to convert carbon containing feedstocks to liquid fuels, chemicals or hydrocarbon waxes, which makes, for instance, the monetisation of stranded gas or associated gas a possibility.

The FT-process is typically carried out in two modes of operation: low temperature Fischer-Tropsch (LTFT) and high temperature Fischer-Tropsch (HTFT). LTFT is normally operated at temperatures of 200 – 250 °C and pressures of 10 – 45 bar to target production of high molecular weight hydrocarbons, while HTFT is operated at 300 – 350 °C and 25 bar to target gasoline production.

The catalytically active metals currently used commercially are iron and cobalt, since product selectivity over nickel is almost exclusively to methane and ruthenium is highly expensive in addition to requiring very high pressures to perform optimally. Fe is much cheaper, but tends to deactivate more rapidly than Co due to oxidation in the presence of high H_2O partial pressures. One of the major drawbacks to using Fe as FT catalyst is the requirement of lower per pass conversion which necessitates tail gas recycle to extend catalyst life and attain acceptable overall conversions. A more active or similarly active but more stable Fe-catalyst would thus be advantageous. For this reason promotion of a self-prepared typical LTFT Fe-catalyst with Ru was investigated.

A precipitated K-promoted Fe-catalyst was prepared by combination of co-precipitation and incipient wetness impregnation and a ruthenium containing catalyst prepared from this by impregnation with $Ru_3(CO)_{12}$. The catalysts, which had a target composition of 100 Fe/30 Al_2O_3/5 K and 100 Fe/30 Al_2O_3/5 K/3 Ru, were characterised using XRD, SEM-EDX, ICP-OES, TPR and BET N_2-physisorption, before testing at LTFT conditions of 250 °C and 20 bar in a continuously stirred slurry phase reactor.

Catalyst characterisation results showed the catalysts to consist of ferrihydrite as major iron phase, while no other structural information pertaining to Al, K or Ru could be determined from the XRD patterns. BET surface areas were high (between 170 and 180 m^2/g) as expected for ferrihydrite. Elemental composition as determined by EDX and ICP were slightly off the targeted values, but Fe/K and Fe/Ru ratios were determined to be within the target range. The TPR investigation showed Ru to be an effective reduction promoter, with clear reduction peak shifts to temperatures 100 – 150 °C lower.

Both catalysts attained very similar levels of CO-conversion at the same tested space velocities and both catalysts were able to attain CO-conversion levels approaching 100%. The Ru-containing catalyst showed an apparent deactivation of 21% over 478 h TOS vs. 27% over 415 h for the non-Ru-containing catalyst, suggesting the Ru-promoted catalyst to be superior in terms of stability.

The Ru-promoted catalyst showed significantly higher selectivity to CH_4 and CO_2 than the catalyst promoted with K only. Olefinicity and C_{5+}-selectivities were also significantly lower over the Ru-promoted catalyst. The higher methane selectivity is thought to stem from a combination of ruthenium's inherent FT activity and an enhancement of the H_2-adsorption. High CO_2-selectivity would seem to be a result of enhancement of the re-carburisation of magnetite facilitated by Ru similarly to what has been proposed for Cu. This alone probably would not account for the large amounts of CO_2 which suggests that Ru also helps to promote the WGS reaction over Fe. The increased WGS activity (leading to lower water partial pressures), coupled with enhanced magnetite carburisation would help in explaining the Ru-containing catalyst's improved stability.

Table of Contents

List of Figures

List of Tables

Nomenclature

2LFh	2-line ferrihydrite
6LFh	6-line ferrihydrite
A	Area
α	Chain growth probability
ASF	Anderson-Schulz-Flory
ATR	Autothermal reforming
BASF	Badishe Anilin und Sodafabrik
BET	Brunauer-Emmet-Teller
ß	Peak width at half intensity
BJH	Barrett-Joyner-Halenda
BTL	Biomass-to-Liquid
C	Concentration
C_{2+}	Products containing 2 carbon atoms or more
C_{5+}	Products containing 5 carbon atoms or more
CFB	Circulating fluidised bed
CNT	Carbon nanotube
CPO	Catalytic partial oxidation
CTL	Coal-to-Liquid
d	Desorption
DCL	Direct coal liquefaction
DFT	Density Functional Theory
DME	Dimethyl ether
EDX	Energy dispersive X-ray spectroscopy
f	Formation
FFB	Fixed Fluidised bed
Fh	Ferrihydrite
FID	Flame ionisation detector
FT	Fischer-Tropsch
FTS	Fischer-Tropsch Synthesis
g	Growth
g_{cat}	Grams of catalyst
GC	Gas chromatography (or gas chromatograph)
GHSV	Gas hourly space velocity

GTL	Gas-to-Liquid
HER	Heat exchange reforming
HTFT	High temperature Fischer-Tropsch
ICL	Indirect coal liquefaction
ICP	Inductively coupled plasma
K	Constant in Sherrer equation (normally taken as 1)
KWI	Kaiser Wilhelm Institute
λ	Wavelength (lambda)
LPG	Liquefied petroleum gas
LTFT	Low temperature Fischer-Tropsch
MFC	Mass flow controller
$\dot{n}$	Molar flow rate
N_C	Number of carbon atoms
$N_{C,(no\ O)}$	Number of carbon atoms not bonded to oxygen
$N_{C,(O)}$	Number of carbon atoms
NTP	Normal temperature and pressure
OES	Optical emission spectroscopy
p	Probability (lower case)
P	Pressure (upper case)
Pr	Product species
r	Rate
R_f	Response factor
RF	Radio-frequency
R&D	Research and development
S_{C5+}	Selectivity toward products containing 5 carbon atoms or more (on the basis of VOC)
S_{CH4}	Selectivity toward methane
S_{CO2}	Selectivity toward CO_2
S'_{CH4}	Selectivity toward methane (on the basis of VOC)
$S_{ole,C}$	Carbon number specific olefin selectivity
SAS	Sasol Advanced Synthol
SEM	Scanning electron microscopy
sin	Sine (trigonometric function)
SMDS	Shell Middle Distillate Synthesis
SMR	Steam methane reforming
sp	Surface species

STP	Standard temperature and pressure
TCD	Thermal conductivity detector
TEM	Transmission electron microscopy
θ	Incident angle (Theta)
TOS	Time on stream
TPR	Temperature programmed reduction
UK	United Kingdom
USA	United States of America
USD	United States Dollar
VOC	Volatile organic compounds
w	Mass/weight fraction
WGS	Water-Gas-Shift
WW1	World War 1 (First World War)
WW2	World War 2 (Second World War)
x	Mole fraction
x_c	Crystallite size
x_d	Interplanar spacing
XRD	X-ray diffraction
Y	Yield
$Y_{ole,C}$	Yield of primary olefins in product fraction with carbon number C
$Y_{par,C}$	Yield of linear paraffins in product fraction with carbon number C

Chemical formulas

Ar	Argon
$Al(NO_3)_3$	Aluminium nitrate
$Al(NO_3)_3 \cdot 9H_2O$	Aluminium nitrate nonahydrate
Al_2O_3	Alumina (Aluminium oxide)
C	Carbon
CO	Carbon Monoxide
CO_2	Carbon Dioxide
C_nH_{2n}	Olefin (Alkene)
C_nH_{2n+2}	Paraffin (Alkane)
CH	Methylidyne
CH_2	Methylene

CH_3	Methyl group
CH_4	Methane
CH_x	Surface species with x-number of hydrogen atoms
CHOH	Enol species
$C_nH_{2n+1}OH$	Linear alcohol
Co	Cobalt
Co_3O_4	Cobalt oxide
Cu	Copper
$5Fe_2O_3 \cdot 9H_2O$	Ferrihydrite (bulk formula)
Fe	Iron
Fe(III)	Iron in valence state 3
FeO	Wüstite
Fe_2O_3	Hematite
Fe_3O_4	Magnetite
FeOCl	Feroxy chloride
$Fe(OH)_3$	Iron (III) hydroxide
FeOOH	Iron oxide hydroxide
$Fe(NO_3)_3$	Iron nitrate
$Fe(NO_3)_3 \cdot 9H_2O$	Iron nitrate nonahydrate
H_2	Hydrogen
HCO_3^-	Bicarbonate
H_2O	Water
He	Helium
K	Potassium
KNO_3	Potassium nitrate
K_2O	Potassium oxide
Mn	Manganese
N_2	Nitrogen
NH_4^+	Ammonium ion
$(NH_4)_2CO_3$	Ammonium carbonate
NO_x	Nitrogen oxides
Ni	Nickel
O_2	Oxygen
Pt	Platinum
Re	Rhenium
Ru	Ruthenium

$Ru_3(CO)_{12}$	Triruthenium dodecacarbonyl
$RuCl_3$	Ruthenium chloride
SiO_2	Silica (Silicon dioxide)
ThO_2	Thoria (Thorium dioxide)
TiO_2	Titania (Titanium dioxide)
ZnO	Zinc oxide

Units

	Angle
°	Degree
	Concentration
ppm	Parts per million
	Current
mA	Milli-ampere (10^{-3} A)
	Distance
Å	Angstrom (10^{-10} m)
m	Metre
μm	Micrometre/micron (10^{-6} m)
nm	Nanometre (10^{-9} m)
	Force
N.m	Newton metre (torque)
	Mass
g	Grams (10^{-3} kg)
mg	Milligram (10^{-6} kg)
ozt	Troy ounce (approximately 31.1 g)
ton	Metric ton (1000 kg)
	Pressure
atm	Atmospheres (equivalent to 101.325 kPa)
bar	Bar (equivalent to 100 kPa)

kPa	Kilopascal (10^3 Pa)
mbar	Millibar (equivalent to 100 Pa)
MPa	Megapascal (10^6 Pa)
Pa	Pascal (1 N/m^2)

Speed

rpm	Revolutions per minute

Temperature

°C	Degrees Celcius
K	Degrees Kelvin

Time

h	Hour (60 min)
min	Minute (60 s)
s	Second

Voltage

kV	Kilovolt (10^3 V)

Volume

cm^3	Cubic centimetre (equivalent to 1 mL)
dm^3	Cubic decimetre (equivalent to 1 L)
L	Litre
m^3	Cubic metre (equivalent to 1000 L)
mL	Millilitre (10^{-3} L)

1

Chapter 1: Introduction

With a growing global population and a more environmentally conscious society, the need to increase energy supply, while reducing mankind's environmental impact, requires scientists to re-evaluate the way in which energy demand is met. A novel approach to supplement the fuels and chemicals derived from natural crude oil reserves with synthetic fuels has been known to researchers since the early 20th century. Commercial production of these synthetic fuels (synfuels) started with coal liquefaction technologies in Germany as a way to gain fuel independence. Germany, like South Africa, is a country with no crude oil reserves, but large quantities of coal. The first technology employed was the direct liquefaction of coal using Bergius's high pressure hydrogenation process. Later an indirect liquefaction method, the Fischer-Tropsch Synthesis (FTS), was discovered and has been applied commercially in South Africa since the 1950's.

The FTS reaction was discovered by Franz Fischer and Hans Tropsch in 1923 – 1926, after Friedrich Bergius's development of the high pressure coal hydrogenation process in 1910 –1925. It offers an indirect route to the production of "synthetic crudes" from carbon containing materials. The FTS is a catalytic conversion of synthesis gas (a mixture of CO and H_2) into a complex spectrum of hydrocarbons which includes olefins, paraffins and oxygenates. The synthesis gas can be obtained from various carbon containing sources, such as coal, biomass or natural gas. Research in FTS has a history dominated by stops and starts. This is mostly linked to the rise and fall of natural crude oil prices, but also other oil crises such as the 1973 Arab oil embargo and the South African boycotts during the Apartheid era.

This chapter, briefly, introduces the concept of synthetic fuels as alternatives to conventional fuels. The Fischer-Tropsch Synthesis, its history, revival and applications is as well introduced in this chapter. This is discussed in more detail in Chapter

2. Additionally, this chapter serves to introduce and discuss the premise for this research project, important research questions, and aims and objectives, and the expected outcomes of the research.

1.1 Synthetic Fuels: Alternatives to crude-derived fuels

The 20th and 21st century synthetic fuel industry evolved in three stages. The first is the invention, followed by the early development, of the Bergius direct coal liquefaction process and the Fischer-Tropsch Synthesis (1910 – 1926). Secondly, Germany's industrialisation of these processes from the late 1920's up to 1945. The third is the global transfer of these technologies to countries such as Britain, Japan, the USA, South Africa, and others from 1930 – 1990's (Stranges, 2007).

The production of synthetic fuels (or synfuels) saw its birth in the early 20th century with the invention of direct coal liquefaction (DCL) technology. Friedrich Bergius, in 1913, invented the high pressure coal hydrogenation process (Williams & Larson, 2003; Dancuart & Steynberg, 2007) which converts coal to a partially refined synthetic crude oil which can be further refined into transportation fuels, as well as liquefied petroleum gas (LPG) (Williams & Larson, 2003). The second technology for the production of synthetic hydrocarbons was discovered by Franz Fischer and Hans Tropsch in 1923. The Indirect coal liquefaction (ICL) process via the Fischer-Tropsch Synthesis (FTS) converts coal into synthesis gas (a mixture of H_2 and CO) and then via catalytic reaction to liquid hydrocarbons (Williams & Larson, 2003).

These synthetic fuel production routes were quickly recognised as an opportunity to attain fuels independence by the German government. The DCL and ICL processes were incorporated into Germany's energy plan and in the 1930's gained considerable support from the Nazi government (Stranges, 2007). It was argued that the German government's involvement played a key role in the synfuel industry's development and advancement as it led to risk-free industry-government collaboration in the 1930's and during World War 2 (Stranges, 2007). Although the Bergius coal hydrogenation process was the main contributor to Germany's transportation fuels requirements during WW2, post-war, DCL (and synfuel research in general) was, for the most part, abandoned when low-cost Middle-East oil became available in the 1950's (Williams & Larson, 2003). Synfuel R&D was revived in industrialised nations during times of oil crises (such as the Arab oil embargo in 1973 and the oil crisis of 1979), but were, in many cases abandoned again with declining oil prices (Williams & Larson, 2003).

Fischer-Tropsch R&D, for the most part, suffered a similar history. With the exception of Sasol in South Africa, the history of research and commercial development of synfuel production via FTS is littered with stops and starts (Davis, 2005; Stranges, 2007). This (as mentioned before) has been mostly linked to fluctuations in crude oil prices and availability (Stranges, 2007). However, concerns over depleting crude, political unrest in major crude exporters, need novel gas monetisation strategies, among other factors have sparked a renewed interest in FT research since the 1970's and late 20th century (Dancuart & Steynberg, 2007; Stranges, 2007; Dasgupta & Wiltowski, 2011; Maitlis, 2013).

Some other technologies for the production of synthetic fuels are as well being considered. These include the conversion of methanol to gasoline and the synthesis of methanol (Williams & Larson, 2003) and dimethyl ether (DME) by ICL as a possible replacement for gasoline and diesel respectively (Larson & Tingjin, 2003; Williams & Larson, 2003). Methanol, however, does have drawbacks associated with its use as a fuel, which limits its use as a gasoline alternative. However, it is being used as starting material to manufacture DME (Williams & Larson, 2003). DME has been proposed for use as a clean cooking fuel or diesel alternative for compression ignition engines due to its high cetane number and clean burning characteristics (Larson & Tingjin, 2003; Williams & Larson, 2003).

1.2 The FT-Process and FT-Synthesis

The Fischer-Tropsch process describes the set of technologies for the production of synthetic fuels and other products from carbonaceous feedstock via the FT synthesis. This process produces high value products from a low value carbon-containing feedstock such as coal, natural gas and increasingly biomass. The process involves synthesis gas production, the Fischer-Tropsch Synthesis, product separation and product workup/upgrading, as can be seen in Figure 1.1.

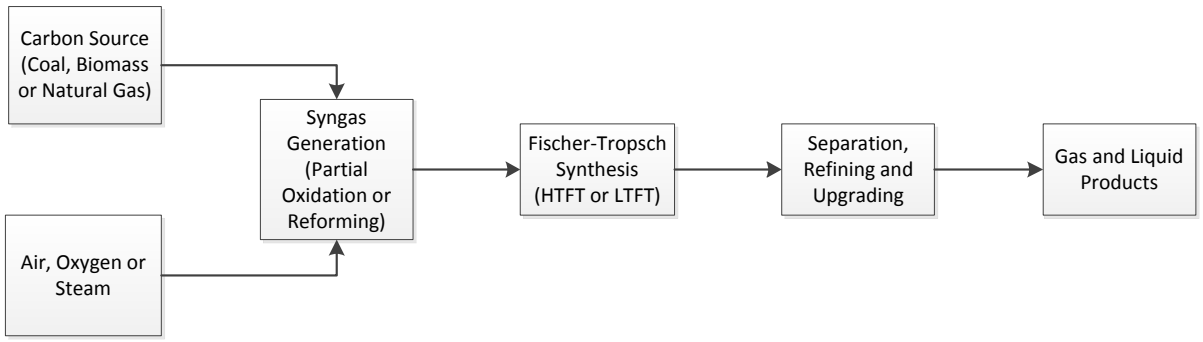

Figure 1.1: Simplified block flow diagram illustrating the FT-process

Synthesis gas production by reacting carbonaceous sources such as coal, biomass or natural gas with air, oxygen, steam or a mixture at high temperature, is the starting point for the FT process. Generally in commercial plants, when using a solid feedstock like coal or biomass to produce synthesis gas, the process is referred to as gasification, while the process of producing syngas from natural gas is achieved via the reforming process (Zennaro *et al.*, 2013; Höök *et al.*, 2014). The reactant (air, oxygen and/or steam) is added in a controlled manner to avoid the complete oxidation to carbon dioxide and water vapour (Zennaro *et al.*, 2013; Höök *et al.*, 2014). In coal gasification the properties of the coal feedstock is of major significance, influencing the choice of gasifier as well as the further processing (Höök *et al.*, 2014). Several types of gasifiers have been developed over the years and can be grouped into four major technologies (each with its own advantages, disadvantages and application): fixed bed-, fluidised bed-, entrained flow- and indirect- gasification (Zennaro *et al.*, 2013).

Natural gas as feedstock tends to have a less significant influence on processing and potentially presents fewer issues when compared to coal due to its greater homogeneity (Höök *et al.*, 2014). The choice of technology is informed majorly by the required syngas composition as well as economic and process optimisation variables. Some of the different options for natural gas reforming are Steam Methane Reforming (SMR), Autothermal Reforming (ATR), Catalytic Partial Oxidation (CPO) and Heat Exchange Reforming (HER) (Zennaro *et al.*, 2013). The preferred technology for FTS is the autothermal reforming because it offers a H_2/CO ratio closer to 2:1 (Höök *et al.*, 2014) as well as being more economical- and requiring less steam than the SMR (Zennaro *et al.*, 2013).

The Fischer-Tropsch Synthesis (FTS) is the catalysed reaction of synthesis gas (a mixture of H_2 and CO) to produce a complex spectrum of hydrocarbons, and water as the main by-product. This complex mixture of hydrocarbons consists of linear and branched

olefins and paraffins, as well as oxygenates (Van der Laan & Beenackers, 1999; Biel, 2004; Blekkan *et al.*, 2007). The major hydrocarbon formation reactions can be summarised as:

$$nCO + (2n + 1)H_2 \rightarrow C_nH_{2n+2} + nH_2O \quad (1.1)$$

$$nCO + 2nH_2 \rightarrow C_nH_{2n} + nH_2O \quad (1.2)$$

In addition to the main reactions, side reactions also take place. These include the water-gas-shift reaction on Fe-catalysts, formation of oxygenated compounds and the Boudouard reaction (Williams & Larson, 2003; Chonco, 2014). The main and side reactions occur to a more or lesser extent depending on the type of catalyst and process conditions employed (Williams & Larson, 2003).

In 1923, Fischer and Tropsch produced a product containing oxygenates (but no hydrocarbons), that they termed Synthol, using an alkali iron catalyst at high temperatures and pressures (400 – 450 °C and 100 – 150 atm, respectively) (Stranges, 2007). At lower pressures they produced hydrocarbons, but found that the Fe-catalyst deactivated more rapidly (Biel, 2004). After further research in 1925 – 1926, with a Co-Fe-catalyst, they completely eliminated the oxygenated products and produced only hydrocarbons at 1 atm and 250 – 300 °C (Stranges, 2007). The FTS is catalysed by the group VIII metals (Biel, 2004; Atashi *et al.*, 2012; Höök *et al.*, 2014). The metals Fe, Co, Ni and Ru are known to be most active for FTS (Van der Laan & Beenackers, 1999). However, only Fe and Co are used commercially and at temperatures and pressures of 200 °C – 300 °C and 10 – 60 bar, respectively (Van der Laan & Beenackers, 1999; Itkulova *et al.*, 2007).

Cobalt-based catalysts have the advantage of higher syngas conversion, higher selectivity toward paraffins (Zennaro *et al.*, 2013) and longer life with clean synthesis gas. Such higher production rates can be achieved with smaller reactors (Graham *et al.*, 2007). Iron-based catalysts have a higher selectivity towards olefins and C_{5+} hydrocarbons, lower methane selectivity and higher tolerance for sulphur compounds. In addition, the Fe-based catalyst can operate in a wider temperature and H_2/CO range. This makes it more suitable for syngas obtained from coal or biomass with a low H_2/CO ratio (Graham *et al.*, 2007). This coupled with its relatively low price and high abundance has made the Fe-based catalyst a very popular FTS catalyst (Wan *et al.*, 2007a; Özkara-Aydınoğlu *et al.*, 2012). The selectivity, activity and stability of the Fe-

based catalyst can be improved by the addition of chemical promoters such as Cu and K, which are the most widely investigated promoters (Özkara-Aydınoğlu *et al.*, 2012).

Nickel and ruthenium are not suited for application as commercial FTS catalysts. This is because Ni is prone to methanation under typical FTS conditions and even though Ru is the most active of the FTS-CO-hydrogenation catalysts, its scarcity make it highly expensive (Van der Laan & Beenackers, 1999; Claeys & Van Steen, 2002; Davis & Maitlis, 2013).

It is known that metallic Ru and metallic Co catalyse the synthesis reaction (Van der Laan & Beenackers, 1999; Davis & Maitlis, 2013), but the active phase (or phases) of Fe for FTS is still debated in literature even though the surface carbidic iron species was believed to be the active phase since the earliest studies (De Smit & Weckhuysen, 2008). Catalyst reduction/activation is done with H_2 for Ru and Co catalysts, because of the requirement that the metals be in the reduced state to be active for FTS. The Fe-based catalyst is pre-treated in H_2, CO or synthesis gas and undergoes phase transformations during FTS. It has been found to consist of a mixture of metallic Fe, Fe-oxides and Fe-carbides (Van der Laan & Beenackers, 1999; De Smit & Weckhuysen, 2008).

Fischer-Tropsch processes are generally carried out at high and low temperatures. The High Temperature Fisher-Tropsch (HTFT) process targets the production of short chain hydrocarbons utilising an iron-based catalyst at relatively high temperature of 300 – 350 °C. Low Temperature Fischer-Tropsch (LTFT) aims at the production of high molecular weight hydrocarbon waxes at relatively low temperatures of 220 – 240 °C using either Co- or Fe-catalysts (Dancuart & Steynberg, 2007; Wood *et al.*, 2012; Kaiser, 2014).

1.3 Why Fischer-Tropsch Synthesis?

The greatest scientific and technological challenge facing the world in the 21st century is the growing demand for energy. This is evident in the annually rising global requirement for more energy (especially in the form of transportation fuels) by modern society (Maitlis, 2013). Putting this in perspective, the global demand for diesel in 2011 was at 25 million barrels/day and this has been forecast to increase to 37 million barrels/day by 2035 (Wood *et al.*, 2012).

Recently, many factors have spurred the interest of researchers to re-evaluate energy forms and sources, especially with regard to transportation fuels. Some of these include the shift from solid to liquid fuels with the recognition of their superior energy content, mass production of automobiles and growing air travels and petroleum powered ships. So also is the desire of countries with limited/no crude oil reserves to achieve energy independence, and a growing global awareness that petroleum reserves are finite (Stranges, 2007). The general rise in the price of crude oil, unrest and uncertainty in the Middle East, rising environmental concerns and stricter legislation with regard to transportation fuels and their production has also led to a renewed interest in synthetic fuels (Dasgupta & Wiltowski, 2011).

One of the major environmental concerns surrounding petroleum as the source of transportation fuels is the considerable amounts of associated gas flared during production (Dung *et al.*, 2008; Nwankwo & Ogagarue, 2011; Wood *et al.*, 2012). This is considered to be the main source of air pollution in oil and gas installations. In the Niger Delta (Nwankwo & Ogagarue, 2011), flaring is the preferred method for the disposal of "waste gas" in the Niger Delta practised by multinational oil companies. In addition to the environmental concerns, the economic loss associated with this practice was already estimated at US $2.5 billion annually in 2008 (with the environmental cost not yet fully quantifiable). Conservative estimates for the Niger Delta alone is that about 50 mscm (million standard cubic meter) of associated gas is flared annually, equivalent to approximately 40% of the African continent's natural gas consumption (Dung *et al.*, 2008).

Other than impacting air quality, the main repercussions of flaring are the formation of acid rain from the emissions, and the contamination of soils and groundwater with heavy metals in surrounding areas (Dung *et al.*, 2008; Nwankwo & Ogagarue, 2011). In the Niger Delta the environmental effects of flaring are quite evident as retardation in crop development has been observed in areas surrounding flare stacks (Dung *et al.*, 2008).

To address the issue of flaring from both an environmental and economic perspective, the "unwanted" associated gas produced during crude oil extraction can be monetised by employing Gas-to-Liquid (GTL) Fischer-Tropsch technology. This utilises the "waste gas" as feedstock to produce liquid hydrocarbons. In addition to being of higher value than natural gas/associated gas, the liquid hydrocarbons are easier to store and transport.

Companies, such as the UK based CompactGTL, are looking into small scale Fischer-Tropsch strategies to utilise associated gas in small modular units. This approach

utilises associated gas by feeding to a methane reformer to produce syngas, which is then converted to a synthetic crude oil, water and a "tail gas" in a FT-reactor. The syncrude is then exported to a conventional refinery for further processing. Even though this approach does not directly produce high-value distillate products on site, it has the advantages of obtaining feed gas at no cost by avoiding flaring and/or costs associated with re-injection. It also extends the application of GTL technology to smaller scale stranded gas applications (Wood *et al.*, 2012).

GTL is considered to present a very attractive gas monetisation strategy for gas producers. The technology will enable them to diversify and expand into the transportation fuel markets. Additionally, this enables more compact- and easy product transportation by converting CH_4 to liquid fuels and valuable liquid hydrocarbon products. The GTL route thus serves as an alternate solution for the utilisation of vast quantities of stranded/isolated natural gas reserves where economical exploitation by conventional means is not possible (Wood *et al.*, 2012). The gas-based FT process has the added advantage that the raw feedstock (associated gas) is far cleaner than coal used in conventional Coal-to-Liquid (CTL) plants.

With the rising concerns pertaining to global warming and climate change, environmentally motivated legislation is getting stricter in most countries. This aims at reducing emissions associated with power generation, transportation, etc. to improve air quality by minimising pollutants and decelerate Global Warming/climate change. The physical and legislative need for cleaner fuels has many researchers looking at alternatives to conventional fuel production.

Of course other methods for the production of synthetic liquid fuels exist, such as the direct liquefaction of coal (coal hydrogenation). High pressure coal hydrogenation, developed by Friedrich Bergius, was the most important source of Germany's synthetic fuel during the Second World War (WW2). However, it is no longer considered a desirable approach to the production of synthetic fuels. Compared to natural gas conversion, coal hydrogenation has a much larger environmental impact and higher cost. Additionally, the high aromatics content of the products is not compatible with modern fuel specifications (Dancuart & Steynberg, 2007).

Another possible route for the production of synthetic transportation fuels is the conversion of methanol to gasoline, where synthesis gas is first converted to methanol. This, however, produces gasoline with high aromatics content and produces virtually no diesel range fuels (Maitlis, 2013). Another synfuel route is the conversion of coal to low molecular weight alkenes and subsequent conversion to gasoline and

diesel. However, the diesel produced is multiple branched, and thus has a low cetane number, making it inferior to FT-derived diesel (Maitlis, 2013). Further possibilities include the synthesis of methanol or dimethyl ether (DME) by ICL as a possible replacement for gasoline and diesel respectively (Larson & Tingjin, 2003; Williams & Larson, 2003; Zennaro *et al.*, 2013). Methanol, however, does have drawbacks associated with its use as a fuel including a low energy density, corrosiveness, toxicity and affinity to water (Williams & Larson, 2003). DME has a high cetane number, is non-carcinogenic and non-toxic, but has an energy density of 55% of number 2 diesel and requires slight compression for liquid storage (Larson & Tingjin, 2003; Williams & Larson, 2003).

The Fischer-Tropsch process for the production of liquid hydrocarbon fuels from synthesis gas is very flexible in the sense that the synthesis gas can, in theory, be obtained from any carbon containing source. The process can be operated utilising Biomass-to-Liquid (BTL), Coal-to-Liquid (CTL) and Gas-to-Liquid (GTL) technologies. The carbonaceous material such as coal, biomass or natural gas is converted into syngas and then to liquid products via the FTS. A green approach to synthetic transportation fuels is thus made possible via BTL since biomass is a renewable resource (Graham *et al.*, 2007).

It is a commercially proven technology and has been operated industrially by Sasol in South Africa since the 1950's (Wan *et al.*, 2008; Höök *et al.*, 2014) and PetroSA since the 1990's (Bingen, 2002; Dancuart & Steynberg, 2007). Other commercial FT operations include the Shell Middle Distillate Synthesis (SMDS) plant in Bintulu, Malaysia. The plant was commissioned in 1993 with an original capacity of 12500 barrels/day, but was upgraded in 2003 to 14700 barrels/day (Wood *et al.*, 2012). In 2007 construction of the Pearl GTL plant in Qatar, jointly owned by Shell and Qatar Petroleum and based on SMDS technology, was started, with 140 000 barrels/day capacity and production commencing in 2011 (Wood *et al.*, 2012; Höök *et al.*, 2014). Another Sasol venture was the Oryx plant in Qatar, a joint venture with Qatar Petroleum, commissioned in 2007 and 2008 with a 32 400 barrels/day design capacity (Wood *et al.*, 2012). These plants are all still operating commercially.

A GTL feasibility study was done by Texaco and SASOL in the Niger Delta in 1998, resulting in the Escravos GTL project agreement between Sasol, Chevron Corporation and the Nigerian National Petroleum Company. The construction of the Escravos plant, of similar scale and design to Oryx GTL, started in 2005 and (after many delays) was expected to start operation in 2013. Due to the delays and increased cost SASOL

withdrew from the project in 2009, however, the FT technology is still used under licence (Wood *et al.*, 2012). Escravos GTL started up in June 2014 and is expected to run at full capacity by 2015 (SASOL, 2014).

FT-derived fuels are attractive due to their low sulphur content and negligible aromatics content (Van der Laan & Beenackers, 1999; Graham *et al.*, 2007; Sehabiague *et al.*, 2008) and these fuels thus usually exceed the environmental properties of conventional crude-derived fuels (Maitlis, 2013). For instance, when comparing the combustion characteristics of FT-diesel and conventional diesel, FT-derived diesel yields much lower nitrogen oxides (NO_x), carbon monoxide (CO), hydrocarbon and nano-particulate matter emissions than the conventional crude derived diesel (Graham *et al.*, 2007).

It is thus fairly certain that FT projects will gain more interest in the light of depleting oil reserves and discovery of more stranded gas reserves, and is likely to become more attractive with rising crude oil prices (Sehabiague *et al.*, 2008). Therefore, the development of more active catalysts with improved properties, such as stability and regenerability, is one of the most significant opportunities for improving the FT-process and meeting today's challenges of alternative fuels supply (Eliason & Bartholomew, 1999; Graham *et al.*, 2007).

The Fe-catalysts are considered by many to be the ideal catalyst when H_2-deficient syngas (obtained from carbon sources such as coal or biomass) is used as feed for FTS due to its high activity for the water-gas-shift reaction and its relatively low cost compared to cobalt and ruthenium (Wan *et al.*, 2007a; Wan *et al.*, 2007b; Chonco *et al.*, 2013). Though it has been operated commercially with success for decades, the Fe-catalysed FT-process still presents some challenges. One of the major remaining challenges is the Fe-based catalyst rapid rate of deactivation due to the oxidation of the catalytically active phase(s) of Fe for FTS to inactive Fe_3O_4 (magnetite) by water, the main by-product of FTS (Satterfield *et al.*, 1986; Claeys & Van Steen, 2002; Biel, 2004; Dalai & Davis, 2008). Satterfield *et al.* (1986) showed the effect of water could be detrimental to iron catalysts, with irreversible deactivation occurring when water was co-fed at 42 mole% of the feed. (Irreversible deactivation here refers to deactivation due to oxidation which was not reversible when returning to initial conditions, i.e. deactivation which was not reversible upon cessation of water co-feeding.) From a commercial viewpoint, this coupled with the associated cost of replacement and/or regeneration, is quite unfavourable (De Smit & Weckhuysen, 2008).

Ruthenium is known to be highly active for FTS, producing high molecular weight hydrocarbons at low temperature and high syngas pressure (Claeys & Van Steen, 2002;

King, 1978; Tang & Li, 2011; Van der Laan & Beenackers, 1999; Davis & Maitlis, 2013). It has also been found to be highly resistant to oxidation as evidenced by its activity in liquid water (Claeys & Van Steen, 2002; Davis & Maitlis, 2013; Hibbitts *et al.*, 2013). Claeys & Van Steen (2002), during water co-feeding experiments on a SiO_2 supported Ru-catalyst, observed an increased reaction rate, C_{5+} selectivity, chain growth probability and olefinicity (and decreased methane selectivity) with increasing water partial pressure. According to Hibbitts *et al.* (2013), H_2O increases chain growth probability by increasing the rate of monomer formation for chain growth occurring via CH_x or the rate constant for chain growth when CO is the monomer. It is therefore thought that promotion of the iron-based catalyst with ruthenium can make make use of this property of ruthenium at high water partial pressures associated with high CO-conversion and that this may make the catalyst more robust (better longevity at high conversion), highly active and more selective toward C_{5+} hydrocarbons.

Kaminsky *et al.* (1985) found Ru seems to be more of a methanation catalyst when supported on carbon at H_2/CO ratio of 3:1 (methane selectivity of more than 75%). However, their experiments were carried out at temperatures above what is considered the upper limit for low temperature synthesis and with very low Fe/Ru ratios. Their findings thus corresponded well with what is known of ruthenium's behaviour at high temperatures and low pressures. Bahome *et al.* (2007) investigated Fe-Ru bimetallic catalysts supported on carbon nanotubes with Fe/Ru ratios of 40:1 and 20:1. As expected, methane selectivity is a bit higher as the Fe/Ru is decreased, but methane selectivities were much lower than that observed by Kaminsky *et al.* (1985) even at much higher conversions. Decreasing the Fe/Ru ratio increased the CO-conversion, but increased the methane selectivity showing ruthenium's low pressure and "high" temperature characteristics to be more pronounced at lower Fe-loadings.

This would imply that promoting Fe with more than $2.5 - 5$ wt% Ru would not be advantageous w.r.t. the FT-product obtained, even if disregarding the high cost of high Ru-loadings. An investigation by Xu *et al.* (2003) on SiO_2 supported Fe promoted with Pt showed an apparent increase in catalyst stability compared to Fe not promoted with Pt and was also capable of higher CO-conversion at the same reactor conditions. However, it did also increase water gas shift activity, leading to slightly higher CO_2 selectivity on the Fe/Pt catalyst compared to Fe only. A decrease in methane selectivity was also observed (however, this will likely not be the case with Ru-promotion). Ru, being a noble metal, is expected to have a similar effect on catalyst stability in addition to its own FTS activity and a similar small increase in CO_2 selectivity may also be expected.

The current industrial practice for Fischer-Tropsch Synthesis using an iron-based catalyst is thus to operate at a relatively low single pass conversion to extend the life of the catalyst. However, this requires an increased reactor size and the need for raw material recycle. Considering the higher capital investment and operating costs associated with this, it has a negative influence on process economics.

1.4 Statements of Research Problem

The productivity of an iron-based Fischer Tropsch (FT) process strongly depends on the synthesis gas conversion. However, iron is known to oxidize significantly at high CO conversion due to the high reactor water partial pressures and in commercial iron-based FT plants this necessitates operation at low single pass conversion, resulting in high separation and recycling cost of the tail gas and the overall economics of the process. Ruthenium has been reported to demonstrate significant stability in the presence of water, hence the employment of a FT catalyst promoted with Ru is expected to permit high CO conversion. In this study the stability of an industrial Fe-based FT catalyst impregnated with ruthenium is investigated.

1.5 Research Aim(s) and Objectives

The study aims at the development of a precipitated iron-based LTFT-catalyst which exhibits improved stability at high synthesis gas conversions while maintaining acceptable product selectivity. To this end the following objectives have been set:

a) Investigate ruthenium's influence on the reducibility of the iron-based FT catalyst.
b) Investigate the influence of the ruthenium addition on the product distribution and selectivity towards C_{5+} hydrocarbons.
c) Investigate how ruthenium promotion affects catalyst stability at high synthesis gas conversion.

1.6 Research Questions

a) Will Fe-based FT catalysts promoted with ruthenium permit high synthesis gas conversion while exhibiting reasonable stability?
b) How does Ru-promotion of the Fe-based catalyst influence the activity of the catalyst?
c) What is the influence of Ru-promotion on the products distribution, including CH_4 selectivity, C_{5+} selectivity, CO_2 selectivity and olefinicity?
d) How does promotion with ruthenium affect the catalyst morphology and reducibility?

1.7 Scope of the Study

The thesis will focus on evaluating the stability of a ruthenium promoted precipitated iron-based LTFT catalyst at high synthesis gas conversions as compared to a non-ruthenium promoted precipitated iron-based catalyst of the same composition. FT runs are done in a slurry bed reactor where GHSV will be altered to achieve high CO-conversion levels. Samples of the product stream will be analysed by GC to gauge performance and compare product selectivities, after which comparative apparent deactivation will be used as an indicator of catalyst stability.

1.8 Expected Contribution to Knowledge

The iron-based FT catalyst has been investigated in many forms and under varying conditions. At the time of writing the author is unaware of much similar research on precipitated, high surface area, iron-based LTFT catalysts having been carried out. The data generated for this type of catalyst, being in industrial use, is expected to be more relevance to industry than previous studies on low iron loading supported catalysts or fused iron catalysts.

1.9 Thesis Outline

Chapter 1 serves to give the background and motivation for the project where the objectives for this work has been briefly outlined. The reader is also introduced, briefly, to the history of synthetic fuels, the Fischer-Tropsch Synthesis and Fischer-Tropsch Process.

Chapter 2 gives a brief history of the Fischer-Tropsch Synthesis and Fischer-Tropsch process. In addition the FT product distribution, most prominent reaction mechanisms, catalysts employed and various reactor systems are discussed.

Chapter 3 provides an overview of catalyst preparation and characterisation techniques. It also provides the methodology employed for catalyst preparation and characterisation, as well as FTS testing and products analysis.

In **Chapter 4** the results of the catalyst characterisation and FTS testing are presented and discussed. The chapter focuses largely on a comparison of product selectivities of the catalysts employed at similar conversion levels as well as with similar systems in literature.

Chapter 5 presents the conclusions of the study with a brief summary of the results in addition to making recommendations for further studies/research. Chapter 5 is followed by a list of references and appendix.

2

Chapter 2: Literature Review

Initially discovered in the 1920's by Franz Fischer and Hans Tropsch, the Fischer-Tropsch Synthesis (FTS) is, most simply put, the catalytic reaction of hydrogen and carbon monoxide to produce hydrocarbons. The wide product spectrum includes hydrocarbon gases, olefins, praffins and oxygenates. Depending on the type of catalyst and synthesis conditions, the product spectrum can be shifted to target the production of specific products such as hydrocarbon fuels or high molecular weight hydrocarbons.

In this chapter the history of FTS (research and commercial application) and coal liquefaction technologies, the FTS reaction, FT-reactors, catalysts and process conditions is discussed. Since the research is focussed on ruthenium promoted iron catalysed FTS, iron and ruthenium catalysts will be discussed in more depth.

2.1 The Fischer-Tropsch Synthesis

The Fischer-Tropsch Synthesis (FTS) is, simply put, the catalysed reaction of synthesis gas to produce hydrocarbons, and water as the main by-product (Van der Laan & Beenackers, 1999; Blekkan *et al.*, 2007). The FT Synthesis is a heterogeneous polymerisation reaction which follows a complicated series of primary and secondary reactions to yield a broad product spectrum that ranges from methane to heavy waxes (Anderson, 1956; Schulz & Claeys, 1999). Fischer-Tropsch products are predominantly linear paraffins and primary olefins, with various amounts of oxygenates (alcohols, aldehydes, ketones and acids) also being formed (Dry, 1981; Gradassi, 1998).

The linear hydrocarbons (n-paraffins and α-olefins) formed during synthesis are regarded as the primary products. Overall reactions for the formation of paraffins ad olefins are shown in Equations 2.1 and 2.2, respectively (Van der Laan & Beenackers, 1999; Dasgupta & Wiltowski, 2011; Maitlis, 2013):

$$nCO + (2n + 1)H_2 \rightarrow C_nH_{2n+2} + nH_2O \quad (2.1)$$

$$nCO + 2nH_2 \rightarrow C_nH_{2n} + nH_2O \quad (2.2)$$

Side reactions occur in conjunction with formation of primary products. These include the water-gas-shift reaction on Fe-catalysts, formation of oxygenated compounds and the Bouduard reaction, as in Equations 2.3 – 2.5 (Van der Laan & Beenackers, 1999; De Smit & Weckhuysen, 2008). In addition, olefins are reactive and can be re-adsorbed to take part in secondary reactions. Depending on the catalyst- and process conditions employed, main and side reactions will occur to a more or lesser extent (Williams & Larson, 2003).

$$CO + H_2O \rightarrow CO_2 + H_2 \quad (2.3)$$

$$nCO + 2nH_2 \rightarrow C_nH_{2n+1}OH + (n-1)H_2O \quad (2.4)$$

$$2CO \rightarrow CO_2 + C \quad (2.5)$$

2.1.1 A Brief History of Fischer-Tropsch

Dancuart and Steynberg (2007) divides the development of the FT industry into five distinct stages:

- Discovery (1902 – 1928)
- The first era of the Co-catalyst (1929 – 1945) during which major commercial development was seen in Germany utilising coal derived synthesis gas
- The Fe-catalyst era (1950 – 1990), majorly focussed around Sasol's construction of commercial plants using coal derived synthesis gas in South Africa.
- The GTL commercial initiation era (1990 – 2004), characterised by accelerated FT research and development using Fe- and Co-catalysts utilising natural gas derived syngas and the construction and operation of commercial plants by PetroSA and Shell GTL.
- Commercial expansion (2004 – present), focussed around the proposal of more GTL projects and –concepts and continued R&D.

The FT process is, historically, the second commercial technology for the production of synthetic hydrocarbons. The first was the Bergius process, a high pressure coal hydrogenation process, developed by Friedrich Bergius (Rheinau-Mannheim) from 1910 – 1925 (Dancuart & Steynberg, 2007; Höök *et al.*, 2014). The process was significantly further developed and improved by the Badishe Anilin und Sodafabrik

(BASF) after Bergius sold the patent rights in 1925 in time to partially fulfil Germany's WW2 liquid fuel requirements (Williams & Larson, 2003; Stranges, 2007).

The discovery of the Fischer-Tropsch synthesis is majorly credited to the work of Fischer and Tropsch leading up to 1923, while at the Kaiser Wilhelm Institute (KWI) for Coal Research in Müllheim, Germany. However, the first reported CO-hydrogenation reaction was that of methane production over a nickel catalyst by Sabatier and Senderens in 1902 (Bartholomew & Farrauto, 2011; Davis & Maitlis, 2013; Maitlis, 2013). BASF, in 1913, patented a process producing liquid hydrocarbons and oxygenated products from syngas containing excess CO in a ratio of CO/H_2 of 2:1. Their hydrocarbon research was abandoned due to the outbreak of WW1 and the priority given to industrialising the synthesis of ammonia and methanol. Fischer, upon learning of the patent, decided to investigate the claims and working with Tropsch started research using a gas with $H_2/CO = 2:1$ to avoid carbon deposition (Stranges, 2007; Bartholomew & Farrauto, 2011). In 1925 Franz Fischer and Hans Tropsch successfully catalytically converted a mixture of CO and H_2 to hydrocarbons and water at atmospheric pressure (Pichler & Schulz, 1970; Stranges, 2007) and reaction temperatures of 250 – 300 °C, completely eliminating the oxygenated compounds, over Co-Fe catalysts (Stranges, 2007). Prior to this, these authors had produced, at high temperature and pressure (400 – 450 °C and 100 – 150 atm), a mixture of oxygenates which they termed "synthol" (Stranges, 2007; Maitlis, 2013). The Co-catalysts instrumental to the success of the FT-process during the war were developed by Fischer and his co-workers during the 1920's – 1930's (Stranges, 2007).

Though synthetic fuel research was of interest internationally during the pre-WW2 era, the majority of the FT-process development occurred in Germany during the 1930's and 1940's. In the early 1930's the Weimar government had already been pushing for Germany's petroleum independence by imposing controls and regulations on the German oil industry. The synthetic fuel industry received a significant push when the Nazi government intensified this, starting in 1933 (Stranges, 2007). By the end of 1935, after demonstrating technical success of FTS using a Co catalyst at Ruhrchemie's Oberhausen-Holten pilot scale plant (after abandoning work on Ni), four commercial scale FT-plants were under construction (Stranges, 2007; Bartholomew & Farrauto, 2011), with the first starting operation in 1936 (Leckel, 2009). By further raising tariffs on imported crude in 1936 synfuel plants were able to show a profit despite their inefficiency. The Nazi government's commitment to- and push for a petroleum independent Germany by the start of WW2 was one of the biggest driving forces ensuring the survival and further development of the synthetic fuel industry. Without

this special relationship between the Nazi government and synthetic fuel industry it would have, more than likely, collapsed (Stranges, 2007).

By 1940 the total synthetic fuel production from Germany's coal hydrogenation plants and FT plants had exceeded the combined total of that produced by crude oil refining and imports. However, despite the significant government intervention, synthetic petroleum produced from coal could not completely solve the German liquid fuel problem and Germany thus never achieved its goal of petroleum independence (Stranges, 2007). During the war effort (1940 – 1945), close to 70% of the German petroleum demand was met through the 21 synthetic fuel producing plants (Dancuart & Steynberg, 2007), providing 90% of the annual motor fuel requirement (Leckel, 2009). Nine of these were FT-plants that had supplied 9% of the German petroleum demand. The main reason for Germany's continued dependence on direct coal liquefaction plants was the low octane FT gasoline that was produced at low temperature and pressure (Dancuart & Steynberg, 2007). Straight run FT distillate was blended with the low cetane number diesel produced by direct coal liquefaction to obtain a 40 – 50 cetane diesel oil (Leckel, 2009).

FT Synthesis was conducted at low temperatures of between 180 °C and 200 °C, over Co/ThO_2/kieselguhr catalysts. The oldest plants were running at pressures of 1 atm, with the newer units designed for operation at up to 10 atm. Coal derived syngas was desulphurised to 5 ppm to extend the lifespan of the catalyst (Dancuart & Steynberg, 2007). After the Second World War most interest in FTS (and synfuels) was lost after major reserve discoveries and consequently lower prices of natural crude. At this stage the process was of more academic than commercial significance. In spite of this a few teams of researchers continued work, primarily basing it on the German's demonstrated technology (Dancuart & Steynberg, 2007). Research and development continued in the USA, Great Britain and Germany. During this time there was a perception of a petroleum shortage and fears that crude prices would increase. Much of the work was based on inexpensive iron FTS catalysts that were developed in Germany towards the end of the war (Stranges, 2007; Bartholomew & Farrauto, 2011).

In the early 1950's the first GTL plant was run in Brownsville, Texas since it used natural gas as feedstock. A HTFT process using an iron catalyst was used to produce 82 octane gasoline (Dancuart & Steynberg, 2007; Stranges, 2007; Leckel, 2009). It also produced a distillate by-product which had a very high cetane number when compared to crude-derived distillate (Leckel, 2009). The plant was plagued by many operational issues in its early years and though these were eventually solved the plant was forced to

shut down due to a significant increase in natural gas prices. Roughly during this time the construction and operation of the Sasol's first coal-based FT plant was starting in Sasolburg, South Africa (Dancuart & Steynberg, 2007; Stranges, 2007; Leckel, 2009; Bartholomew & Farrauto, 2011; Höök *et al.*, 2014). In reaction to the 1970's oil crisis as well as the world's reaction to the apartheid regime, Sasol expanded their operations by constructing two FT plants in Secunda in 1970's and 1980's (Stranges, 2007; Leckel, 2009; Höök *et al.*, 2014).

Sasol developed two LTFT and two HTFT systems. At the Sasolburg plant, the original LTFT ARGE reactors were an optimised Ruhrchemie design and they are still in use today. The original HTFT reactors were circulating fluidised bed (CFB) reactors based on the original Kellog concept. These CFB reactors had many teething problems, forcing significant changes and resulting in the Synthol CFB reactors (Steynberg & Dry, 2004; Dancuart & Steynberg, 2007). The second generation CFB reactors installed in Secunda were improved and scaled up versions of the Synthol CFB reactors (Steynberg & Dry, 2004; Dancuart & Steynberg, 2007; Leckel, 2009). These reactors were also installed in the, then Mossgas, Mossel Bay plant in the early 1990's. However, only PetroSA's Mossel Bay plant still operates these second generation CFB reactors, since Sasol had replaced all their CFB's with fixed fluidised bed Sasol Advanced Synthol (SAS) reactors by 1999 (Steynberg & Dry, 2004; Leckel, 2009; Höök *et al.*, 2014).

Though investigated during the 1950's and 1960's, slurry phase reactors for LTFT were not commercially operable due to limited knowledge. Original investigations were done at space velocities too low to judge commercial performance and effective wax-catalyst separation had not yet been developed. During the 1970's Sasol revisited the concept. After evaluation, further development and testing of an effective separation device in 1990, a commercial unit was brought on-line in 1993 with a production capacity equivalent to five of the ARGE reactors (Steynberg & Dry, 2004). The Sasolburg plant's process scheme changed again in 2004 with the replacement of coal gasification with natural gas reforming, turning Sasol One into a GTL plant (Dancuart & Steynberg, 2007; Leckel, 2009).

In 1993 the Shell Middle Distillate Synthesis (SMDS) plant was commissioned in Bintulu, Malaysia. The plant uses an LTFT GTL process for the conversion of natural gas. Multi-tubular fixed bed reactors are used to target paraffinic wax production over a high activity Co-catalyst, which is subsequently hydrocracked to transportation fuel products (Steynberg & Dry, 2004; Dancuart & Steynberg, 2007; Leckel, 2009; Höök *et al.*, 2014).

A 2001 agreement between Sasol and Qatar Petroleum resulted in the Oryx GTL plant in Qatar. After delays and budget overruns, the 32 400 barrel/day plant was completed in 2008. Syngas is generated via autothermal reforming and converted in LTFT slurry phase FT reactors followed by isocracking product upgrading to produce mainly diesel (Leckel, 2009; Höök *et al.*, 2014). Since both use a similar refining concept in the processing of FT synthetic crude, products from the Oryx GTL plant are very similar to those produced by the SMDS (Leckel, 2009).

Sasol ended up withdrawing from the Nigerian Escravos project in 2009 due to delays and cost overruns. The joint venture started as a 1998 GTL feasibility study together with Texaco. The project agreement between Sasol, Chevron and the Nigerian National Petroleum Company was completed in 2002 and used the same design as the Oryx plant (Dancuart & Steynberg, 2007; Höök *et al.*, 2014). The plant started production in mid-2014 (Okereke, 2016), targeting the production of principally diesel (Höök *et al.*, 2014; Okereke, 2016).

Construction of the Pearl GTL plant in Las Raffan, Quatar, a joint venture between Shell and Qatar Petroleum, started in 2007. Production started in 2011, with full production capacity of 140 000 barrel/day being reached in 2012. Much of Shell's experience from the Bitulu SMDS plant was used in the design of this project (Dancuart & Steynberg, 2007; Höök *et al.*, 2014).

2.1.2 Synthesis gas

The starting point for the FT process is synthesis gas generation from carbonaceous sources such as coal, biomass and natural gas reacted with air, oxygen, steam or a mixture at high temperature. When using a solid feedstock like coal or biomass to produce synthesis gas, the process is referred to as gasification. The reaction occur by the addition of the reactant (air, oxygen and/or steam) in a controlled manner to avoid the complete oxidation to carbon dioxide (Zennaro *et al.*, 2013; Höök *et al.*, 2014). In coal gasification the properties of the coal feedstock (such as carbon content, sulphur content, plasticity, etc.) is of major significance, since the synthesis gas, choice of gasifier and further processing is largely influenced by this (Höök *et al.*, 2014).

Several types of gasifiers have been developed over the years and can be grouped into four major technologies: fixed bed, fluidised bed, entrained flow and indirect gasifiers. The fixed bed gasifier is the oldest technology, with its main advantage lying

in its simple design. Its disadvantages lie in the production of a low heating value syngas and high tar yields. Fluidised bed gasifiers have seen extensive use. The bed is fluidised by the reactant gas (oxygen, air, steam, or a mixture), achieving a more even temperature distribution and higher quality syngas. Entrained flow gasifiers use a gas-, powder- or slurry fuel mixed with a high temperature steam/oxygen stream at pressures above 20 bar. The process requires significant preparation of the carbon fuel source, but produces an almost tar-free synthesis gas. In addition, the high heat production is undesirable and must therefore be utilised for power generation if reasonable process efficiency is to be achieved. Indirect gasifiers are two stage systems consisting of two reactors: a gasifier and a combustor, both of which are circulating fluidised beds. The bed material is removed from the gas in cyclones and exchanged between the reactors. Residual char from the gasifier is burned in the combustor, thus heating the bed material and upon re-entering the gasifier provides the necessary heat for gasification (Zennaro *et al.*, 2013).

Due to it being more homogeneous, natural gas as feedstock has a less significant influence on processing and potentially presents fewer issues when compared to coal (Höök *et al.*, 2014). When the synthesis gas generation step uses natural gas as raw feedstock, the process is referred to as reforming. Different options for natural gas reforming exist, e.g. Steam Methane Reforming (SMR), Autothermal Reforming (ATR), Catalytic Partial Oxidation (CPO) and Heat Exchange Reforming (HER) to name a few (Zennaro *et al.*, 2013). The preferred technology is autothermal reforming since it offers a better H_2/CO ratio for FTS (Höök *et al.*, 2014). In autothermal reforming a mixture of steam, methane and oxygen is fed over a Ni-based catalyst. The heat required for the endothermic steam reforming reaction and water gas shift reaction (Equations 2.8 and 2.3) is provided by the exothermic oxidation reactions in Equations 2.6 and 2.7 (Zennaro *et al.*, 2013).

$$CH_4 + 2O_2 \rightarrow CO_2 + 2H_2O \quad (2.6)$$

$$CH_4 + \tfrac{1}{2}O_2 \rightarrow CO + 2H_2 \quad (2.7)$$

$$CH_4 + H_2O \rightarrow CO + 3H_2 \quad (2.8)$$

ATR is an adiabatic process and produces syngas with a H_2/CO ratio of close to 2:1. The process requires excess steam to prevent soot formation, but much less than for steam reforming alone. In spite of the additional cost required for a cryogenic oxygen plant,

ATR is generally more economical than conventional steam reforming (Zennaro *et al.*, 2013).

2.1.3 Modes of Operation of the Fischer Tropsch Process

The commercial Fischer-Tropsch process can be subdivided into two processes: Low Temperature Fischer-Tropsch (LTFT) and High Temperature Fischer-Tropsch (HTFT). The low temperature process is typically operated at relatively low temperatures of 200 – 250 °C (Dancuart & Steynberg, 2007; Subiranas, 2008; Maitlis, 2013; Kaiser, 2014) and pressures of 10 – 45 bar (Jager, 2003). LTFT typically targets the production of higher molecular weight hydrocarbons (diesel and linear waxes) (Dry, 2004; Thomas & Thomas, 2015). Chain growth probabilities of as high as 0.92 – 0.95 on cobalt or iron catalysts have been reported for LTFT processes (Claeys & Van Steen, 2004).

The high temperature process operates at relatively high temperatures and a medium pressure of 300 – 350 °C (Dancuart & Steynberg, 2007; Subiranas, 2008; Wood *et al.*, 2012; Kaiser, 2014) and 25 bar (Jager, 2003; Wood *et al.*, 2012), respectively. Chain growth probabilities for the HTFT process is typically in the range of 0.65 – 0.7, which is low enough to minimise the formation of liquid products at reaction conditions (Claeys & Van Steen, 2004). This is a process requirement to prevent catalyst agglomeration and loss of fluidisation in the fluidised bed reactors (Steynberg & Dry, 2004). The target of HTFT is the production of low carbon number alkenes and gasoline range hydrocarbons (Subiranas, 2008; Thomas & Thomas, 2015).

2.1.4 The Fischer-Tropsch Product Distribution

As a general approximation, the amount of product in an individual carbon number fraction will decline exponentially with carbon number (Claeys & Van Steen, 2004). Some of the early researchers, such as Herington (1946), noticed this behaviour as being indicative of a polymerisation reaction proceeding via stepwise C_1-monomer addition (Claeys & Van Steen, 2004). The simplest case of such polymerisation reaction will be briefly discussed.

The FTS reaction is regarded as a polymerisation reaction where the chain initiating species as well as the monomeric building blocks are produced in situ. For illustration of

the basic principle the simplest form the growth scheme will be considered: i.e. the assumption of the formation of a single product type. After the formation of a surface species with one carbon atom, two possibilities exist: Desorption (termination) to form a product species containing one carbon atom, or monomer addition (chain growth) will occur to produce a surface species with two carbon atoms. Each consecutive surface species will face the same two possibilities of desorption to form a product species or growth through monomer addition to form a new surface species. This process is presented graphically in Figure 2.1.

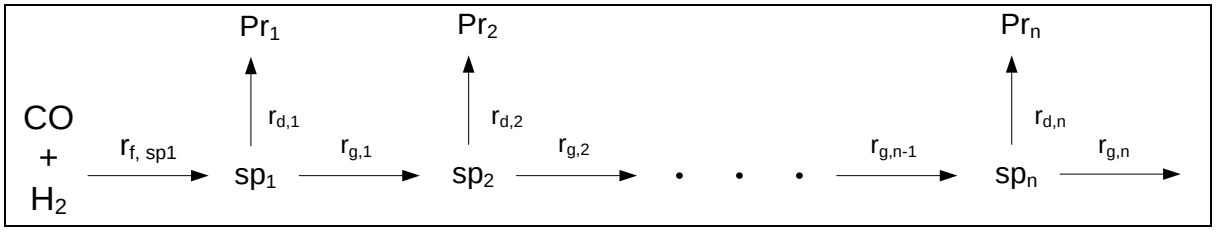

Figure 2.1: Simplified ideal growth scheme assuming single product type [Reproduced from Claeys & Van Steen (2004)] (f = formation, d = desorption, g = growth, Pr = product species, sp = surface species)

For any surface species containing n carbon atoms (sp_n), the probability of chain growth (often expressed as α_n) is the ratio between the rate of chain growth and the sum of the rates of chain growth and –desorption.

$$\alpha_n = p_{g,n} = \frac{r_{g,n}}{r_{g,n} + r_{d,n}} \tag{2.9}$$

Conversely the probability of the surface species being desorbed instead of experiencing chain growth is defined as in Equation 2.10:

$$p_{d,n} = 1 - p_{g,n} = 1 - \frac{r_{g,n}}{r_{g,n} + r_{d,n}} = \frac{r_{d,n}}{r_{g,n} + r_{d,n}} \tag{2.10}$$

Since product formation occurs via desorption of a surface species, the rate of formation of a product species with n carbon atoms (Pr_n) is equal to the rate of desorption of the surface species with n carbon atoms:

$$r_{Pr_n} = r_{d,n} \tag{2.11}$$

Mathematical manipulation of Equation 2.11 yields Equation 2.12:

$$r_{Pr_n} = r_{d,n} \frac{(r_{g,n} + r_{d,n})}{(r_{g,n} + r_{d,n})} \tag{2.12}$$

Substitution of Equation 2.10 into Equation 2.12 yields Equation 2.13:

$$r_{Pr_n} = p_{d,n}\left(r_{g,n} + r_{d,n}\right) \tag{2.13}$$

At steady state, the net rate of formation of surface species sp_n will equal zero, since the rate at which sp_n forms through chain growth (via monomer addition to sp_{n-1}) is equal to the rate at which sp_n is consumed through chain growth and desorption, to form sp_{n+1} and Pr_n, respectively (Claeys & Van Steen, 2004).

$$r_{g,n-1} = r_{g,n} + r_{d,n} \tag{2.14}$$

Substituting Equation 2.14 into Equation 2.13 yields Equation 2.15. By similar manipulation and substitution as was done in Equations 2.12 and 2.13, one arrives at Equation 2.16.

$$r_{Pr_n} = p_{d,n} r_{g,n-1} \tag{2.15}$$

$$r_{Pr_n} = p_{d,n} r_{g,n-1} \frac{\left(r_{g,n-1} + r_{d,n-1}\right)}{\left(r_{g,n-1} + r_{d,n-1}\right)} = p_{d,n} p_{g,n-1}\left(r_{g,n-1} + r_{d,n-1}\right) = p_{d,n} p_{g,n-1} r_{g,n-2} \tag{2.16}$$

Finally,

$$r_{Pr_n} = p_{d,n} p_{g,n-1} p_{g,n-2} \cdots p_{g,1} r_{f,sp_1} \tag{2.17}$$

Since all compounds must contain one carbon atom originating from the initiating surface species sp_1, the rate of formation of surface species sp_1 can be determined as the sum of the rates of formation of all product species (Claeys & Van Steen, 2004).

$$r_{f,sp_1} = \sum_{n=0}^{n=\infty} r_{Pr_n} \tag{2.18}$$

The molar fraction of a product species, Pr_n, within the product spectrum can be written as:

$$x_n = \frac{r_{Pr_n}}{\sum_{n=0}^{n=\infty} r_{Pr_n}} = \frac{p_{d,n} p_{g,n-1} p_{g,n-2} \cdots p_{g,1} r_{f,sp_1}}{r_{f,sp_1}} = p_{d,n} p_{g,n-1} p_{g,n-2} \cdots p_{g,1} \tag{2.19}$$

A special, simplified, case can be derived when the probability of chain growth is assumed independent of carbon number. Thus $\alpha_n = p_{g,n} = \alpha$, so that:

$$x_n = p_{d,n} p_{g,n-1} p_{g,n-2} \cdots p_{g,1} = p_d p_g^{n-1} \tag{2.20}$$

$$x_n = p_d p_g^{n-1} = \left(1 - p_g\right) p_g^{n-1} = (1-\alpha)\alpha^{n-1} \tag{2.21}$$

This equation was first developed by Schulz (1935) and Flory (1936) to describe homogeneous polymerisation. Anderson *et al.* (1951) developed a similar equation from the perspective of stepwise monomer addition (Biel, 2004).

A semi-logarithmic plot of this equation versus carbon number (as in Figure 2.2) yields a straight line, with the slope equal to the logarithm of the chain growth probability. These plots are commonly referred to as the Anderson-Schulz-Flory (ASF) distribution in literature.

The expression can be rewritten in terms of weight fraction, as follows (Van der Laan, 1999; Maitlis, 2013):

$$\frac{w_n}{n} = (1-\alpha)^2\alpha^{n-1} \qquad (2.22)$$

Making a semi-logarithmic plot of w_n/n versus carbon number yields a similar straight line ASF plot (similar to Figure 2.2).

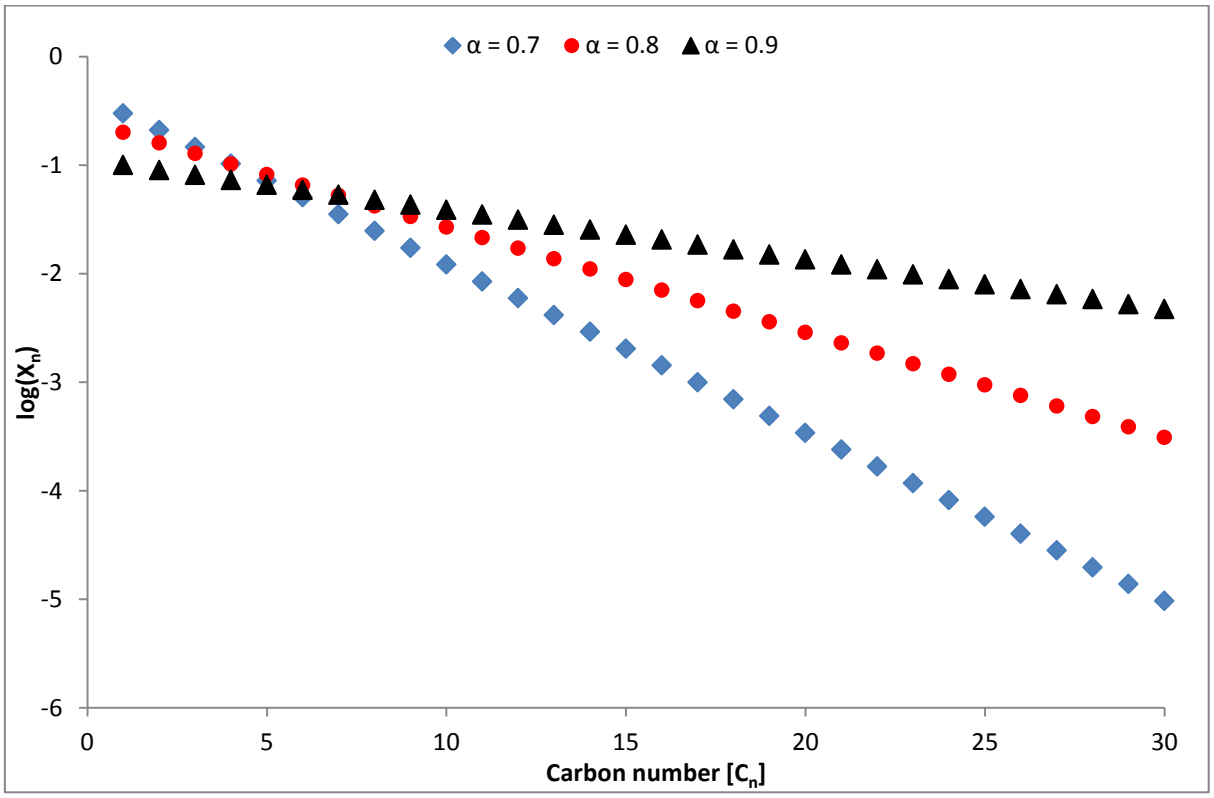

Figure 2.2: Ideal molar product distributions following ASF kinetics with carbon number independent chain growth probability (calculated using Eq. 2.21)

2.1.4.1 Real product distributions (Deviations from ASF)

The ideal ASF distribution (with a single product type) serves as a good approximation to describe product selectivity trends. However, because these kinetics are not observed, with more than one type of product being formed, a predictive model would have to account for the observed deviations. In an attempt to account for this, selectivity models have been developed by a number of authors, including Zimmerman *et al.* (1992), Iglesia *et al.* (1993), Van der Laan & Beenackers (1999) and Visconti *et al.* (2007), for the prediction of FT product selectivities utilising different catalysts and reaction conditions.

The four most commonly observed deviations from ideal ASF behaviour are (Van der Laan & Beenackers, 1999; Claeys & Van Steen, 2004):

- Molar CH_4 content is higher than predicted by ASF
- The molar C_2 content is lower than predicted/expected
- The chain growth probability (α) shows an increase with increasing carbon number
- An exponential decrease in olefin/paraffin ratio with increase in carbon number

Since the primary objective of FTS is the production of transportation fuels, CH_4 is the most undesired of the products (Yang *et al.*, 2014). This is especially true if the synthesis gas was obtained from natural gas. It is worth noting, though, that the molar CH_4 content is not of as great economic significance as the carbon based CH_4 content. A large molar fraction of CH_4 does not necessarily mean a large carbon based content of methane, since the latter is highly dependent on the chain growth probability. The exact cause for the larger than expected molar values of methane has not truly been explained. It has been proposed that excess methane is produced due to an increased termination probability of the methane precursor surface species (Wojciechowski, 1988). More recently, somewhat in line with the supposition of Riedel *et al.* (1999) that chain growth and methanation occur independently so that some active sites may favour the formation of CH_4, it has been suggested that methane may be preferentially formed at sites with a high degree of coordination, while at sites with low coordination chain growth is promoted (Schulz *et al.*, 2002).

The deviations from ideal ASF can also be explained by the occurrence of secondary reactions. Van der Laan & Beenackers (1999) pointed out that the reason most reported for the anomalous C_2 product formation is most probably the occurrence of secondary reactions: 1) ethane is incorporated into growing chains, 2) ethane is rapidly readsorbed, 3) ethane is hydrogenated to ethane, and 4) ethane undergoes hydrogenolysis. The

resultant oscillating product distribution which would result from the proposal that ethene might be used as a monomer/building block for FTS has not been observed (Glebov & Kliger, 1994). The latter three reactions would explain the decreased ethene yield and associated increased ethane and higher hydrocarbons yield (Van der Laan & Beenackers, 1999).

The increase in chain growth probability and decrease in olefin/paraffin ratio is a somewhat interrelated topic. These deviations are best and most reasonably explained by the occurrence of secondary reactions (reinsertion, hydrogenolysis, hydrogenation and isomerisation) according to Kuipers *et al.* (1995). Secondary reactions (and readsorption) are directly influenced by space velocity and is dependent on chain length. This tendency results in a decrease in the olefin/paraffin ratio as well as increase in growth probability with an increase in chain length.

2.1.4.2 The chain growth probability (α) and product selectivity

The influence of the chain growth probability on product distribution can be seen more clearly from Figure 2.3, where product weight fractions are plotted against chain growth probability assuming ideal ASF kinetics. It can also clearly be seen that ASF kinetics imposes some constraints on the theoretically achievable product selectivities. At a chain growth probability of zero only methanation takes place, while it can be seen that at low values of α methane is the preferred product. The formation of the gasoline range hydrocarbon fraction reaches a theoretical maximum of just under 40% at a chain growth probability in the range of 0.75, while at a value of around 0.88 a theoretical maximum of about 40% in diesel range hydrocarbon fraction is obtained.

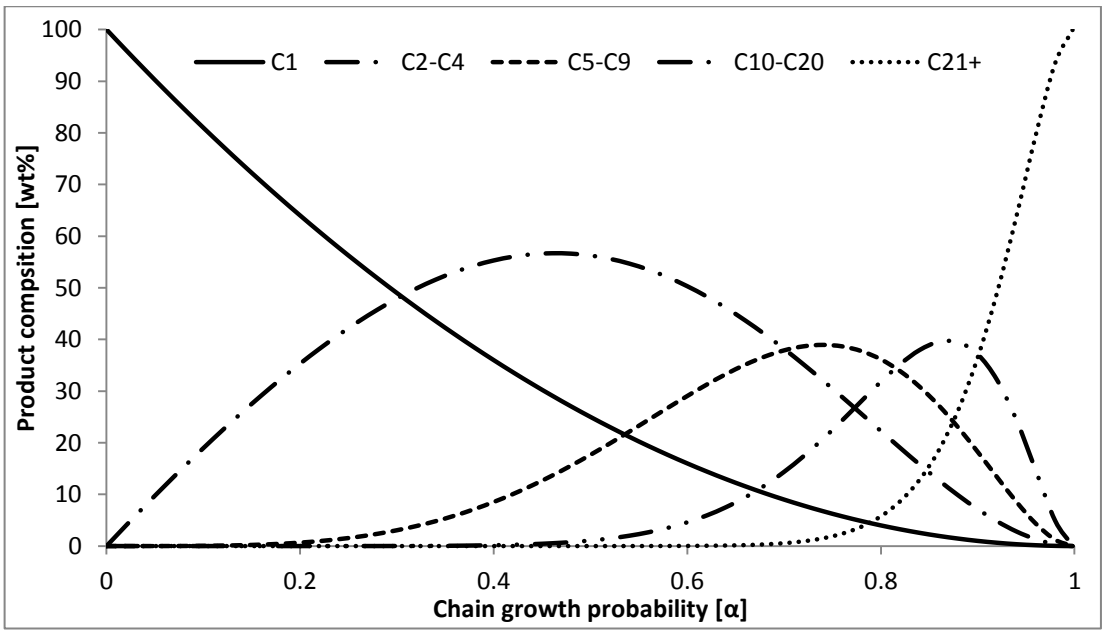

Figure 2.3: Ideal ASF product composition (wt%) as a function of chain growth probability (α) [reproduced from Claeys & Van Steen (2004)]

The FTS reaction is kinetically controlled. Thus the chain growth probability, and consequently the product distribution, depends highly on the type of catalyst employed and process variables such as temperature, pressure, H_2/CO ratio, etc. (Biel, 2004; Chonco, 2014). A summary of the effects of process parameters on product selectivities is presented in Table 2.1.

The effect of increasing reaction temperature is an increased CH_4 selectivity and a shift toward products with a lower carbon number (Dry, 1981; Dictor & Bell, 1986). Consequently lower reaction temperatures favour the formation of longer chain hydrocarbons due to an increased chain growth probability. An increase in olefin/paraffin ratio is observed with increasing temperature on K-promoted precipitated Fe-based catalysts (Anderson, 1956; Dictor & Bell, 1986), but a decreased olefin selectivity is reported when increasing reaction temperature for unalkalised iron (Dictor & Bell, 1986). Oxygenate selectivity is reported by Liu *et al.* (2007) to increase with increasing reaction temperature on Fe-Mn over a temperature range of 260 – 280 °C. Similarly, Dry (1981) notes that for an iron catalyst the oxygenate selectivity increases as operating conditions shift from that of LTFT to HTFT.

Table 2.1: Effect of process conditions on FTS product selectivity [Adapted from Van der Laan & Beenackers (1999), Cairns (2008) and Chonco (2014)]

	Parameter				
	Temperature	**Pressure**	**H_2/CO**	**Conversion**	**Space Velocity**
Methane Selectivity	↑	↓	↑	↑	↓
Olefin Selectivity	↕	↕	↓	↓	↑
Oxygenate selectivity	↓	↑	↓	↓	↑
Carbon deposition	↑	↕	↓	↑	↕
Chain Growth/ Length	↓	↑	↓	↕	↕
Chain Branching	↑	↓	↑	↕	↕

Increase with increase in parameter: ↑
Decrease with increase in parameter: ↓
No clear effect/Complex relation: ↕

When increasing total pressure, most studies report product selectivities to shift towards heavier products and more oxygenates (Dry, 1981), while an increase in H_2/CO ratio results in lighter hydrocarbons (negative impact on chain growth) and decreases olefin selectivity (Dictor & Bell, 1986; Donnelly & Satterfield, 1989). High CO partial pressure is said to promote chain growth as the catalyst coverage of adsorbed monomers is high, whereas lower CO partial pressure results in lower surface coverage and increased probability of desorption (Grobler, 2008).

Increasing space velocity (decreasing residence time), in addition to decreasing conversion, has been found to increase the olefin/paraffin ratio (Bukur *et al.*, 1990; Iglesia *et al.*, 1991; Kuipers *et al.*, 1996). On a commercial iron catalyst Bukur *et al.* (1990) found no correlation between the product's molecular weight distribution of hydrocarbons and space velocity, while on ruthenium Iglesia *et al.* (1991) reported an increasing average molecular weight of the products with decreasing space velocity. On Co/TiO_2 Iglesia *et al.* (1993) observed increased CO-conversion and C_{5+} selectivity, as well as decreasing methane selectivity, with decreasing space velocity. Over Fe-Mn, (Liu

et al., 2007) reported an increase rate of oxygenate formation upon increasing space velocity, but upon further increase this decreased to some extent.

2.1.5 Fischer-Tropsch Reaction Mechanisms

The common consensus is that the Fischer-Tropsch Synthesis forms its products through surface polymerisation reaction, characterised by key steps: adsorption of the reactants to the catalyst surface, the subsequent (in situ) generation of a chain initiator species as well as monomer species, chain growth by addition of the monomer species, desorption of products from the catalyst surface, and reactive products re-adsorbed for further reaction (Chonco, 2014). A number of possible reaction pathways have been proposed for the FTS reaction over the years, all of which share the common theme of initiation, propagation and termination, referring to the formation of a chain starting species, chain growth by the in situ produced monomer addition and product desorption from the catalyst surface, respectively (Claeys & Van Steen, 2004).

For a mechanistic model to be acceptable it is expected to account for all of the aspects of FTS product spectrum (Dry, 1996). These include:

- FT products are predominantly linear, with aromatics formed at higher temperatures only,
- high olefin content and lower than thermodynamically predicted paraffin to olefin ratio,
- the olefin content consists of mainly α-olefins,
- there is a large amount of mono-methyl branching and a decrease in degree of branching with increasing chain length.

With a vast possible product spectrum and some unique aspects such as the abovementioned, the exact chemical identity of the monomeric building block and method of chain propagation on the catalyst surface remains elusive and a controversial subject (Van Dijk, 2001). The four most popular of the proposed mechanisms are the *alkyl, alkenyl, enol* and the *CO-insertion* mechanisms (Dry, 1981; Claeys & Van Steen, 2004). It is worth noting that due to the FT reaction's complexity, it is in general accepted by many that more than one mechanism may be operating on the surface of the catalyst at any given time (Claeys & Van Steen, 2004).

2.1.5.1 The Alkyl Mechanism

Currently this mechanism seems to be the most widely accepted for chain growth (Claeys & Van Steen, 2004) and was developed from the carbide theory for chain growth, which was first suggested by Fischer and Tropsch in 1926 (Dictor & Bell, 1986; Shroff *et al.*, 1995; Claeys & Van Steen, 2004). In this earlier mechanism proposed the reaction to proceed via metal carbide formation, where carbon in the carbide phase is hydrogenated to CH_2-species which would then polymerise. It has been subsequently shown that only iron forms stable carbides under FTS conditions and that the carbon content of products originating from metal carbides is very small, leading to the rejection of this mechanism (Claeys & Van Steen, 2004). In the alkyl mechanism, chain initiation is proposed to occur via the dissociative adsorption of CO on the catalyst surface. Surface oxygen is removed by reaction with adsorbed hydrogen or -carbon monoxide to result in either water or carbon dioxide, respectively. The adsorbed surface carbon species is then sequentially hydrogenated to CH, CH_2 and CH_3. The methyl species (CH_3) is regarded as the chain initiator and the surface methylene species (CH_2) is proposed as the monomer responsible for propagation of the chain. Primary products are desorbed by hydrogen elimination or –addition to yield α-olefins or n-paraffins, respectively (Claeys & Van Steen, 2004; De Smit & Weckhuysen, 2008). The formation of oxygenates is inexplicable by means of the alkyl mechanism, however it has been suggested by Johnson *et al.* (1991) to be possible via OH-group coupling with an alkyl group (Van Steen & Claeys, 2008). A schematic representation of the alkyl mechanism follows in Figure 2.4.

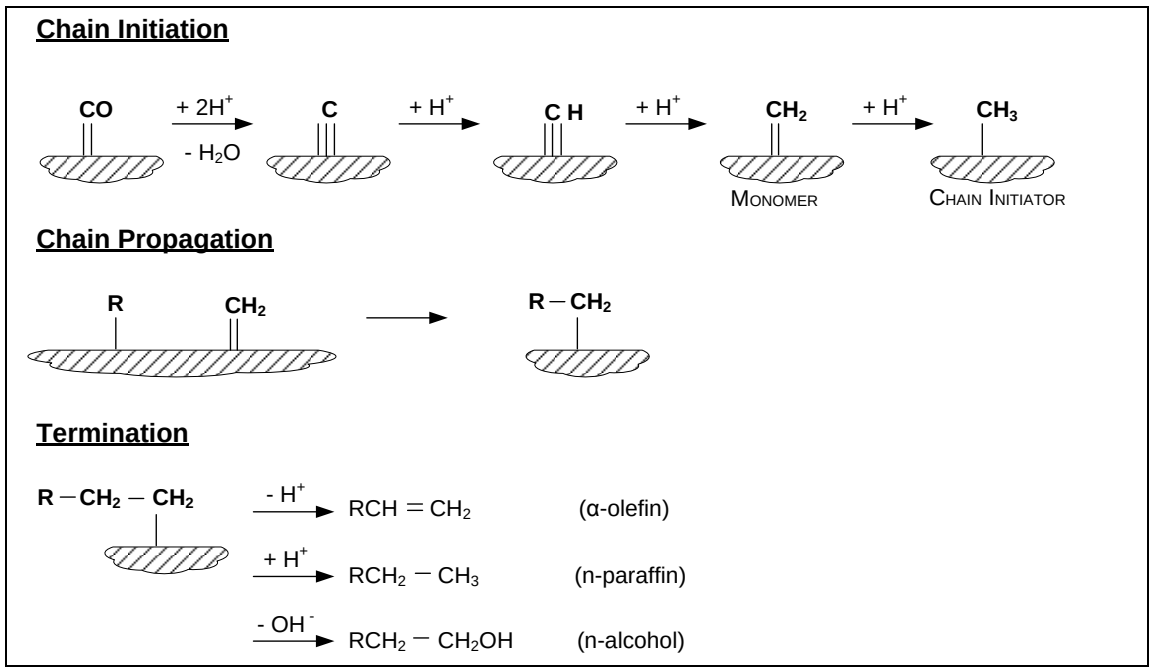

Figure 2.4: The alkyl mechanism (Claeys & Van Steen, 2004)

2.1.5.2 Alkenyl Mechanism

In the alkenyl mechanism, monomer formation is identical to that of the alkyl mechanism. A surface carbon species undergoes subsequent hydrogenation to methylene. The chain initiator is a surface vinyl species which is formed by the combination of a surface methylene species (CH_2) and a surface methylidyne species (CH). Propagation takes place via stepwise addition of the methylene species to the vinyl species which yields a surface allyl species, and after isomerisation yields a surface alkenyl species. Termination produces α-olefins as primary products upon desorption after hydrogen addition. This mechanism, proposed by Maitlis and co-workers (1996), does, however, not explain the formation of n-paraffins or –alcohols (Claeys & Van Steen, 2004). A schematic representation of the mechanism follows in Figure 2.5.

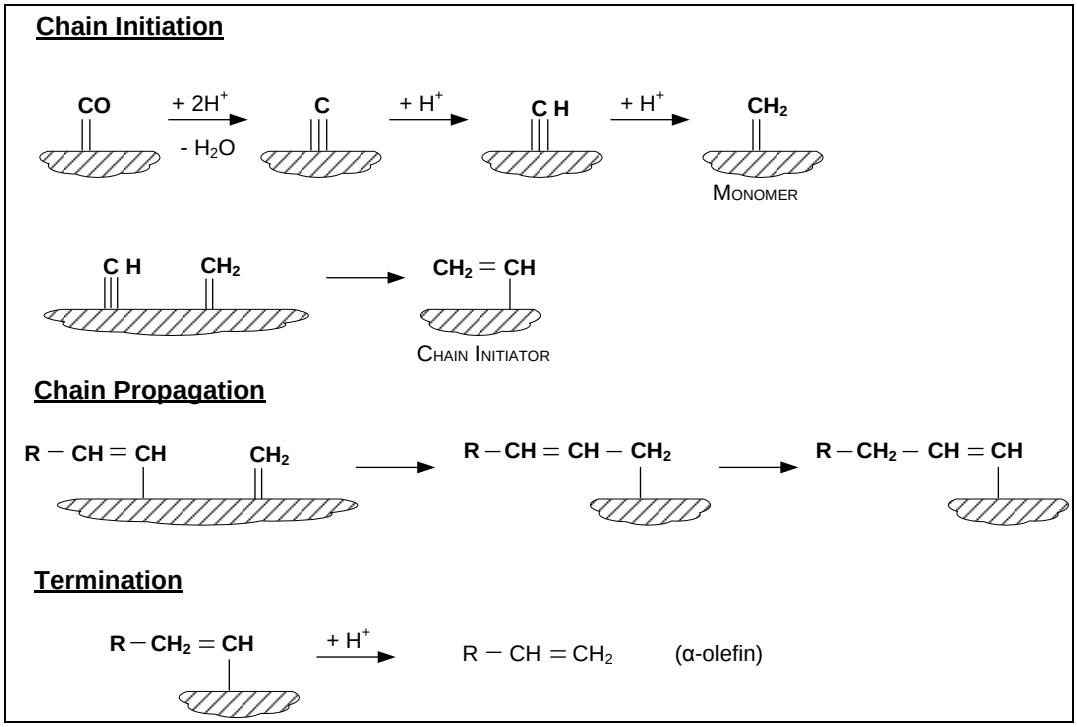

Figure 2.5: The alkenyl mechanism (Claeys & Van Steen, 2004)

2.1.5.3 Enol Mechanism

A mechanism proposed by Storch *et al.* (1951) proposes a surface enol species (M=CHOH), formed by the hydrogenation of adsorbed carbon monoxide, as chain initiator. Propagation occurs via the condensation reaction of two surface enol species and the removal of water. Termination yields oxygenates or α-olefins as primary products. This mechanism does not explain the primary formation of n-paraffins, but is

described as a secondary reaction by the hydrogenation of the primarily formed olefins (Claeys & Van Steen, 2004; De Smit & Weckhuysen, 2008). A schematic representation follows in Figure 2.6:

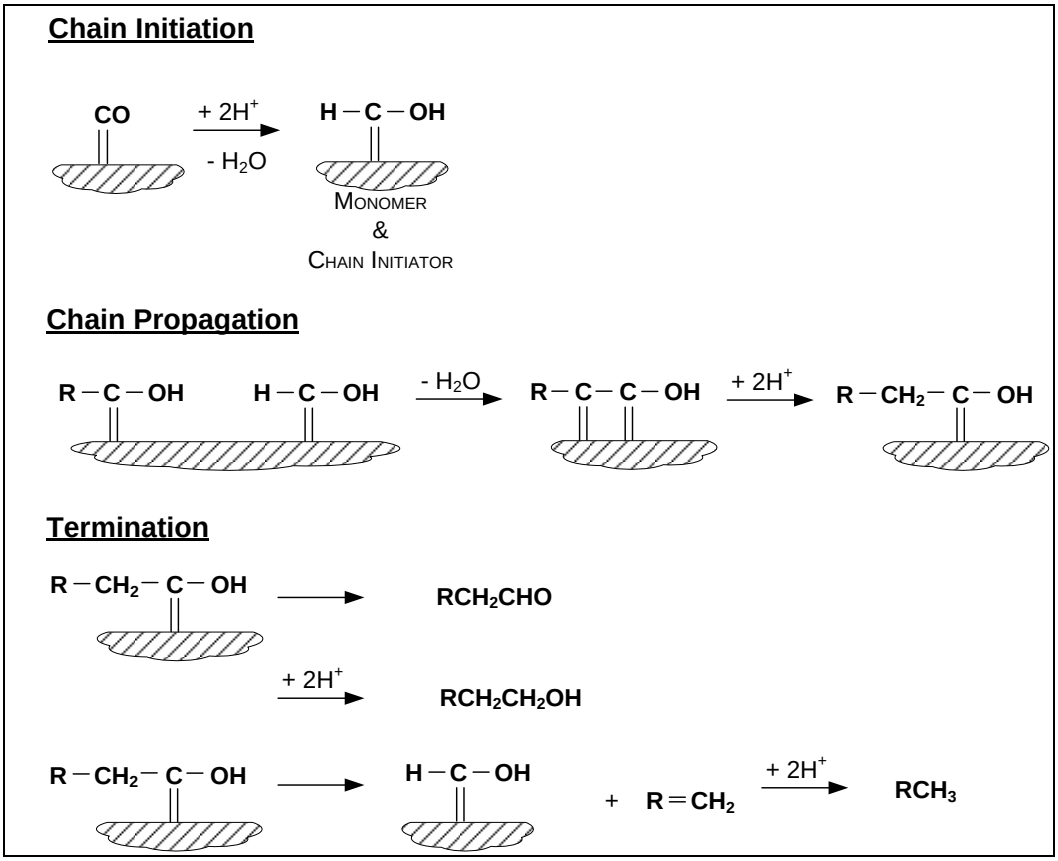

Figure 2.6: The enol mechanism (Claeys & Van Steen, 2004)

2.1.5.4 CO-insertion Mechanism

This is believed to be the main reaction pathway for the formation of oxygenates (Anderson & Ekerdt, 1985; Dry, 1990). Originally formulated by Sternberg & Wender (1959) and Roginski (1965) (Claeys & Van Steen, 2004), with additional refinement by Pichler and Schulz (1970), this mechanism assumes CO as the monomer and a surface methyl species as the chain initiator. The formation of the methyl species differs from the alkyl mechanism in that oxygen is eliminated from the surface species. Chain growth occurs by the insertion of CO into the metal-alkyl bond to form an acyl surface species. Hydrogenation eliminates oxygen (producing water) and produces an alkyl species. Termination or desorption can occur via the same path as proposed in the alkyl mechanism to yield n-paraffins or α-olefins as primary products, while termination of the oxygen containing species would yield aldehydes and alcohols as primary products

(Claeys & Van Steen, 2004; De Smit & Weckhuysen, 2008). Figure 2.7 illustrates the initiation and propagation steps of the CO-insertion mechanism:

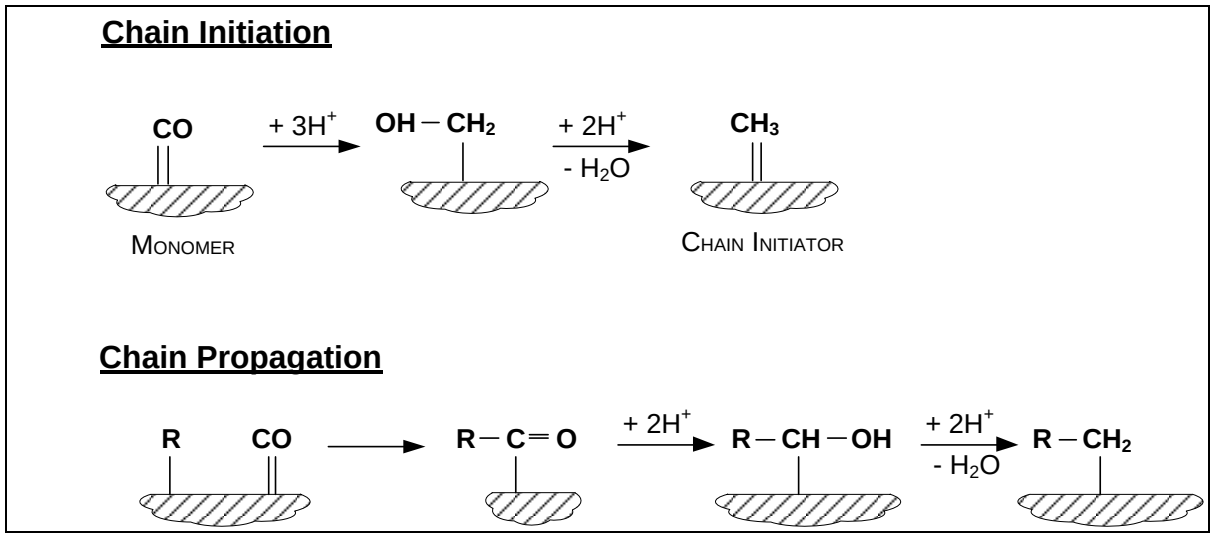

Figure 2.7: The CO-insertion mechanism (Claeys & Van Steen, 2004)

2.2 Fischer-Tropsch Reactors

There are four types of FT reactors in commercial use: circulating fluidised bed, fluidised bed, tubular fixed bed and slurry phase reactors (Steynberg & Dry, 2004). Two phase fluidised bed reactors are used for HTFT applications, while the fixed bed and slurry phase reactor operate under LTFT conditions (Steynberg & Dry, 2004). The key distinguishing feature between these is that the HTFT reactors do not have a liquid phase present outside the catalyst particles, since the presence of a liquid phase would lead to agglomeration and loss of fluidisation (Steynberg & Dry, 2004; Steynberg & Nel, 2004).

2.2.1 Low Temperature Fischer-Tropsch Reactors

LTFT reactors may employ either precipitated Fe catalysts or supported Co catalysts, with the choice of either being a function of various parameters. Heavy hydrocarbons are produced and are present in the form of liquid wax (Steynberg & Dry, 2004). Industrial LTFT technology was pioneered in Germany. Early reactors were tube cooled fixed bed reactors, originally employing a kieselguhr-supported cobalt catalyst and operating at 1 atm. Development of the German medium pressure synthesis utilised the same catalyst at higher pressure of 1 MPa, increasing productivity and extending

catalyst life, but used a tube-in-tube design for the fixed bed reactor. Post-WW2 a more practical approach was the use of multi-tubular fixed bed reactors. Though slurry bed reactors were also investigated during the 1930's and 1950's its commercial application was not possible until refinement by Sasol (De Klerk *et al.*, 2013).

2.2.1.1 Fixed Bed Reactors

Fixed bed reactors for the middle pressure synthesis used a tube-in-tube design to achieve the required heat transfer rates. However, this design was mechanically complicated (De Klerk *et al.*, 2013). Thus the preferred fixed bed reactor is a multi-tubular fixed bed reactor with the catalyst inside the tubes, with cooling on the shell side (Steynberg & Dry, 2004). This design, resembling a vertical shell and tube heat exchanger, is more practical and achieves the same goal. The robustness of this design is evidenced by Sasol's original ARGE reactors, commissioned in 1955, still being in operation (De Klerk *et al.*, 2013).

Feed gas enters from the top and leaves at the bottom of the reactor, which aids the removal of liquid wax from the reactor tubes. Heat transfer is optimised by high linear gas velocities (ensuring turbulent flow) and the use of narrow tubes (short distance between catalyst particles and tube walls). The more active the catalyst, the narrower the tubes should be to ensure minimal radial temperature gradients (Steynberg & Dry, 2004).

Though maximum average temperature is required for maximum conversion, due to axial and radial temperature gradients this is limited to the maximum allowable temperature peak. Temperatures higher than this will lead to excessive carbon formation, leading to catalyst break-up and, in turn, blockages (Jager & Espinoza, 1995). After the liquid wax, oils and water knock-out, a portion of tail gas is recycled, increasing the percentage conversion (on fresh feed basis) as well as increasing linear gas velocity to aid in improvement of the heat transfer rate (Steynberg & Dry, 2004).

Fixed bed reactors are easy to operate, requiring no additional separation equipment for catalyst-wax separation since the liquid wax simply trickles down the catalyst and is then collected downstream in a knockout pot. One of the greatest advantages to the multi-tubular fixed bed is that large scale commercial reactor performance can be relatively easily predicted based on single tube pilot unit performance (Jager & Espinoza, 1995; Steynberg & Dry, 2004; De Klerk *et al.*, 2013).

If slippage of catalyst poisons through syngas purification sections occurs, only the top portion of the catalyst will be deactivated (leaving the rest of the bed intact), while with slurry phase reactors all of the catalyst will be affected (Jager & Espinoza, 1995; Steynberg & Dry, 2004; De Klerk *et al.*, 2013). One of the downsides to such reactors, especially when using iron catalysts, is the requirement for periodic replacement of the catalyst, making the reactor maintenance and labour intensive (Jager & Espinoza, 1995; De Klerk *et al.*, 2013). In addition this, product selectivity also changes with time on stream. Large pressure drops over the reactor coupled with high recycle needs translates to considerable recompression costs (Jager & Espinoza, 1995).

Multi-tubular reactors are normally unsuited to high temperature operation and because they can consist of thousands of tubes, construction costs are high. Because such reactors are heavy, this limits scale up since transportation can become a limiting factor (Steynberg & Dry, 2004).

The five multi-tubular ARGE reactors that were installed in the 1950's, jointly designed by Ruhrchemie and Lurgi, are still in operation at Sasol. These utilise extruded Fe-based catalysts, operate at 2.7 MPa and 230 °C and have a production capacity of 500 barrel/day, each (Steynberg & Dry, 2004; Spivey *et al.*, 2015). Shell's Bitulu plant in Malaysia uses four Lurgi designed multi-tubular reactors with wider overall diameters than the Sasol units. High activity cobalt catalysts are employed and thus the tube diameters are smaller than those in the Sasol reactors to achieve higher heat exchange rates for temperature control. The Shell reactors ran at an original capacity of 3000 barrel/day per reactor, but with new generation higher activity catalysts this has been increased to 8000 barrel.day (Steynberg & Dry, 2004).

In summary, despite apparent drawbacks of multi-tubular fixed bed reactors (temperature control, construction cost, significant bed pressure drop, transport limitations in large catalyst particles and labour intensive catalyst replacement), they remain the dominant LTFT reactor technology due to the following advantages (Steynberg & Dry, 2004; De Klerk *et al.*, 2013):

- Robust operation, demonstrated by many decades of industrial operation
- A certain level of poisoning resistance (to contaminants like H_2S), since the top layer of catalyst is affected and acts a guard bed to the rest of the catalyst bed
- No requirement for catalyst-wax separation equipment
- Straightforward scale-up
- Catalysts do not require appreciable attrition resistance

2.2.1.2 Slurry Phase Reactors

The slurry bed reactor was developed for wax production in low temperature FT applications, with the liquid wax being the medium in which the catalyst is suspended (Steynberg & Dry, 2004). During the 1950's and 1960's various sizes of slurry bed reactor were tested in Germany, England and the USA. However, the space velocities used were very low which made judging performance at likely commercial space velocities impossible. Additionally, a practical and efficient means of separating the catalyst from the product was an integral step that was not successfully developed until much later, with a suitable system being demonstrated in 1990 by Sasol (Steynberg & Dry, 2004; De Klerk *et al.*, 2013).

Typically under same operating conditions slurry reactors produce heavier products than fixed bed reactors (Jager & Espinoza, 1995). In the late 1970's Sasol decided to revisit and evaluate the slurry system on pilot plant scale (Steynberg & Dry, 2004). The fixed bed and slurry bed systems were compared for wax production at the temperatures normally used in the fixed bed units and utilising the same precipitated iron catalyst used in the commercial multi-tubular reactors (with the only difference being the size of the catalyst particles). Hard wax selectivity and the percentage (H_2 + CO) conversion obtained in the slurry phase reactor were as good, if not better, than those obtained in the fixed bed unit, despite the three-fold lower catalyst loading in the slurry phase reactor. The higher activity per mass of catalyst was ascribed to the much smaller particle size used in the slurry phase system. With the rate of the FT reaction being pore diffusion limited even at low temperatures this results in a higher observed activity for a smaller catalyst particle (Steynberg & Dry, 2004; De Klerk *et al.*, 2013).

The slurry reactor system and the two phase (gas-catalyst) reactor systems at higher temperatures, normally used for the production of gasoline, were also compared using the same fused catalyst used in the HTFT reactors. High temperature slurry phase operation was deemed impractical as at the reaction temperature of 324 °C the wax inside the reactor was continuously being hydrocracked, requiring the daily addition of wax. Also, although the slurry bed gave the same product selectivities, the percentage (CO + CO_2) conversion was considerably lower than that obtained in the two-phase fluidised bed unit. This was mainly because the slurry system did not have the advantage of a smaller catalyst particle size compensating for the lower catalyst loading (Steynberg & Dry, 2004).

Though the low temperature slurry system was very promising, further development was somewhat delayed because of the problem of satisfactory wax-catalyst-

separation. An efficient separation device was successfully tested in 1990 in a 1m ID demonstration unit, after which a commercial unit was brought on-line in 1993. The capacity of this reactor (22m high, 5m ID) is about 2500 barrel/day (10 million tonnes per year); equal to the total production capacity of five 3m diameter multi-tubular fixed bed ARGE reactors. Slurry bed reactors with a capacity of at least 20 000 barrel/day (85 million tonnes per year) are feasible (Jager & Espinoza, 1995; Steynberg & Dry, 2004; De Klerk *et al.*, 2013).

For Fe catalysts, the advantages of the slurry phase reactor over multi-tubular fixed bed reactors are (Jager & Espinoza, 1995; Steynberg & Dry, 2004; De Klerk *et al.*, 2013):

- The reactor train cost is 25% of the same capacity multi-tubular reactor system
- Catalyst consumption per ton product is 4 times lower than in fixed bed units due to lower catalyst loadings in slurry reactors
- Gas compression cost is decreased since typical pressure drops over slurry reactors are 0.1 MPa vs. 0.4 MPa for multi-tubular units
- Higher average temperature operation and resultantly improved reactant conversion is possible due to the slurry bed being more isothermal
- Higher average conversions and longer reactor runs are possible with online addition and removal of catalyst

2.2.2 High Temperature Fischer-Tropsch Reactors

Neither slurry bed reactors, nor fixed bed reactors are suited to HTFT operation for producing lighter FT products. Instead two-phase fluidised bed reactors are utilised: Turbulent or fixed fluidised bed (FFB) and circulating fluidised bed (CFB) reactors. The turbulent reactors are known as Sasol Advanced Synthol (SAS) reactors, named after its developer (Steynberg & Dry, 2004).

A high degree of turbulence means that fluidised beds exhibit very high heat exchange rates. They can therefore cope with large amounts of reaction heat at high conversions and high feed gas throughputs achievable at high operating temperature. The reactors are very isothermal and a temperature difference between the top and bottom of the reactor is only a few degrees (Steynberg & Dry, 2004). Development of HTFT technology had its origins in the USA. The technology was, however, perfected by Sasol in South Africa (Steynberg & Dry, 2004; De Klerk *et al.*, 2013). Two-phase HTFT reactors require process conditions to be such that selectivity to long chain hydrocarbons is limited to

prevent excessive condensation in catalyst pores as well as agglomeration due to surface wetting so that loss of fluidisation does not occur (Steynberg & Dry, 2004).

2.2.2.1 Circulating Fluidised Bed (CFB) Reactor

Sasol's fluidised bed reactors for the original Sasolburg plant were the CFB reactors developed by Kellogg (Steynberg & Dry, 2004; De Klerk *et al.*, 2013; Spivey *et al.*, 2015). The linear gas velocities in CFB's are 3-4 times higher than turbulent fluidised beds. Several design- and catalyst formulation changes were made, which resulted in satisfactory performance of the reactors. These were renamed Synthol reactors and served Sasol for 30 years (Steynberg & Dry, 2004).

Aerated catalyst flows down a standpipe, with the rate being controlled by a slide valve. Catalyst is swept up the reaction section by feed gas preheated to 200 °C. Around 40% of the reaction heat is absorbed by the heat exchangers and the rest by the feed gas and products. The catalyst and gas disengages in a wide settling hopper. Aerated catalyst drops down into the standpipe and entrained catalyst fines is removed in the cyclones and returned to the standpipe. Remaining fines are removed by heavy oil scrubbers downstream of the reactor (Steynberg & Dry, 2004; De Klerk *et al.*, 2013). A high catalyst loading is required in the reaction zone for a high conversion. However, the loading cannot be so high that the pressure drop over the reaction zone exceeds the pressure drop over the standpipe. If this happens gas will flow up the standpipe, choking the cyclones and resulting in massive losses of catalyst. Also no heat exchange will take place in the standpipe, resulting in catalyst damage due to temperature runaway (Steynberg & Dry, 2004).

Significant amounts of carbon are deposited on the iron catalyst operating at 340 °C. This causes particle disintegration, increased fines loss through the cyclones as well as a loss of density of the catalyst particles. Lighter particles are transported more rapidly, less catalyst back mixing occurs and reaction zone catalyst loading decreases, which results in a decrease in conversion rate with time on stream. Online catalyst removal and addition is an adopted practice that attempts to resolve this problem (Steynberg & Dry, 2004; Spivey *et al.*, 2015).

Second generation CFB's were installed in the Secunda and Mossel Bay plants. These were larger and operated at 2.5 MPa instead of 2.0 MPa to increase capacity threefold. The reactors had improved heat exchangers and standpipe slide valves. However, the only CFB reactors currently operating are the Mossel Bay CFB's since by 1999 the

Secunda reactors had been replaced by higher capacity Sasol Advanced Synthol (SAS) reactors (Steynberg & Dry, 2004; Spivey *et al.*, 2015).

2.2.2.2 Sasol Advanced Synthol (SAS) Reactors

In the late 1970's Sasol further investigated the potential of Fixed Fluidised Bed (FFB) reactors, as the R&D pilot units, used for improved catalyst development and the study of process variables, were performing very well and easy to operate. After much development a demonstration reactor was built, coming online in 1984. Using the same catalyst and process conditions as the CFB reactors, higher conversions were obtained with similar product selectivities. A commercial unit came on stream in 1989, performing as expected. The 16 second generation CFB's at the Secunda plant were replaced by 8 SAS reactors between 1995 and 1999, which increased the plant's capacity by 2 x 10^6 tons per year (Steynberg & Dry, 2004; Spivey *et al.*, 2015).

Gas enters the bottom of the reactor, passing through a grid plate (or gas distributor) fluidising the catalyst bed, which operates in the turbulent fluidisation regime. The gas distributes the gas evenly throughout the catalyst bed to prevent preferential flow patterns and stagnant regions. It has an additional function, acting as a support for the catalyst bed during slumps when there is no gas flow. The Fischer-Tropsch and side reactions occurring in the reactor are highly exothermic, requiring cooling coils to remove heat by generating steam in the coils. This, together with rapid mixing in the fluidised bed, results in isothermal conditions. The product gas leaves the bed, entraining some catalyst particles carrying some catalyst particles. Before leaving the reactor, the gas passes through cyclones to separate the entrained solids from the gas. The solids collected in the cyclones are then returned to the reactor via diplegs (Steynberg & Dry, 2004).

Since fluidisation regime changes can occur as a result of a change in the particle density and size distribution, an on-line catalyst removal and catalyst addition policy was implemented to maintain the fluidised bed density of the SAS reactors within certain limits to prevent uncontrolled bed expansion and blockage of the cyclones. This could occur due to the formation of free carbon (from the Bouduard reaction) and deposition of this on the catalyst. To reduce the risk of potential dipleg blockages due to powder classification changes, the diplegs are provided with constant aeration (Steynberg & Dry, 2004). The SAS reactors have some major advantages over CFB's (Steynberg & Dry, 2004; De Klerk *et al.*, 2013):

- Lower construction cost mainly due to the smaller reactor size, as well as simpler construction of the support structure
- Higher conversion. SAS reactors utilise all catalyst particles while the CFB uses only a portion at any given time
- Increased capacity. SAS reaction section is wider, accommodating more cooling coils and higher syngas feeds by increased flow or operating pressure.
- Lower overall catalyst consumption. Problems associated with reduced catalyst density due to carbon deposition are less significant if allowances are made for bed expansion. High conversion can be maintained with lower online catalyst removal and replacement rate.
- Lower linear gas velocities, catalyst velocities and pressure drop over reactor.
- Lower gas compression cost as well as less abrasion and consequently longer operation before maintenance inspection.

2.3 Fischer-Tropsch Synthesis Catalysts

Catalysts that are most active for the Fischer-Tropsch Synthesis are the group VIII metals Fe, Co, Ru and Ni (Schulz, 1999; Dry, 2004; Derouane *et al.*, 2006; Spivey *et al.*, 2015). Of these, only cobalt and iron are viable commercially (Dry, 2004; Van Steen & Claeys, 2008). This is due to process, product and cost considerations. Although the optimum catalyst for FT is still being debated, most will agree, based on operational considerations, the Fe-based catalyst is the better choice for use with a CO-rich syngas derived from coal or biomass (Chonco *et al.*, 2013; Spivey *et al.*, 2015). Ru and Co show little to no water-gas-shift activity and as such their use is not recommended with hydrogen lean synthesis gas.

In terms of cost, Fe-based catalyst is the cheapest, followed by Co and then Ru. In 2015 for instance, Ru is substantially cheaper compared to about 10 years ago (870 USD/ozt). However, its price still far exceeds that of iron or cobalt. In late 2015 the cost of Ru was 42 USD/ozt, equivalent to ±1.35 million USD/ton (Matthey, 2016), whereas iron (iron ore) was 50 – 55 USD/ton (Quandl, 2016a; Quandl, 2016b) and cobalt cost ±23 700 USD/ton (Infomine, 2016). In relative terms the cost of Co and Ru is around 450 and 26 000 times as expensive as iron, respectively.

There exists a range of operating conditions over which either Co or Fe will be more productive. Generally, under LTFT conditions Co is more selective toward linear paraffins, while under the same conditions Fe favours the formation of a more olefinic

product, as well as producing more oxygenates (Steynberg & Dry, 2004; Derouane *et al.*, 2006). When comparing, under the same conditions, based on space velocity, Fe is more productive at higher space velocities and conversely Co is more productive at lower space velocities. Co catalysts therefore show greater productivity under higher per pass conversion regimes than iron catalysts (Steynberg & Dry, 2004).

Since this work is concerned with the Ru-promotion of a precipitated iron catalyst, this section will be focussed more around iron and ruthenium catalysts.

2.3.1 Nickel

Although nickel does catalyse the FT reaction, it is too hydrogenating at relevant FTS conditions (Dry, 2004). As such Ni has a very high selectivity to methane and with increasing temperature the selectivity shifts towards almost exclusively methane (Schulz, 1999; Dry, 2004; Spivey *et al.*, 2015). This tendency is associated with cobalt and ruthenium as well, but is less excessive (Schulz, 1999). In addition Ni forms volatile carbonyls at elevated pressures and lower temperatures, and the catalyst is thus lost from the reactors (Schulz, 1999; Dry, 2004; Spivey *et al.*, 2015).

In atmospheric pressure pilot plant studies performed by Fischer and Ruhrchemie in the 1930's, Ni was demonstrated as being overall capable of FTS. There were significant problems though as the catalyst provided a low yield, had a very short lifespan and significant losses of catalytic metals occurred upon regeneration. Therefroe, due to its poor performance, Ruhrchemie and Fischer abandoned Ni as FT-catalyst and resumed work on Co-catalysed FTS (Stranges, 2007).

2.3.2 Cobalt

Cobalt catalysts have a higher activity and hydrogenation activity than that of iron and resultantly Co is more selective to linear paraffins (Dry, 2004). The cobalt based catalyst is employed in the low temperature synthesis only. Unlike iron, cobalt has very little, if any, water gas shift activity (Dry, 2004; Spivey *et al.*, 2015). Though both Fe and Co catalysts are oxidised by water, cobalt shows more resistance to re-oxidation and thus has a longer lifespan (Jager, 2003).

Due to the relatively higher cost of Co-catalysts, when compared to Fe, it is of vital importance that the minimum amount of Co is employed whilst a high activity and long

effective catalyst life be maintained. Cobalt is therefore dispersed on high surface area oxides in order to maximise the specific surface area. Co-catalysts show better activity when decreasing crystallite size and increasing dispersion of the active phase (Dry, 2004; Kunene *et al.*, 2014). However, when decreasing crystallite size too much performance suffers, partially due to increased metal-support interaction leaving more unreduced Co-oxide (De Beer *et al.*, 2014b; Spivey *et al.*, 2015). It has also has been found that Co crystallites smaller than 6nm are more prone to oxidation at high conversion and H_2O partial pressure, rendering them inactive (Dry, 2004; De Beer *et al.*, 2014b; Kunene *et al.*, 2014; Spivey *et al.*, 2015). A narrow particle size distribution above this threshold value is thus required. However, small particles have a tendency to sinter, resulting in a loss in surface area and thus activity (Van Steen & Claeys, 2008). Despite this, it is reported that the intrinsic FT activity per metal site of cobalt is about three times that of iron (Dry, 2004; Van Steen & Claeys, 2008; De Beer *et al.*, 2014b).

It is preferable to avoid the use of expensive cobalt catalysts with coal derived synthesis gas, irrespective of the reactor type used. This concern is based mainly on possible catalyst poison slippage that may occur through the syngas purification section (Steynberg & Dry, 2004).

From the published kinetic equations for Co, the effect of the partial pressure of produced water is low, which means that under the same operating conditions, using the same reactor and feed gas flow, a Co-catalyst will have a much higher conversion of syngas than a Fe-catalyst (Dry, 2004; De Beer *et al.*, 2014a). Cobalt catalysts will normally be selected for natural gas applications where synthesis gas will have a H_2/CO ratio around 2:1. This is because higher per pass conversion is possible with Co catalysts in addition to avoiding the formation of CO_2, associated with iron catalysts (Steynberg & Dry, 2004; Van Steen & Claeys, 2008; De Beer *et al.*, 2014a). Unlike with iron catalysts, operating pressure has a pronounced effect on product selectivities and an increased wax selectivity is observed with increased pressure (Jager & Espinoza, 1995).

Supported Co catalysts using cobalt nitrate are typically synthesised via impregnation onto the support. Drying of the precursor leads to cobalt nitrate droplet formation and subsequent calcination of the droplets to Co_3O_4 crystallites (Van Steen & Claeys, 2008). The most used supports for Co include alumina, silica and titania (De Beer *et al.*, 2014b; Spivey *et al.*, 2015). These supports retain a large portion of their high surface areas after high calcination temperatures required to reduce cobalt (Van Steen & Claeys, 2008; De Beer *et al.*, 2014b; Spivey *et al.*, 2015).

An active Co catalyst requires a high degree of reduction and thus reduction promoters are added (Van Steen & Claeys, 2008). The metals Pt, Re and Ru are the most widely used as reduction promoters (De Beer *et al.*, 2014b). Due to the noble metals' associated cost they are used in small amounts ranging from 0.1 – 1.0 wt% (De Beer *et al.*, 2014b; Spivey *et al.*, 2015). It is believed that noble metal promoters such as Pt improve reducibility by means of H_2 spill over (De Beer *et al.*, 2014b). Ag has also investigated as a possible candidate. It's much lower price compared to Pt makes it an interesting alternative though the promotional effect seems to be lower (Spivey *et al.*, 2015).

2.3.3 Iron-based Catalysts

In terms cost to synthesise FT catalysts, Fe is the least expensive. It is employed commercially as a catalyst in FT processes and can be used in either LTFT or HTFT, but is normally not suited for GTL applications due to its high CO_2-selectivity (Spivey *et al.*, 2015). Classical Fe catalysts have chain growth probabilities of between 0.65 and 0.70, which yields an optimum in gasoline range hydrocarbons (Thomas & Thomas, 2015). Generally LTFT iron catalysts produce less methane and a more olefinic product when compared to cobalt (Jager & Espinoza, 1995).

It is the cheapest of the metals that are active for FTS and also has the ability to catalyse the water-gas-shift (WGS) reaction (see section 2.1). This reaction and property of the Fe-based catalyst is important when dealing with CO-rich synthesis gas. As mentioned before, even though the optimum FTS catalyst is still debated, it is argued that Fe catalysts are a better choice for FT processes utilising H_2-lean synthesis gas (Chonco *et al.*, 2013; Spivey *et al.*, 2015) which has a low H_2/CO ratio ≈ 1. The iron catalyst's ability to catalyse the WGS reaction means that the H_2/CO usage ratio matches the H_2/CO ratio of the syngas, which then simplifies the gas loop surrounding the FT-reactor (De Smit & Weckhuysen, 2008; Chonco *et al.*, 2013). This characteristic of iron allows high per pass conversion in LTFT applications utilising H_2-lean synthesis gas, since the WGS activity keeps water partial pressures low, staving off deactivation due to oxidation.

However, when utilising synthesis gas derived from natural gas (or with H_2/CO ratios approaching 2:1) water production becomes inevitable. To prevent rapid deactivation due to oxidation, H_2O partial pressures must be kept below 3 bar, in turn requiring severe per pass conversion restriction (Steynberg & Dry, 2004). Published kinetic equations for the iron catalyst also show that the partial pressure of product water has a

strong negative effect, requiring lower single pass conversion to achieve conversions comparable to cobalt catalysts. Feed gas flow thus has to be lower, a large portion of the tail gas recycled and more reactors are required, increasing operating costs (Jager & Espinoza, 1995; Dry, 2004). Compared to Co, the Fe-catalyst seems to be a bit more resistant to sulphur poisoning (Bartholomew & Bowman, 1985) and except in cases of severe poisoning, sulphur poisoning does not appear to have an effect on product selectivity (Jager & Espinoza, 1995).

Typical LTFT Fe-catalysts are precipitated catalysts consisting, on a mass basis, of 100 Fe/ 25 SiO_2/ 5 Cu/ 5 K_2O (De Smit & Weckhuysen, 2008). Catalyst precursors normally consist of nm-sized crystallites of iron oxide, with pre-treatment/activation done in situ using H_2, CO or syngas (De Smit & Weckhuysen, 2008; Spivey *et al.*, 2015) which converts the catalyst precursor to the active form (De Smit & Weckhuysen, 2008). When H_2 is used as reduction medium, iron oxide is reduced to metallic iron (Chonco *et al.*, 2013). During FTS, after exposure to synthesis gas, a complex mixture of iron phases is formed. Generally it is recognised that metallic iron, iron carbides and iron oxides coexist after activation with CO or syngas and during FTS (De Smit & Weckhuysen, 2008). Since the earliest studies it was believed that the surface carbidic iron species was the active phase for FTS. However, the exact identity of the active phase still remains controversial after numerous characterisation studies and is still an issue of debate among researchers considering the complex catalyst composition under FT-conditions (De Smit & Weckhuysen, 2008; Spivey *et al.*, 2015).

To obtain a highly active iron based catalysts, the addition of promoters is required (Van Steen & Claeys, 2008). These in include structural promoters (also referred to as supports or binders) and chemical promoters. Structural promoters are added to precipitated iron catalysts to prevent the total collapse of the precipitated iron oxide/hydroxide during the calcination and reduction steps (Van Steen & Claeys, 2008). Alumina, silica, zirconia and zinc oxide are potential structural promoters and dispersion aids with good activity (De Smit & Weckhuysen, 2008; Van Steen & Claeys, 2008). Silica is often used as binder/structural promoter and reportedly shows little to no metal support interaction when added as binder, as opposed to during the precipitation step (Spivey *et al.*, 2015). Addition of alumina or silica during the precipitation step typically yields a less reducible catalyst, so these binder materials are preferably added during spray-drying (Van Steen & Claeys, 2008).

Typically copper is added as a reduction promoter (De Smit & Weckhuysen, 2008; Chonco *et al.*, 2013). It facilitates the reduction of trivalent iron and is used in a typical

molar ratio of Cu/Fe ~ 0.03 – 0.07 (Chonco *et al.*, 2013). The presence of copper permits low temperature reduction to suppress crystal growth and ensure maximal surface area is retained (Davis, 2013; Spivey *et al.*, 2015; Thomas & Thomas, 2015) as well as inhibiting the formation of iron silicates or aluminates (Van Steen & Claeys, 2008). Cu is introduced in the catalyst precursor, mostly, by co-precipitation of copper/ferrous nitrate solutions, and less often by impregnation on oxadic precursors. Typically a distinct Cu phase is not observed in the oxadic precursor, but it is known that intimate Fe-Cu-contact is essential for effective promotion with copper. However, the precise location of the Cu-ions in the catalyst precursor's structure after precipitation and/or calcination remains unknown (Chonco *et al.*, 2013). Promotion with Cu also increases the catalyst's WGS activity as well as decreasing methane selectivity and increasing long chain hydrocarbon production (Spivey *et al.*, 2015).

Alkali metals (mainly K) are used for the promotion of Fe-catalysts to yield a high activity catalyst. Promotion with potassium increases CO adsorption and CO dissociation (De Smit & Weckhuysen, 2008; Spivey *et al.*, 2015), inhibits CH_4 production, increases the Fe carburisation rate (Spivey *et al.*, 2015) and tends to increase chain growth probability (Thomas & Thomas, 2015). Potassium would seem to be the most cost effective chemical promoter for enhancing activity. A two to four fold enhancement of the activity factor can be obtained when promoted with the optimum amount of potassium, whereas overdosing will lead to reduced catalyst activity due to blockage of the active surface (Van Steen & Claeys, 2008). Depending on the loading, K-promotion can increase or decrease WGS activity. Potassium is highly mobile due to its low melting point and also makes the catalyst more prone to carbon deposition. Both of these effects decrease catalyst stability under typical FTS conditions (Spivey *et al.*, 2015).

The main challenge still associated with Fe-based catalysts for FTS is the high deactivation rate (due to oxidation in the presence of high water partial pressure and sintering) which limits per pass conversion. This, in turn, makes the iron catalyst less attractive when compared to the higher per pass conversions achievable over Co catalysts (Jager & Espinoza, 1995; Dry, 2004; De Beer *et al.*, 2014b). The rapid rate of deactivation in conjunction with the costs associated with catalyst replacement and/or regeneration are, from a commercial point of view, a challenge (Dry, 2004; De Smit & Weckhuysen, 2008; De Beer *et al.*, 2014a; De Beer *et al.*, 2014b).

2.3.4 Ruthenium

Ru is the most active of the transition metals for CO hydrogenation and is highly resistant to oxidation (Derouane *et al.*, 2006; Spivey *et al.*, 2015). It is prone to methanation at relatively low pressures, but is selective toward high molecular weight hydrocarbons at low temperature and high syngas pressures (temperatures below 150 °C and pressures above 100 bar) (King, 1978; Van der Laan & Beenackers, 1999; Claeys & Van Steen, 2002; Tang & Li, 2011).

Due to its scarcity, Ru is highly priced and was abandoned as industrial FT catalyst mainly due to this limitation (Dry, 1996; Dry, 2004; Davis & Maitlis, 2013). Though cheaper than ± 10 years ago at US $ 870 per troy ounce, it is still far more expensive than iron or cobalt, standing at $42/ozt (±1 350 USD/kg) since August 2015 (Matthey, 2016), compared to iron (iron ore) at $50 – 55 tonne (Quandl, 2016a; Quandl, 2016b) or cobalt at around $ 23 700/tonne (Infomine, 2016). If one were to normalize the price of iron to be equal to one, based on these figures the cost of Co is about 430 – 470 and Ru around 24 500 – 27 000 times more expensive. That is Co is more than 400 times the price of Fe while Ru is almost 60 times as expensive as Co. Comparing the results obtained in studies by Pichler *et al.* (1964) and Everson *et al.* (1978) it seems that, in addition to the cost implications of the catalyst, for Ru to perform optimally as a standalone catalyst and produce high molecular weight products, rather high operating pressures are required.

Ruthenium has been of interest for many years and has received considerable attention in laboratory studies. Much of the early work was done by Pichler who reported Ru to likely be more active than either Fe or Co. It was reported that high molecular weight products were formed at high pressures (1000 atm) and mild temperatures (≤ 140 °C), while only methane was formed at 300 °C and atmospheric pressure (Davis & Maitlis, 2013).

A composition cycling study by Ross *et al.* (1987) showed that at 484 K and 446 kPa, with feed H_2/CO ratios between 3:1 and 2:1, product selectivity is majorly olefinic (75% selectivity). This trend was shown to increase with decreasing H2/CO ratio. This could possibly be extended to operation at higher pressures where longer chain hydrocarbons are produced. It was also found that the stoichiometric feed ratio (H_2/CO = 2:1) favoured the formation of higher hydrocarbons.

Iglesia *et al.* (1992) conducted experiments on supported Ru catalysts ranging from 1 – 10 wt% supported on TiO_2, SiO_2 or Al_2O_3. Operating conditions were 476 K, 560 kPa,

$H_2/CO = 2.1$ and CO-conversions of 45 – 60%. For unsupported Ru, methane selectivity was 2% and C_{5+} selectivity 95%. They also reported CH_4 selectivities around 5% and C_{5+} selectivities in the range of 90% in the majority of cases over the range of supported Ru catalysts. Taking into account the relatively high operating temperature and low pressure of this study and suggestions madde by Pichler in his work, with operation at higher pressure and lower temperature similar or better results in terms of CH_4 and C_{5+} selectivities could be expected.

In a study on supported Ru-catalysts by Abrevaya *et al.* (1986), a catalyst consisting of 1% Ru supported on Al_2O_3 was reported to have achieved $C_1 – C_4$ selectivities in the range of 3 – 4 times lower than for the Arge catalyst (at the time). This was at a CO-conversion level of 87% and operating conditions of 225 °C and 35 atm. In other experiments, during the same study, an improved 2.8% Ru, Al_2O_3 supported catalyst, incorporating an undisclosed set of modifiers, was tested at 208 °C and 62 atm with a H_2/CO ratio of 2:1. This catalyst was reported to have $C_1 – C_2$ selectivity of 1.5% at 80% CO-conversion. The catalyst was also reported to show little to no apparent deactivation over 800 hrs time on stream. This result would imply, by virtue of low methane selectivity, significant selectivity to higher hydrocarbons at relatively high CO-conversions as well as pronounced resistance to deactivation despite high water partial pressures.

Ru remains in the metallic state under FTS conditions and is the known active phase for FTS. Since Ru shows little to no WGS activity, it is not suited to use with H_2-deficient syngas (Van der Laan & Beenackers, 1999). Ruthenium seems to tolerate the effects water very well; evidenced by its resistance to oxidation and being active even if suspended in liquid water (Claeys & Van Steen, 2002). Pulse studies by Nijs & Jacobs (1980) with water co-feeding over supported Ru-catalysts showed that the presence of water seemed to promote chain growth. A direct mechanistic involvement of H_2O in FT-synthesis with Ru has thus been suggested (Claeys & Van Steen, 2002).

Claeys and Van Steen (2002) conducted experiments in a continuously operated stirred slurry reactor at various H_2O partial pressure. With a supported Ru catalyst they found that with increasing water partial pressure, the selectivity towards methane declined and the C_{5+} selectivity increased. In a density functional theory (DFT) study by Hibbitts *et al.* (2013) it was concluded that water plays a mechanistic role in FTS over ruthenium and may act as a co-catalyst, increasing chain growth probability by increasing the rate of monomer formation or –inclusion.

2.4 Catalyst Preparation Techniques

There are essentially two main methods for the production of heterogeneous catalysts: Impregnation of preformed supports with active metal precursor salts or co-precipitation of the active metal (s) with the support (Lok, 2009). Though considered more difficult, since it requires accurate control of conditions such as pH, crystallite size and degree of dispersion, precipitation- and co-precipitation techniques remain some of the most industrially relevant and widely used since catalysts with the same properties cannot be produced by other methods (Schüth *et al.*, 2008; Lok, 2009). This is due to the high degree of dispersion that can be achieved using these techniques (Schüth *et al.*, 2008) as well as the high attainable metals loading up to- and in excess of 60% (Lok, 2009).

2.4.1 Precipitation and Co-precipitation

Precipitation is defined as a process whereby a solid is produced from a homogeneous solution after supersaturation is achieved with respect to the precipitating solid (Schüth *et al.*, 2008). In general the term precipitation is used for processes where solid formation is induced by chemical reaction or a reduction in the solubility due to the addition of a precipitating agent. Normally this involves high supersaturation and amorphous intermediates are formed (Schüth *et al.*, 2008; Lok, 2009). The precipitation process consists of three major steps: 1) liquid mixing, 2) nucleation and crystal growth and 3) aggregation of primary particles (Lok, 2009).

Related phenomena are crystallisation (where a solid is directly obtained in crystalline form at low supersaturation and the precipitation is induced by lowering temperature or evaporation of the solvent) and sol-gel synthesis (where a container spanning hydro-/alcogel is formed in a sol-gel reaction) (Schüth *et al.*, 2008). However, no clear phase separation takes place in sol-gel synthesis (Schüth *et al.*, 2008). For the purposes of this work precipitation will refer to precipitation induced by chemical precipitating agents.

Precipitation and co-precipitation is more demanding than several other preparation methods due to the necessity of product separation as well as the generation of large volumes of salt solutions (Schüth *et al.*, 2008; Lok, 2009). In spite of this it remains the most common applied method for the preparation of several catalytically relevant materials, especially support materials, such as oxides of aluminium, silicon and titanium, as well as zirconia- and iron-oxides (Schüth *et al.*, 2008).

When catalysts based on more than one metal are to be produced, the method of co-precipitation can be employed. Co-precipitation is defined as the simultaneous precipitation of a normally soluble component with a macrocomponent from the same solution via the formation of mixed crystals, adsorption, occlusion or mechanical entrapment (Schüth *et al.*, 2008).

As a method of catalyst (and support) preparation, the technique has as its main advantages the possibility of creating very pure materials and a process that is flexible with regard to the final product quality. In addition the method of co-precipitation is especially suited for obtaining a homogeneous distribution of catalyst components and creating a catalyst precursor with definite stoichiometry (Schüth *et al.*, 2008; Lok, 2009). These precursors can also be easily converted to an active catalyst by calcination and/or reduction steps. When the catalyst precursor is a stoichiometrically defined compound of the final catalyst constituents, calcination and/or reduction creates a catalyst with small and intimately mixed crystallites of the catalyst components (Schüth *et al.*, 2008).

2.4.2 Incipient Wetness Impregnation

This method is generally employed to adsorb a precursor on the surface of a support and achieve a relatively low loading. Often this method is used in the preparation of supported precious metal catalysts where generally low loadings are required (Geus, 2007). The procedure involves adding an impregnating solution to dried or evacuated support bodies (Geus, 2007; Lekhal *et al.*, 2007) where the precursor is in the form of a metal salt (Lekhal *et al.*, 2007). In most cases the impregnating solution is water-based. However, in the case of a hydrophobic support surface or when hydrolysis of the support is to be avoided, non-aqueous solutions are used (Lekhal *et al.*, 2007). Applying a volume of impregnating solution equal to the support body pore volume is most effective. The uptake of liquid by the support body proceeds fast and thus impregnation can be performed rapidly as the dissolved precursor is transported by convection into the pores. An analogous procedure is dripping impregnation, where support bodies are immersed in a solution containing the precursor and subsequently drained. Here the dissolved precursor must diffuse into the pores of the support before being adsorbed (Geus, 2007).

3

Chapter 3: Experimental

This chapter presents the experimental method followed to generate empirical data to provide answers to the research questions as set out for the study. Catalysts used in the study were prepared by a combination of co-precipitation and incipient wetness impregnation. Iron oxide with an alumina binder was precipitated, washed, dried, crushed and classified before proceeding with consecutive impregnations with potassium and ruthenium. The catalysts were characterised using XRD, TPR, SEM-EDX, ICP-OES and BET before exposure to FTS conditions. Catalysts were tested in a slurry reactor under relevant LTFT process conditions to compare the behaviour of an iron catalyst promoted- and not promoted with Ru.

3.1 Catalyst Preparation

3.1.1 Preparation of Fe-based catalysts

Catalyst preparation was done using a combination of co-precipitation and incipient wetness impregnation techniques. The catalysts were prepared from a precipitated base of Fe- and Al oxides, where alumina acts as binder on the basis of 100 Fe/30 Al_2O_3. This Fe-Al-base was promoted with potassium via the incipient wetness impregnation technique to have a composition of 100 Fe/ 30 Al_2O_3/ 5 K. A portion of this was used to prepare the Ru-promoted catalyst via simple impregnation using $Ru_3(CO)_{12}$ as precursor to yield a Ru-concentration of 3 wt% based on Fe-content (100 Fe/30 Al_2O_3/5 K/3 Ru). This yielded two catalysts; a K-promoted Fe/alumina catalyst and a Ru- and K-promoted Fe/alumina catalyst.

For ease of reference the catalysts and their precursors will be referred to as in Table 3.1:

Table 3.1: Catalysts and their composition

Catalyst	Theoretical composition	Description	Promoters
Fe/Al	$100Fe/30Al_2O_3$	Upromoted uncalcined Fe-catalyst	-
Fe/Al/K	$100Fe/30Al_2O_3/5K$	Calcined K-promoted Fe-catalyst	K
Fe/Al/K/Ru	$100Fe/30Al_2O_3/5K/3Ru$	K- and Ru-promoted Fe-catalyst (using $Ru_3(CO)_{12}$)	K, Ru

3.1.2 Unpromoted Fe-catalyst preparation

The Fe-based catalyst with alumina binder was synthesised via the co-precipitation method, using ammonium carbonate as the precipitating agent and the nitrates of iron and aluminium as precursor salts. The precipitation reactions, when using ammonium carbonate as precipitating agent, are as in Equations 3.1 and 3.2:

$$2Al(NO_3)_3 \cdot 9H_2O + 5(NH_4)_2CO_3 \rightarrow Al_2O_{3\,(s)} + 8N_2 + 38H_2O + 5CO_2 \quad (3.1)$$

$$Fe(NO_3)_3 + 3(NH_4)_2CO_3 + 2H_2O \rightarrow FeOOH_{\,(s)} + 6NH^+_{4\,(aq)} + 3HCO^-_{3\,(aq)} \quad (3.2)$$

60 g of $Al(NO_3)_3 \cdot 9H_2O$ (Sigma-Aldrich, 99.998%), , 196 g $Fe(NO_3)_3 \cdot 9H_2O$ (Sigma Aldrich, 99.95%) and 462 g of $(NH_4)_2CO_3$ (Sigma Aldrich, 99.999%) was weighed with the aim of producing 50 g of Fe/Al base catalyst with a composition of 100 Fe/30 Al_2O_3. A three times molar excess of the precipitating agent was used to ensure a complete precipitation of the aluminium and iron ions in the precipitation reaction.

The weighed masses of Fe- and Al-nitrate nonahydrate salts were added in a 2 L beaker and dissolved in about 300 mL of warm deionised water and placed on a hotplate (Heidolph MR3001K) and heated to around 90 ^{O}C. The required amount of ammonium carbonate was dissolved in a 1 L beaker with about 700 mL warm deionised water and brought to the boil on a second hot plate (of the same make and model). When both the solutions of the precursor salts and precipitating agent were at the boil, the ammonium carbonate solution was added to the nitrates solution under continuous stirring using a Heidolph RZR1 overhead stirrer, with a paddle mixer at 150 rpm while still maintaining the heating. This incremental addition of the ammonium carbonate solution was done in

order to prevent spillage or boiling over due to the evolution of CO_2 during the precipitation reactions. As more precipitating agent was added to the nitrates solution and the nucleation-precipitation proceeded, a thickening slurry of Fe- and Al-oxides/oxyhydroxides was formed. This required the mixer speed to be adjusted until a final speed of 600 rpm was reached. The reaction mixture was then left under heating and stirring for a further 20 min, after the last of the precipitating agent was added, to allow the process to complete. The stirrer and hot plate was then switched off and the suspension was allowed to stand for 30 min before filtering.

The dark brown precipitate slurry was vacuum filtered using a Büchner filter setup and washed with about 5 L of boiling deionised water until the presence of nitrate and ammonium ions could not be detected. The washed precipitate was dried in an oven at 100 °C for 24 h and the dried filter cake crushed with a pestle and mortar. The catalyst particles were classified using sieves with aperture sizes of 300 µm, 250 µm, 212 µm, 125 µm and 53 µm. Oversized particles larger than 300 µm were crushed again and reclassified, until finally ±25 g of catalyst particles in the 250 – 300 µm size range was obtained. The undersized particles were kept aside.

The 250 – 300 µm catalyst was calcined for 16 h at 350 °C in a glass calcination tube under nitrogen flow at a flow rate of 60 mL/min NTP. A heating rate rate of 1 °C/min was used, with a one hour hold at 100 °C to allow for drying of the uncalcined catalyst before raising the temperature to the calcination temperature of 350 °C at a rate of 1 °C/min. The calcination temperature was held for 16 h, after which the reactor and furnace was allowed to cool under N_2 flow before removing the calcined catalyst. A relatively mild temperature of 350 °C was chosen so as to limit/avoid sintering, and an associated loss in surface area, as far as possible.

Promotion of the Fe/Al catalyst base with potassium was done after calcination by simple impregnation using the incipient wetness technique in a Buchi R-215 Rotavapor with Buchi B-491 heating bath and Buchi V-700 vacuum pump. Potassium nitrate was used as precursor salt to achieve a weight based Fe/K ratio of 20:1. The required mass of potassium nitrate was calculated assuming the calcined catalyst consisted of Fe and Al in the form of hematite and alumina (on a 100 Fe/30 Al_2O_3 basis), respectively. All of the calcined catalyst was added to the "vacuum bowl" of the rotary evaporator and about 2 g of KNO_3 (Sigma Aldrich, 99.9%) was weighed and added. 50 mL of deionised water was added to this to form a slurry. The bath temperature of the rotary evaporator was set to 40 °C and the pressure lowered to 100 mbar in 20 mbar decrements to evaporate the solvent under vacuum and continuous rotation at 50 rpm. To ensure the solvent was

completely removed, the pressure was further reduced to 72 mbar, while increasing the temperature of the water bath to 60 °C. Once completely dry, the catalyst was removed from the "vacuum bowl" and calcined again using the same method as described earlier.

3.1.3 Ru-promoted Fe-catalyst preparation

Ruthenium promotion was done after characterisation of the Fe/Al/K catalyst. Since Ru salts are expensive, and the Ru-content is dependent on the Fe-content, it is imperative that the true Fe-content be known before promotion.

The Ru-promoted catalyst was prepared by simple impregnation with triruthenium dodecacarbonyl. 0.3 g $Ru_3(CO)_{12}$ (Sigma Aldrich, 99%) was weighed and dissolved in 800 mL of n-hexane (Merck) in a 1 L flask at ambient pressure and temperature, yielding a relatively bright orange translucent solution. To this solution, 6.5 g of the Fe/Al/K catalyst powder was added, the container sealed and allowed to stand for three days (72 h) while monitoring the change in colour of the solution. During this time the solution turned a more translucent pale yellowish-orange as more of the organometallic salt was adsorbed to the catalyst surface. After 72 hours the colour had stabilised, since the change in colour was insignificant compared to at 48 hours. At this point the solvent was removed by evaporation, in the same rotary evaporator used for K-promotion, allowing the rest of the salt to be impregnated on the catalyst surface, recovering the solvent for disposal. Under constant rotation of 50 rpm and a water bath temperature of 40 °C, the pressure was lowered to 335 mbar, gradually, in 20 mbar decrements. Nearing the end of the evaporation process, the pressure was reduced further to 300 mbar while increasing the bath temperature to 50 °C. When completely free of solvent, the Ru-promoted catalyst was removed from the vacuum bowl and stored in a clean sample container.

The catalyst was not calcined after promotion since $Ru_3(CO)_{12}$ has been shown to decompose thermally to Ru-metal in an inert atmosphere at a temperature of 175 °C (Banditelli *et al.*, 1976). Since the reactor, and catalyst, is heated in an inert atmosphere prior to activation, a calcination step was not deemed necessary as the organometallic complex would be in the reduced metallic state before reaching the activation temperature of 270 °C.

Prior to this, Ru-promotion with $RuCl_3$ as precursor salt was attempted, but proved unsuccessful. Upon activity testing in a fixed bed reactor it was observed that CO-

conversion was exceptionally low and did not increase upon increasing residence time. It is thought that the catalyst was deactivated during calcination with the formation of FeOCl and that this inhibited reduction as well as carburisation of the catalyst during syngas activation. Consequently, this catalyst was abandoned and ruthenium dodecacarbonyl, as alternative ruthenium precursor, was used for Ru-impregnation.

3.2 Catalyst Characterisation

Techniques employed for the characterisation of all catalysts used in the study were X-Ray Diffraction (XRD), Scanning Electron Microscopy with Energy Dispersive X-Ray Diffraction Spectroscopy (SEM-EDX), Inductively Coupled Plasma Optical Emission Spectrometry (ICP-OES), Temperature Programmed Reduction (TPR) and Brunauer Emmet Teller N_2-Chemisorption (BET).

3.2.1 SEM-EDX

Scanning electron microscopy is used to examine the surface of a specimen by scanning with an electron beam and collecting the secondary- and back-scattered beam of electrons. The surface must be electrically conductive, but polishing or etching is not a prerequisite. Magnification of 10 to more than 50 000 times is possible and the use of accessory equipment permits qualitative and semi-quantitative elemental analysis of localised surface areas (Callister, 2007).

Electron microscopy is a relatively straightforward technique for the determination of the size and shape of supported particles. Electrons have characteristic wavelengths of less than 1 Å. Crystallographic information is obtained from diffracted electrons. The back-scattering of electrons becomes more effective as atomic mass of the sample increases, making large regional concentrations of heavier elements/atoms distinguishable due to the higher yield of back-scattered electrons. Additionally Auger electrons and X-Rays are formed (Chorkendorff & Niemantsverdriet, 2003). Scanning Electron Microscopy involves rastering a narrow high energy electron beam over the sample surface and detecting the yield of secondary- or backscattered electrons as a function of primary beam position. Secondary electrons have low energies and originate from the surface of the sample, while backscattered electrons come from deeper and carry compositional information (Rothenberg, 2000; Chorkendorff & Niemantsverdriet,

2003). SEM thus gives a three-dimensional image of the catalyst, albeit at a lower resolution than transmission electron microscopy (TEM) (Rothenberg, 2000).

Energy dispersive X-Ray spectroscopy allows for a qualitative elemental analysis using the X-rays formed in the relaxation of core-ionised atoms. The X-Rays that are emitted are characteristic to an element (much like in bulk phase identification using X-ray diffraction). This allows determination of the chemical composition of a selected part of the sample (Chorkendorff & Niemantsverdriet, 2003).

A FEI NanoSEM 230 with Oxford X-Max silicon drift EDX detector was used in the characterisation of the catalyst samples. A small amount of the sample was sprinkled onto a carbon glue covered aluminium stub. The sample was then carbon coated in a Balzers evaporation coater, after which it was inserted into the SEM. Operating conditions in the SEM were a 5 mm working distance, 20 kV and a beam current of 1.6 nA, which are settings ideal for the generation of X-Rays. X-Rays were collected using the Oxford X-Max detector and INCA software, displaying the elements present in the sample in weight percent, with the areas where the EDX spectra were collected also viewable.

3.2.2 XRD

X-ray diffraction (XRD) is a characterisation method used for the identification of bulk crystalline phases present in materials and for obtaining an indication of crystallite size (Rothenberg, 2000; Chorkendorff & Niemantsverdriet, 2003). This is also one of the oldest and most frequently applied techniques for the characterisation of catalysts (Chorkendorff & Niemantsverdriet, 2003).

X-Ray diffraction is a result of the elastic scattering of X-Ray photons by atoms in a crystal lattice with sufficient crystallographic order. As such, diffraction is a consequence of the specific phase relationships between scattered waves. When monochromatic X-rays are scattered and have a difference in path length that is an integer number, the waves are in phase and mutually reinforce one another, giving rise to constructive interference. For this constructive interference or diffraction to occur, Bragg's law (Equation 3.3) must be satisfied (Rothenberg, 2000; Chorkendorff & Niemantsverdriet, 2003; Callister, 2007).

$$n\lambda = 2x_d \sin\theta ; \quad n = 1,2, \ldots \tag{3.3}$$

In this relation λ is the X-ray wavelength, n is the order of reflection, x_d is the interplanar spacing (also referred to as the :"d-spacing") and θ is the incident angle for constructive interference (Chorkendorff & Niemantsverdriet, 2003; Callister, 2007). The d-spacings, can be determined from the Bragg relation if the 2θ angles, where constructive interference occurs, are measured. These d-spacings are characteristic for a particular compound and thus allows for the positive identification of bulk crystallographic phases present in the sample (Rothenberg, 2000; Chorkendorff & Niemantsverdriet, 2003).

Characterisation using XRD has an important limitation in that clear diffraction peaks are observed only when the sample possesses sufficient long range crystallographic order. This, however, also imparts information regarding the dimensions of the reflecting planes since there is a relationship between the aforementioned and the diffraction peak width (Chorkendorff & Niemantsverdriet, 2003). An estimate of the crystallite size can be determined from the obtained diffractogram and the Scherrer equation (Equation 3.4).

$$x_c = \frac{K\lambda}{\beta \cos\theta} \tag{3.4}$$

Here x_c is the crystallite diameter, β is the peak width at half intensity and K is a constant, often taken as 1. Though quick, X-Ray line broadening does not always offer a reliable estimate of the crystallite size (Chorkendorff & Niemantsverdriet, 2003).

X-Ray diffraction patterns were collected for the Fe/Al, Fe/Al/K and Fe/Al/K/Ru catalysts using a Bruker D8 Advance X-ray diffractometer with a Co-Kα source (λ = 1.78897 Å) and position sensitive Bruker Vantec detector (operating at 35 kV and 40 mA).

Before loading the sample, the sample holder was cleaned thoroughly with ethanol to prevent contamination of the catalyst sample. The sample was then loaded into the sample holder, taking care to ensure a flat sample surface and the excess removed from the sample holder. This was placed in the automatic sampling tray and secured. A scanning range of 10° to 130° 2θ was used with a scanning rate of 1°/min and a step size of 0.01°.

3.2.3 ICP-OES

Inductively Coupled Plasma Optical Emission Spectroscopy is a technique is based on the spontaneous emission of photons from atoms and ions that have been excited in a radio-frequency (RF) discharge. The wavelengths of the emitted photons are then used to identify the elements from which they originated, which the total number of photons directly proportional to the concentration of the originating element (Hou & Jones, 2006; Juncosa, 2008).

When analysing solid samples, they require extraction or acid digestion so that the elements to be analysed will be present in solution. The sample solution is then converted to an aerosol and directed into the central channel of the plasma, where it is quickly vapourised, and the elements liberated as free atoms in the gaseous state, as the inductively coupled plasma (ICP) sustains a temperature of approximately 10 000 K. Further collisional excitation within the plasma imparts additional energy to the atoms to promote them to excited states. Sufficient energy is often available for the conversion of the atoms to ions and subsequent promotion of the ions to excited states. Both the atomic and ionic excited state species may then relax to the ground state via the emission of a photon which has a characteristic energy determined by the quantized energy level structure for the atoms or ions (Hou & Jones, 2006). The wavelength and intensity serves to identify the element and its concentration (Hou & Jones, 2006; Juncosa, 2008).

Compared to the commonly used analytical atomic spectrometry techniques, ICP-OES probably has the fewest interferences. In contrast with a low temperature flame, where chemical interference can be a severe problem, the argon plasma is inert. The high temperature of the plasma also helps reduce chemical interference and is high enough to break down most species into atoms or ions for excitation and subsequent emission (Boss & Fredeen, 1999; Hou & Jones, 2006).

3.2.4 BET

The Brunauer-Emmet-Teller (BET) method determines surface area by relating the total surface area of a solid to the volume of gas that adsorbs at a given temperature and pressure. An adsorption isotherm is a graph showing the dependence of the amount gas adsorbed on the equilibrium pressure of the gas at a constant temperature (Rothenberg, 2000; Juncosa, 2008). It is the most common method for the calculation of surface area

of metal oxides (Juncosa, 2008) and remains a very important characterisation technique for a wide range of porous materials, with nitrogen remaining universally pre-eminent as adsorbate (Sing, 2001).

Langmuir's work on monolayer adsorption renewed interest in the interpretation of adsorption data. It was realised in the 1930's that multilayer adsorption of nitrogen could occur at a temperature of 77 K and in 1938 the BET-theory, the first successful attempt in modelling multilayer adsorption, was published (Sing, 2001; Bartholomew & Farrauto, 2011). To obtain the specific surface area Brunauer, Emmett and Teller assumed the completed monolayer adsorption to be in a close-packed state (Sing, 2001). The BET theory is based on a very simplified model of physisorption, where, as in the Langmuir theory, the adsorbent surface is assumed uniform and pictured as an array of equivalent sites where molecules are adsorbed randomly (Sing, 2001; Juncosa, 2008). The probability of the occupation of a site is assumed independent of the occupancy of neighbouring sites and there is assumed to be no lateral interactions between the adsorbed molecules. Molecules in the first layer act as sites for molecules in the second layer, which in turn are sites for the next layer and so on. Though lateral interactions are not allowed, all the layers above the first are assumed "liquid-like". Due to the artificial nature of the theory, the range of applicability of the BET equation is, however, limited to a portion of the nitrogen isotherm and the best fit rarely extends above $P/P_0 = 0.30$. The location and extent of the linear region of a BET plot is mostly dependent on the adsorbent and adsorbate, as well as the operational temperature. Thus the BET monolayer capacity derivation is recommended from the best linear fit for that part of the isotherm. The calculation of the BET specific surface area is dependent on the average area occupied by each molecule in the completed monolayer, which in the case of N_2 at 77 K is usually taken as 0.162 nm^2. This is the value originally proposed by Emmett and Brunuaer, based on the liquid form close-packed monolayer structure assumption. Other researchers have, however, proposed alternative values ranging from $0.13 - 0.20$ nm^2 (Sing, 2001).

The use of nitrogen adsorption for pore size analysis dates back to the late 1940's, based on the application of the Kelvin equation with a correction for the multilayer thickness on the pore walls. The method was devised by Barrett, Joyner and Halenda (BJH) in 1951 and remains the most popular way pore size distribution determination from an appropriate nitrogen isotherm (Sing, 2001).

Nitrogen physisorption was carried out according to the Brunauer-Emmet-Teller (BET) method using a Micromeritics Tristar II 3020 for the determination morphological properties such as surface area and pore volume.

3.2.5 TPR

Temperature Programmed Reduction forms part of a class of techniques where a chemical reaction is monitored with a linear time-dependent increase in temperature. Typically a reactor, charged with catalyst, is heated at a linear rate of 0.1 – 20 °C/min while the outlet gas composition is monitored by thermal conductivity detector. TPR is a useful measure of the temperature needed for complete reduction of catalysts (Chorkendorff & Niemantsverdriet, 2003). By plotting signal intensity against sample temperature a TPR profile is obtained, making it possible to identify reduction peaks corresponding to the metal oxide reduction steps.

The TPR studies were conducted using a Micromeritics Autochem HP2950. Quartz wool was tamped into the wider end of a quartz u-tube reactor. A sample mass of ± 50 mg or 100 mg was weighed, recorded and loaded in the reactor. The reactor is fixed in the Autochem HP2950 with stainless steel fasteners, each with a rubber o-ring to give a leak proof seal. The o-rings were inspected visually to make sure that they are not torn or show appreciable deformation/flattening prior to fixing the reactor in place. The furnace was carefully closed, ensuring that the reactor is not subjected to unnecessary stresses. This ensures that the tube does not break/shatter upon closing the furnace or upon heating the reactor. A 5% H_2 in Ar mixture was used as reduction gas and a flow rate of 50 mL/min NTP. Prior to reduction the sample was dried for two hours at 120 °C in flowing Ar at 50 mL/min NTP. The temperature was increased linearly to 120 °C at a rate of 10 °C/min and held for 2 hours to allow the sample sufficient drying time. After drying the sample furnace was set to cool at a rate of 10 °C/min to reach a sample temperature of 60 °C. Once the sample temperature reached 60 °C, flow of the reducing gas was initiated, and sample temperature increased at a rate of 10 °C/min to a final temperature of 920 °C. Thermal conductivity measurements of the outlet gas were logged every second. Upon reaching 920 °C, this final temperature was held for 2 hours before initiating inert gas flow and terminating the experiment.

3.3 Fischer-Tropsch Experiments

Catalysts were tested at industrially relevant LTFT conditions of 250 °C and 20 bar in a 1 dm^3 stirred, slurry reactor (stirring rate: 350 rpm). The reactor is fed from the main gas lines with H_2, CO and Ar at a ratio of 2:1:1. Flow is controlled via mass flow controllers (Brooks 5850S). System pressure is controlled and maintained with a back pressure regulator. The system is fitted with a CO guard bed (at 230 °C) for carbonyl decomposition, hot knockout (at 210 °C) to remove waxes and cold knockout (at ambient temperature) for the collection of water and liquid products. The remaining tail gas is passed through an online GC-TCD, using Ar as internal standard, for the determination of tail gas composition before being vented. Samples of the product gas is taken using the ampoule sampling method and analysed offline using a GC-FID fitted with an ampoule breaker. Ampoule sampling points are located on the feed side, product side and in the tails line (feed side and tails side to be used if offline analysis is necessary). Figure 3.1 shows a process flow diagram of the rig setup.

The slurry reactor itself consists of a reactor pot and head assembly which is fitted with an agitator, inlet and outlet lines, and a pressure relief valve. The reactor pot is mated with the head assembly by raising the pot into position with a scissor jack stand. A copper gasket ensures a tight, leak free, seal between the surfaces once the head and pot is mated and torqued.

To ensure that the reactor and rig is operating both correctly and safely due to the pressures, temperatures, feed and products involved in the FTS reaction, the following preparation is required: Pressure testing the system, calibrating the mass flow controllers (MFC's) and calibration of the GC-TCD.

3.3.1 Pressure Testing

The reactor was pressure tested to ensure that there are no leaks in the system, the rig can be operated safely and tail gas composition can be measured more reliably. The feed to the reactor, consisting of CO and H_2, is potentially dangerous due to the toxicity of CO and the potential flammability/explosion hazard associated with H_2. It is thus imperative these gases be confined to the system. Additionally, the reactor product stream consists of unreacted feed gases and a wide range of hydrocarbon products that are highly flammable, under pressure and, due to the nature of the FTS, has a wide range boiling- and flash points. The pressure test was conducted by charging the

system with an inert, non-toxic, gas (Ar) to mitigate possible explosion, flammability and toxicity hazards.

The copper gasket of the reactor pot was inspected visually to establish whether any imperfections are present that may cause imperfect sealing between the head and pot, resulting in pressure loss. The reactor pot was raised into position to meet the head assembly, the six bolts to secure the head were inserted and finger tightened, the heating jacket was fixed to the reactor pot, the reactor insulation placed over this and the system heated to operating conditions. Heating was done incrementally, in 30 °C increments, to ensure the heaters do not overshoot and trip the system. All the "hot" lines were heated to 210 °C and the CO guard bed heated to 230 °C, while the reactor was first heated to a temperature of 120 °C for torqueing down the head. Upon reaching 120 °C, the bolts were torqued to 60 N.m in 10 N.m increments in a "criss-cross" fashion to ensure even pressure distribution across the head. After torqueing down the head, the reactor temperature was increased to 250 °C. Once at temperature, the backpressure regulator was set to 30 bar and the reactor charged with Ar. After reaching a reactor pressure of close to 30 bar the flow was ceased and the inlet valve to the reactor shut. The reactor was left for one hour to allow the pressure to fully stabilise and then monitored for 24 h. This procedure was repeated for each reaction run.

The pressure testing results are also given in Tables A1 and A2 in Appendix A. For the Fe/Al/K run a pressure loss of 0.35 bar over the 24 h period was observed, equivalent to 0.015 bar/h. A pressure loss of 0.44 bar was recorded for the Fe/Al/K/Ru run, equivalent to 0.018 bar/h for the 24 h period. This was considered a negligible and acceptable loss so that the system is considered essentially "leak proof" when taking into account that the system will be operating at 20 bar.

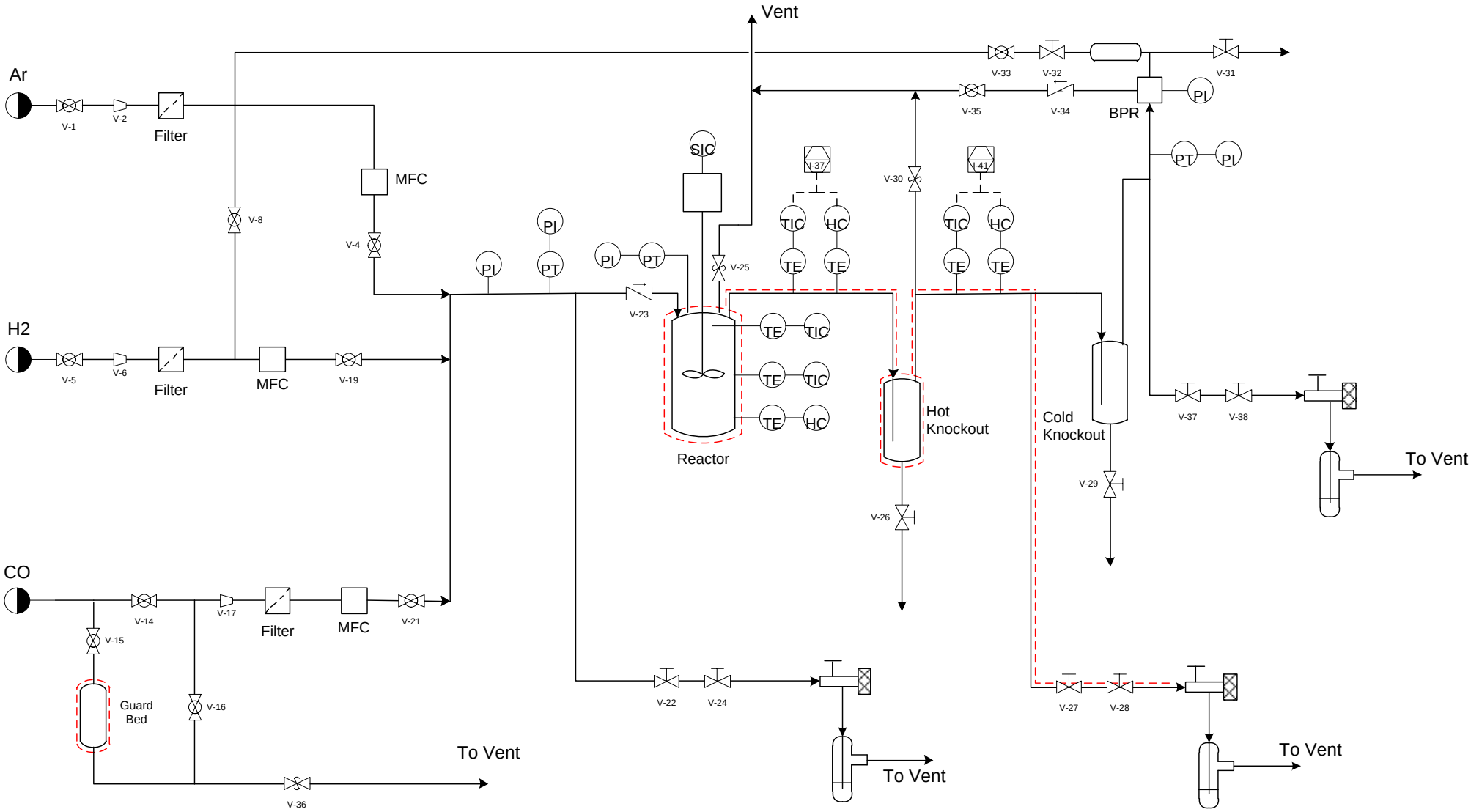

Figure 3.1: PFD of slurry reactor setup

3.3.2 MFC Calibration

The MFC calibration ensures that the MFC's deliver the specified flow. A calibration curve was drawn by setting each MFC to specified percentages of the maximum flow rate and measuring the delivered flow rate using a soap bubble flow meter. A high degree of linearity was observed for all the MFC's over the range of interest. R^2 values of 0.9974, 0.9998 and 0.9992 were obtained for CO, H_2 and Ar, respectively, indicating a very good fit over the measured ranges. To ensure minimal error in measurement, each of the flow rates was measured 10 times and then averaged. (See Tables A7, A8 and A9 in Appendix A for the raw measurement data.) The calibration curves for the CO, H_2 and Ar MFC's are viewable in Figures A3, A4 and A5, respectively in Appendix A.

3.3.3 GC-TCD Calibration

A gas chromatograph with thermal conductivity detector (GC-TCD) was used for online analysis of the tail gas using 3 columns to detect the non-condensable gases for the determination of CO-conversion, CH_4-selectivity and CO_2-selectivity (GC specifications in Table A4 in Appendix A). Column 1 used H_2 as carrier gas to detect Ar, CH_4 and CO, while column 2 used He as carrier to detect CO_2 and column 3 used for the detection of H_2 with Ar as carrier gas. However, since column 3 was not functioning correctly, only columns 1 and 2 were used for the detection of CO, CO_2, CH_4 and Ar.

A calibration gas, with composition as in Table 3.2, was used to determine the response factors for the different gases in the different columns, which relate the concentrations of all other gases to the concentration of Ar.

Table 3.2: Calibration gas composition

Gas	Fraction (%)
H_2	39.6
N_2	5.2
CO	20.1
CH_4	15.2
CO_2	9.8
Ar	10.1

Retention times for Ar, CH_4 and CO in channel 1 were 0.87 min, 1.71 min and 2.6 min, respectively. The retention time of CH_4 and CO_2 in channel 2 was 0.37 min and

0.42 min, respectively, while the retention time for H_2 in channel 3 could not be determined due to the column not functioning correctly.

Response factors, $R_{f,TCD}$, were determined for each of the gases based on their peak areas and concentrations with respect to the peak area and concentration of Ar according to Equation 3.5. The response factors were rechecked for accuracy before running each experiment.

$$R_{f,TCD} = \frac{A_i/C_i}{A_{Ar}/C_{Ar}} \tag{3.5}$$

Here A_{Ar} is the measured peak area of Ar in the TCD chromatogram, C_{Ar} is the concentration of Ar in the gas, A_i is the peak area of the compound i in the chromatogram and C_i is the concentration of compound i in the gas. The calculated response factors that were used are summarised in Table 3.3. (See Tables A5 and A6 in Appendix A for the TCD measurements for response factor determination.)

Table 3.3: GC-TCD response factors

	$R_{f,TCD}$	
Gas	**Channel 1**	**Channel 2**
CH_4	1.069	1.217
CO	1.054	-
CO_2	-	1.644

It was observed that the retention time of CO tends to shift over time from multiple measurements. When the CO retention times had shifted by 0.2 min or more the column was baked at its maximum allowable temperature for a few hours.

3.3.4 Catalyst FTS testing

All the hot lines were heated to 210 °C, as well as heating the CO-guard bed and hot knockout to 230 °C and 210 °C. As during pressure testing, this was done in 30 °C increments to avoid gross overshooting. The heating jacket and insulation was fixed to the reactor pot and the pot lifted into position. Heating to 120 °C was initiated. Upon reaching this temperature, the reactor was filled with 300 g of FT hard wax (Sasol, 99.9%) and the wax melted at 120 °C, after which 5 g of catalyst was added to the melted wax. The reactor was sealed and -heated to the activation temperature under stirring at 350 rpm and constant argon flow at atmospheric pressure.

The catalyst was activated *in situ* for 16 h at 270 °C and 1 bar using synthesis gas with a composition of H_2/CO of 2:1 and a GHSV of 150 mL/min.g_{cat} (NTP). After the 16 h activation the reactor was purged with Ar while lowering the temperature to 250 °C. The cold knockout was drained post-activation and thereafter both the cold- and hot knockout was drained every 24 hours for the duration of the reaction run.

Upon reaching the synthesis temperature of 250 °C, the backpressure regulator was set to 20 bar and the reactor pressurised to 20 bar with Ar, after which synthesis gas flow, consisting of H_2/CO/Ar = 2:1:1, at a GHSV of 200 mL/min.g_{cat} (NTP) was initiated. CO-conversion, CH_4- and CO_2-selectivity was monitored by analysing the tail gas passed through the online GC-TCD at regular intervals. Analysis of the FTS product spectrum was done offline by sampling using the ampoule sampling technique and analysing the ampoules on GC-FID fitted with an ampoule breaker. The reactor was allowed to run for 72 h to achieve steady state before taking ampoule samples of the product gas, after which the flow rate was lowered to 160 mL/min.g_{cat}. A period 36 – 48 h at these conditions was allowed for the system to reach steady state before taking ampoule samples and adjusting the flow rate to 120 mL/min.g_{cat}. This procedure was repeated a further five times using flow rates of 100, 80, 60, 40 and 20 mL/min.g_{cat}, before returning to initial conditions at 200 mL/min.g_{cat}.

After completing the reaction run, the system was purged with Ar and depressurized to ambient pressure. The reactor temperature was lowered to 120 °C and the wax in the reactor pot removed while still liquid using a modified ladle (the catalyst particles settle out and accumulate at the bottom of the reactor pot). When the system had cooled to ambient temperature a thin wax tablet containing the spent catalyst was extracted.

3.3.5 Selectivity calculation

Overall methane selectivity and CO_2 selectivity is defined as follows:

$$S_{CH_4} = \frac{Y_{CH_4}}{X_{CO}} \tag{3.6}$$

$$S_{CO_2} = \frac{Y_{CO_2}}{X_{CO}} \tag{3.7}$$

Methane selectivity and C_{5+} selectivity on the basis of volatile organic compounds (VOC) is defined as follows:

$$S'_{CH_4} = \frac{Y_{CH_4}}{X_{CO+CO_2}} \tag{3.8}$$

$$S_{C_{5+}} = 1 - S'_{CH_4} - S'_{C_2} - S'_{C_3} - S'_{C_4} \tag{3.9}$$

The carbon number specific primary olefin selectivity (commonly referred to by some texts as the olefin/paraffin ratio) is determined as in Equation 3.10. This can be extended to include a carbon number range, e.g. determination of the olefin selectivity within the $C_2 - C_4$ product fraction.

$$S_{ole,C} = \frac{Y_{ole,C}}{Y_{ole,C} + Y_{par,C}} \tag{3.10}$$

3.3.6 GC-FID (product analysis)

A gas chromatograph with flame ionisation detector (GC-FID) equipped with ampoule breaker was used for the offline analysis of organic products that are in the vapour phase under reaction conditions. (Specifications in Table A3 in Appendix A) The ampoule collected during the FTS run sampling was placed into the heated ampoule breaker, where it was broken under N_2 flow. This flow is introduced into the split injector of the gas chromatograph through a system of valves, where after the carrier gas was switched to hydrogen.

The FID response is carbon specific. However, all carbon atoms do not show an equal response depending on the type and size of the compound. Theoretical incremental response factors (Table 3.4) suggested by Kaiser (1969) account for this. These are used to calculate compound specific FID response factors using Equation 3.10, where $R_{f,FID}$ is the specific response factor of compound i, $N_{C,i}$ is the number of carbon atoms in compound i, $N_{C,(no\ O)}$ is the number of carbon atoms in compound i not bonded to oxygen and $N_{C,(O)}$ is the number of carbon atoms in compound i with a single bond to oxygen.

Table 3.4: Kaiser theoretical incremental response factors

Carbon atom type	**Response factor**
Carbon without oxygen atoms	1.00
Carbon with single bond to oxygen	0.55
Carbon with double bond to oxygen	0.00

$$R_{f,FID} = \frac{N_{C,i}}{N_{C,(no\ O)} + 0.55N_{C,(O)}} \tag{3.10}$$

Methane as detected by online GC-TCD is used as reference compound to obtain all other flow rates in GC-FID analysis. Using the response factors and molar flow rate of methane, the flow rate of any compound can be determined using Equation 3.11, where $\dot{n}_i$ is the molar flow rate of compound i, $\dot{n}_{CH_4}$ is the molar flow rate of CH_4 as determined from GC-TCD, A_i is the GC-FID peak area of component i, A_{CH_4} is the GC-FID peak area of CH_4. The flow rate can also be expressed in terms of moles of carbon using Equation 3.12, where $\dot{n}_{i,C}$ is the molar flow rate of compound i on a carbon atom basis.

$$\dot{n}_i = \dot{n}_{CH_4} \frac{A_i}{A_{CH_4}} \frac{R_{f,FID}}{N_{C,i}} \tag{3.11}$$

$$\dot{n}_{i,C} = \dot{n}_{CH_4} R_{f,FID} \frac{A_i}{A_{CH_4}} \tag{3.12}$$

Product sampling for offline analysis on GC-FID was done using the glass ampoule sampling technique. The glass ampoules were prepared using commercially available Pasteur pipettes which were evacuated and subsequently sealed with a propane torch.

The capillary end of the sealed and evacuated ampoule was inserted into the heated ampoule sampling point, through the airtight septum and past the breaking fork. The breaking fork was rotated 90° to break off the tip of the capillary and suck the volatile organic compounds into the ampoule. A butane torch was then used to melt the capillary end and seal the ampoule. These samples were then analysed using a GC-FID equipped with a special ampoule breaking device.

4

Chapter 4: Results and Discussion

The results of the catalyst characterisation before exposure to FT Synthesis conditions as well as the results of the FTS experimental catalyst testing are given and in this chapter.

The XRD profiles of the catalyst samples indicate it to consist of majorly ferrihydrite (Fh), which is the only phase of iron detected. The presence of Al_2O_3, K_2O or $Ru_3(CO)_{12}$ was not observed in the XRD patterns. It is thought that these materials are too disperse for positive identification. BET surface areas of the catalysts were in accordance with values reported in literature, though slightly lower. This is likely due to the double calcination, where some sintering would have occurred, which the Fh reported on in literature did not undergo. The elemental composition of the catalysts before exposure to FTS as determined by ICP-OES and SEM-EDX was determined to be close to the theoretical composition when considering the weight based Fe/K ratio of 20:1 and Fe/Ru ratio 100:3 to be most important. Variability in the SEM-EDX measurements can be ascribed to sample homogeneity and analysis method, since EDX takes into account only the first few μm of the surface layer. The TPR profiles obtained for the catalysts showed two distinct reduction peaks. Reduction peaks are observed at lower temperatures in the Fe/Al/K/Ru profile, where, as expected, Ru acts as reduction promoter.

During FTS testing CO-conversion increased with increasing residence time, as is the expectation. High conversions over 95% were achieved for both catalysts. The doubly promoted catalyst (K and Ru) had a higher CH_4- and CO_2-selectivity than the catalyst promoted with K only. The methanation is thought to stem from Ru operated temperatures in excess of 180 – 200 °C and pressures below 100 bar, where Ru is known to be more selective to methane in addition to its chemical promoter effects on Fe. The high CO_2-selectivity is indicative of high WGS activity and may be linked to the presence of Ru as well, where Ru acts similarly to Cu in promoting WGS over Fe. In addition to higher

CO_2-selectivity, C_{5+}-selectivity is typically 10 – 15% lower on Fe/Al/K/Ru over the range of space velocities. Considering the loss associated with high CO_2-selectivity, a reduction in product quality is most undesirable. Additionally, both Fe/Al/K and Fe/Al/K/Ru produces a product spectrum less olefinic than reported in literature for K-promoted Fe, with Fe/Al/K/Ru underperforming when compared to Fe/Al/Cu/K or Fe/Si/Cu/K systems. Though selectivity to CH_4 and other gaseous hydrocarbons increased over Fe/Al/K/Ru, the catalyst showed increased stability as evidenced by a lesser degree of apparent deactivation of 21% over 478 h TOS vs 27% over 415 h TOS for Fe/Al/K.

4.1 Catalyst Characterisation

4.1.1 XRD

X-Ray diffractograms were obtained for the Fe/Al, Fe/Al/K and Fe/Al/K/Ru catalysts and presented in Figure 4.1. (The definitions for Fe/Al, Fe/Al/K and Fe/Al/K/Ru can be viewed in Table 3.1 in Section 3.1.3)

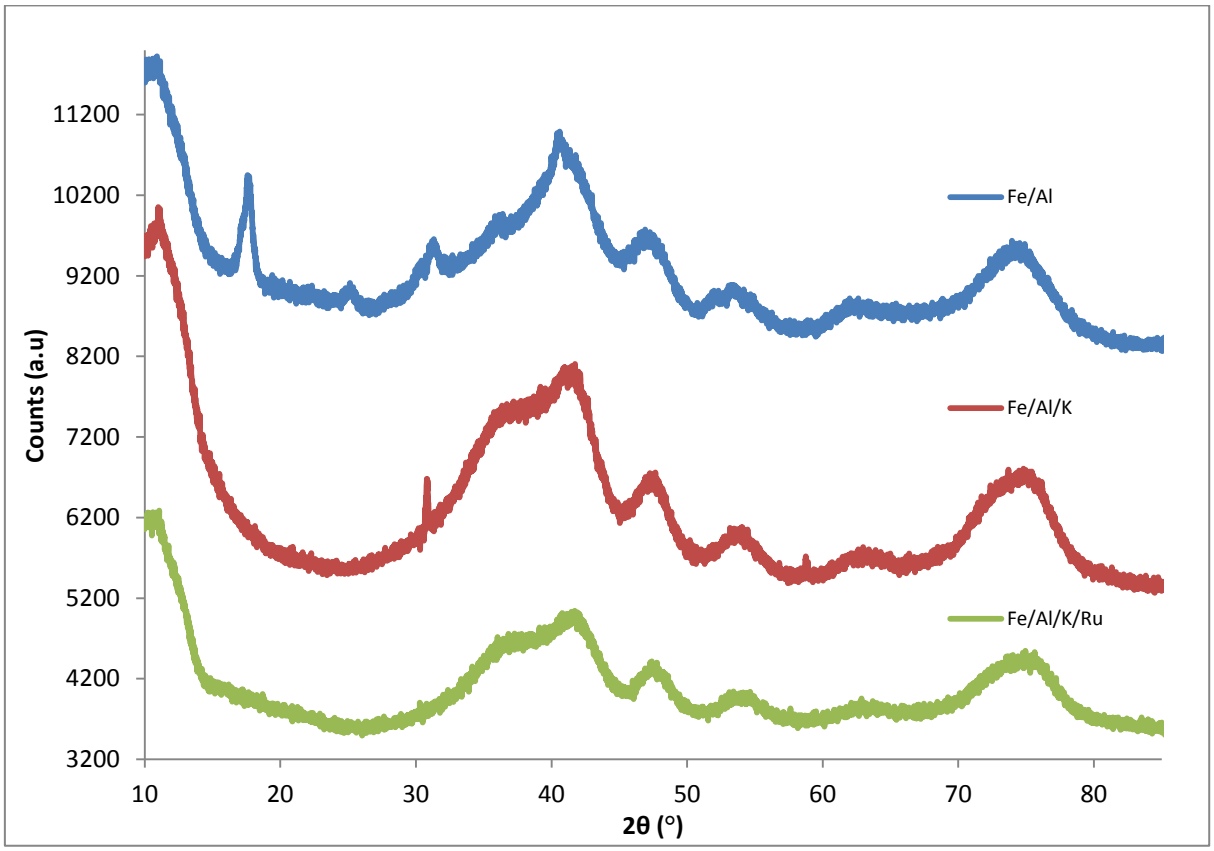

Figure 4.1: XRD patterns for the Fe-based catalysts before exposure to FTS conditions

The XRD patterns obtained for the three catalysts closely resemble that of ferrihydrite, more specifically that of 6-line ferrihydrite, and match up well to the XRD profile obtained by (Majzlan *et al.*, 2004) and the d-spacings reported by Janney *et al.* (2000) and Pan *et al.* (2006). Typically four to five broad peaks in each of the XRD patterns obtained for the catalysts are observable, corresponding to d-spacings characteristic to ferrihydrite.

Ferrihydrite (Fh) is a Fe(III) oxyhydroxide with a suggested bulk formula of $5Fe_2O_3 \cdot 9H_2O$ (Jansen *et al.*, 2002; Cudennec & Lecerf, 2006). It typically possesses only short range structural order and is characterised by poor crystallinity, small particle sizes and high dispersion, showing from two to up to seven broad range XRD peaks dependent on the degree of crystallinity (Jansen *et al.*, 2002; Majzlan *et al.*, 2004; Cudennec & Lecerf, 2006; Abdus-Salam & M'civer, 2012). The exact structure of ferrihydrite is still being debated and a number of structural models have been suggested. Its structure was first described by Towe & Bradley (1967), with the most recent suggestion by Drits *et al.* (1993) being a two phase model consisting of a defect free phase and a defective phase made up of a random distribution of the two structural fragments of the defect free phase (Jansen *et al.*, 2002; Cudennec & Lecerf, 2006).

Ferrihydrite appears in 2 main forms according to the number of observable peaks that can be found on the X-ray powder diffractogram: 2-line ferrihydrite (2LFh) and 6-line ferrihydrite (6LFh). 2LFh is the least crystalline, showing two broad peaks, while 6LFh is the most crystalline variety showing 5 – 7 broad peaks (Majzlan *et al.*, 2004; Cudennec & Lecerf, 2006). At room temperature the major d-spacings for 6LFh are reported to be 3.66 Å, 3 – 3.2 Å, 2.5 – 2.6 Å, 2.02 Å, 1.86 Å, 1.76 Å, and 1.45 – 1.58 Å (Janney *et al.*, 2000; Jansen *et al.*, 2002; Pan *et al.*, 2006).

Table 4.1 shows a summary of the expected peak positions at the reported d-spacings for 6LFh using a Co-Kα source with $\lambda = 1.78897$ Å.

Table 4.1: Expected ferrihydrite 2θ peak positions at reported d-spacings

d-spacing (Å)	Expected 2θ peak position
3.66	28.3°
3 – 3.2	32.4° – 34.7°
2.5 – 2.6	40.2° – 41.9°
2.02	52.55°
1.86	57.5°
1.76	61.1°
1.45 – 1.58	68.9° – 76.1°

The relatively sharp peak at ± 17° in the Fe/Al XRD profile did not match any possible compounds expected to be in the sample (based on the element present) and could not be identified. It was initially thought to be a shifted peak attributed to the 3.66 Å d-spacing. This peak would be expected at ± 28°. The small peak at ± 24° would be a more likely candidate for this d-spacing. Also a peak shift of 10° seems unlikely. Thus the 17° peak remains unidentified. Similarly the spike at ± 31° in the Fe/Al/K pattern does would match the 3 Å d-spacing for Fh, but its sharp and narrow nature does not conform to the broadness expected in Fh patterns and neither does it seem to belong to other expected compounds.

Ferrihydrite commonly occurs as a corrosion product in the iron- and steel industries (Jansen *et al.*, 2002). It is also a naturally occurring meta-stable mineral, being one of the eight naturally occurring iron ores (Abdus-Salam & M'civer, 2012). Due to its meta-stable nature it is known to be a precursor to more stable and crystalline minerals like hematite and goethite (Majzlan *et al.*, 2004; Cudennec & Lecerf, 2006; Abdus-Salam & M'civer, 2012). It is most formed by the rapid oxidation of Fe^{2+} solutions followed by hydrolysis in the presence of crystallisation inhibitors. In high pH precipitations it would seem to be the primary precipitate formed as a precursor to goethite (Jansen *et al.*, 2002). Due to the high surface area associated with ferrihydrite, it is most widely investigated for its adsorbent properties (Abdus-Salam & M'civer, 2012).

The X-ray diffractograms show no visible peaks that can be ascribed to Al_2O_3. This makes sense if one takes into account the relatively low percentage of Al_2O_3 in the catalyst samples and possibly the amorphous precipitated Al_2O_3 was not able to attain sufficient crystallinity during calcination at 350 °C or the phase is too dispersed within the bulk iron phase. The XRD patterns for Fe/Al/K and Fe/Al/K/Ru also show no peaks to indicate the presence of K_2O. Considering the amount of K-salt used for impregnation, the formation of large discernible crystallites is unlikely. If the catalysts

are, for the most part, very homogeneous it is very likely that very small crystallites of Al_2O_3 are present and highly dispersed within the bulk Fe-phase and very small K_2O crystallites are scattered widely over the entire surface area of the catalyst. This would make any structural information regarding Al_2O_3 and K_2O indiscernible as it would be obscured by the broad ferrihydrite XRD pattern.

The Sherrer equation was used for the estimation of the average ferrihydrite crystallite size. This was determined as ranging from $20 - 32$ Å ($2 - 3.2$ nm). Since diffraction peaks belonging to Al_2O_3, K_2O and $Ru_3(CO)_{12}$ were indiscernible, crystallite size estimation using the Sherrer equation was not possible for the other components of the catalysts.

4.1.2 Elemental composition (ICP-OES and SEM-EDX)

SEM-EDX and ICP-OES results were normalised to show metals content only and compared to the targeted elemental composition for the catalysts. This is shown in Table 4.2.

Table 4.2: Normalised elemental compositions of the catalysts (wt%)

	ICP-OES				SEM-EDX				Target			
Catalyst	**Fe**	**Al**	**K**	**Ru**	**Fe**	**Al**	**K**	**Ru**	**Fe**	**Al**	**K**	**Ru**
Fe/Al/K	57.24	8.45	2.53	-	57.02	9.5	2.6	-	48.83	7.75	2.44	-
Fe/Al/K/Ru	59.70	8.76	2.3	1.72	49.91	6.86	1.60	1.40	38.78	6.42	2.02	1.95

It is assumed that the percentage of adsorbed water (water that is adsorbed eternally and does not form part of the ferrihydrite structure) is negligible and thus its impact on the results should be negligible. Also, it is further assumed that even though EDX cannot detect hydrogen, the error associated with this is negligible since hydrogen would make up less than 2% of the catalyst mass assuming the catalyst to consist of majorly ferrihydrite based on the targeted Fe, Al, K and Ru percentages.

ICP-OES results are in fairly close agreement with one another, though the Fe and Al percentages in Fe/Al/K/Ru are slightly higher than expected and exceed those obtained for Fe/Al/K. This is a somewhat illogical result since the iron content of a sample diluted by further addition of promoters should not increase. It is suspected that a contributing factor to this inconsistency may be the decomposition of $Ru_3(CO)_{12}$ during digestion

which decreases the sample mass by ± 98% and is not accounted for when using the raw sample mass. Additionally, it may also be that some volatiles are formed during the digestion and that the sample contained some adsorbed water that is lost in the analysis. It may be that either or both of these factors have influenced the measurement to some degree.

There is some variability in the EDX results confirming that the techinique is inherently somewhat flawed and dependent on homogeneity of the sample as well as specific particle targeting. The discrepancy between the ICP- and EDX- as well as individual sample results may be partly explained by assumption of homogeneity, which may not always hold true, especially for smaller samlple subsets. It may, however, be true for the bulk. Adittionally, EDX only provides information on the first few μm of the outer surface area of individual particles and this does necessarily reflect the bulk composition of the particle itself. When taking into account the limited control during precipitation and impregnation, the outer surface area will not necessarily reflect the inner surface area of the particle, or its bulk composition for that matter. It is thus worth noting that the assumption of complete homogeneity is an over simplification during the characterisation and that individual samples used in the analyses may differ to a certain degree, but that the sample in broader terms may show a geater degree of homogeneity. That being said, EDX does, however, provide a quick and easy ball park estimate of the elemental composition.

It is noteworthy that the EDX and ICP results were highly similar for Fe/Al/K. Taking this result into account, it is highly likely that differences in individual particle composition could have played a major role in the discrepancies observed between ICP and EDX measurements.

Overall, though, the elemental compositions are not too far off the mark from the targetted compositions if one takes into account the targetted Fe/K ratio and Fe/Ru ratio of 20:1 and 100:3, respectively. Assuming ICP-OES to be the more reliable of the measurement techniques, Fe/K ratios of about 23:1 and 26:1 were obtained for Fe/Al/K and Fe/Al/K/Ru catalysts, respectively, while a Fe/Ru ratio of about 104:3 was obtained for Fe/Al/K/Ru. Though a Fe/Al ratio of roughly 25:4 was targeted and the ICP measuremnts puts the ratio at about 27:4 for both catalysts, meaning a slightly higher Fe/binder ratio, this is not expected to affect the catalysts' performance too significantly, if at all.

4.1.3 N_2-Physisorption (BET)

The N_2-physisorption results can be seen in Table 4.3.

Table 4.3: N_2-physisorption results for the Fe/Al/K and Fe/Al/K/Ru catalysts

	Catalyst	
Parameter	**Fe/Al/K**	**Fe/Al/K/Ru**
BET surface area (m^2/g)	176.6	171.9
BJH desorption surface area of pores 1.7 nm – 300 nm (m^2/g)	273.4	247.9
BJH desorption cumulative volume of pores 1.7 nm – 300 nm (cm^3/g)	0.29	0.26
BET average pore diameter (nm)	5.54	5.16
BJH desorption average pore diameter (nm)	4.3	4.2

BET surface areas were calculated as 176.6 m^2/g and 171.9 m^2/g for Fe/Al/K and Fe/Al/K/Ru, respectively. BJH adsorption cumulative pore volumes, in the same order, were 0.29 cm^3/g and 0.26 cm^3/g, repectively.

The surface area results compare well with the ultrahigh surface area claim in the range of up to 200 m^2/g for ferrihydrite as reported by Abdus-Salam & M'civer (2012). Calculated catalyst BET surface area results are also in relative agreement with the value of 186.8 m^2/g by Juncosa (2008) for 6LFh, 183 m^2/g for the 100 Fe/18 SiO_2/5 Cu/5 K catalyst by Chun *et al.* (2014) (which consisted of a mixture of hematite and >80% ferrihydrite), as well as the Fe/Cu/K/SiO_2 catalyst prepared by Hayakawa *et al.* (2006) with a surface area of 175 m^2/g. Though differing in preparation, compositionally the catalyst prepared by Chun *et al.* (2014) is similar to Fe/Al/K/Ru in that a similar binder loading was used and similar promoter loadings were used (promotion with Cu was at 5%, whereas Fe/Al/K/Ru used Ru at 3%).

The BET surface area of 175 m^2/g and pore volume of 0.273 cm^3/g for the 100 Fe/0.3 Cu/2 K/8.8 SiO_2 catalyst prepared by Hayakawa *et al.* (2006) also closely matches that obtained for Fe/Al/K and Fe/Al/K/Ru. The XRD profile for their catalyst does differ though, but is highly similar to that of ferrihydrite, when comparing to the x-ray diffractograms of Majzlan *et al.* (2004), where two very distinct broad peaks are observed. However, the authors ascribe the profile to supressed Fe_2O_3 crystal growth or SiO_2-stabilised non-crystalline FeOOH. Juncosa (2008) reported a BET surface area of 44.6 m^2/g for synthetic goethite, while Laberty & Navrotsky (1998) reported surface areas of 39.2 – 41.2, 40.2 and 35.2 m^2/g for goethite, akageneite and lepidocrocite, respectively. Goethite and lepidocrocite is known to be crystalline, leaving only

akagenite as possible non-crystalline iron phase. However, the surface area measured by Hayakawa *et al.* (2006) is more than four times what would be expected for akageneite, suggesting that the catalyst's major iron phase is ferrihydrite. In that case their catalyst matches up very well to the data in Table 4.3.

The lower obtained values of surface area for the Fe/Al/K and Fe/Al/K/Ru catalyst samples make sense considering the catalysts were calcined twice for 16 h at 350 °C. The 6LFh prepared by Juncosa (2008) was not calcined, whereas the Fe-catalyst prepared by Chun *et al.* (2014) underwent a single calcination of 8 h at 400 °C. Though the calcination temperature of 350 °C was chosen to be mild enough to prevent gross surface area loss due to sintering, some loss will still occur. Also the catalysts were both promoted with potassium and it may have been a factor contributing to surface area loss by surface enrichment with K, which would be consistent with findings by Özkara-Aydınoğlu *et al.* (2012) on their K-promoted Fe-catalysts. It would thus not be unreasonable to presume the uncalcined catalysts had a higher surface area in the range of that reported by Juncosa (2008) and Chun *et al.* (2014) or even approaching 200 m^2/g.

Pore size and pore surface area results would suggest the catalyst samples to be majorly mesoporous. Average pore diameters calculated using BET were 5.5 nm and 5.2 nm and from BJH desorption were 4.3 nm and 4.2 nm, for Fe/Al/K and Fe/Al/K/Ru, respectively. The majority of the calculated cumulative pore area (± 72%) falls within the pore diameter range of 2 – 50 nm for both the Fe/Al/K and Fe/Al/K/Ru catalysts.

4.1.4 TPR

The TPR profile for the Fe/Al/K and Fe/Al/K/Ru catalyst is shown in Figure 4.2. The difference in TCD signal intensity is due to the difference in sample mass used for the TPR experiments, Fe/Al/K/Ru being 100 mg and Fe/Al/K being 50 mg.

Typically a two or three peak reduction profile is obtained for iron catalysts. The first two peaks are ascribed to the reduction of CuO to Cu and Fe_2O_3 to Fe_3O_4 in the case of Cu-promoted Fe-catalysts. Sometimes these two peaks overlap. The third peak represents the reduction of Fe_3O_4 and residual Fe_2O_3 to α-Fe.

The TPR profile of the Fe/Al/K catalyst shows two distinct reduction peaks; a primary peak at ± 345 °C and a much broader secondary peak at around 750 °C. The TPR profile of the Fe/Al/K/Ru catalyst shows a primary peak at ± 200 °C and a broad secondary peak around 620 °C. Unlike with Fe-Cu systems, where a small peak is sometimes visible

before the Fe_2O_3 reduction peak, as is the case with the Fe/Cu catalyst prepared by Wan *et al.* (2008), Fe/Al/K/Ru shows only 2 distinct reduction peaks. Since Ru was deposited as $Ru_3(CO)_{12}$ and the organometallic complex decomposes thermally to Ru at 175 °C, a major TCD response is not expected. A slight bulge at the start of the primary reduction peak is observed which may be ascribed to the TCD response to the decomposition products in the tail gas.

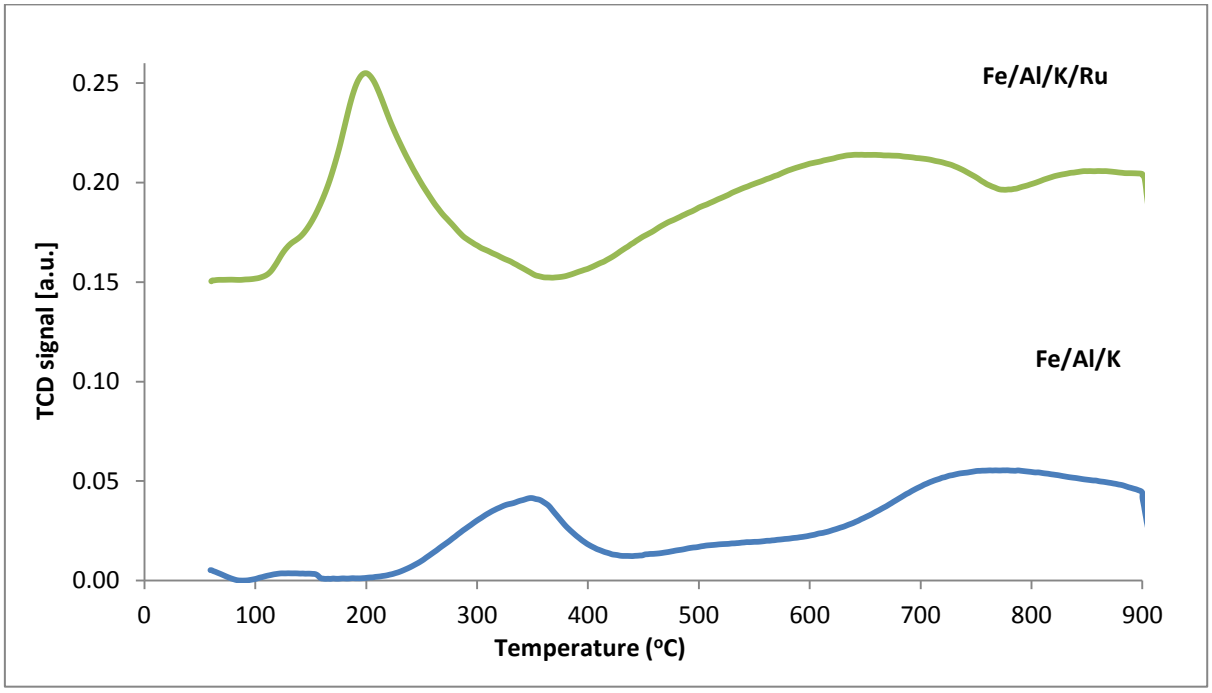

Figure 4.2: H_2-TPR profiles for the Fe/Al/K and Fe/Al/K/Ru catalysts

Comparing the effects of the promoters in the TPR profiles obtained by Wan *et al.* (2008) for Fe/Cu, Fe/Cu/K, Fe/K and Fe, it is clear that Cu served to reduce the reduction peak temperatures (normally by around 100 – 150 °C) when comparing Fe to Fe/Cu and Fe/K to Fe/Cu/K. A similar trend is seen when comparing the TPR profiles for Fe/Al/K and Fe/Al/K/Ru, where a primary- and secondary reduction peak temperature shift of about 150 °C and 130 °C, respectively, was observed. Here ruthenium thus acts similarly to copper in lowering the reduction temperature and thereby improving the reducibility of the catalyst.

The shift to lower reduction temperatures (similar to Cu and what has been found for other noble metals) is expected with the addition of Ru, based on the observations of authors such as Berry *et al.* (1985), van der Kraan *et al.* (1986) and Bahome *et al.* (2007). Based on the observations by authors such as Li *et al.* (2002), the effect of Ru is expected to be stronger than that of copper. It was found that Ru acts similarly to Cu

and Pt in its reduction promoting effect. In the study on platinum promoted, silica supported Fe-based catalysts by Xu *et al.* (2003) with a 10% Fe- and 1% Pt-loading, TPR profiles showed comparable trends as in Figure 4.2. The addition of platinum served to reduce reduction peak temperatures by about 100 °C when comparing the non-potassium promoted Fe/SiO_2 and $Fe/Pt/SiO_2$ catalysts. Similar results were seen with carbon nanotube (CNT) supported Fe/Ru catalysts prepared by Bahome *et al.* (2007). Shifts to lower reduction temperatures were seen on catalysts with the same Fe/Ru ratio, but higher metals loading, as well as on catalysts with the same Fe-loading, but higher Ru-loading. The latter illustrates that the effect is ascribed to the presence of Ru rather than Fe crystallite sizes and the existence of metal-support interactions as the authors pointed out. This is very similar to the observation for Fe/Al/K vs. Fe/Al/K/Ru.

What is also seen in the TPR profiles by Wan *et al.* (2008) is that incorporation of K into the catalyst serves to increase reduction temperature, as evidenced by the 50 – 100 °C higher primary reduction peak temperatures of Fe/K vs. Fe and Fe/Cu/K vs. Fe/Cu. This was also seen in the TPR profiles obtained for SiO_2-supported Fe/Pt and Fe/Pt/K by Xu *et al.* (2003), where reduction peak temperatures increased by around 50 °C. A study by Wan *et al.* (2007b) on unpromoted Fe-catalysts with and without Al_2O_3 binder the TPR showed that the presence of Al_2O_3 increased the temperature of the primary reduction peak. These findings would suggest the use of a reduction promoter when structurally promoting Fe-catalysts as well as when chemically promoting with K to be fairly important.

The TPR profile obtained by Chun *et al.* (2014) with peaks at around 250 °C and 650 °C for their 100Fe/18 SiO_2/5 Cu/5 K closely resembles that obtained for Fe/Al/K/Ru with peaks at 200 °C and 620 °C. The catalysts resemble one another fairly closely in composition when looking at Fe/binder ratio and dominant Fe phase being ferrihydrite. Cu-loading is 5% vs. 3% for Ru and K-loading is around 5% for both. It is thus not surprising that the profiles should look similar. In a study on binder effects by Wan *et al.* (2007a), comparing SiO_2 and Al_2O_3, it was found that SiO_2 seems to facilitate reduction whereas Al_2O_3, as in the TPR experiment of Wan *et al.* (2007b), decreases the catalyst reducibility. Keeping the findings of Wan *et al.* (2007a) and Wan *et al.* (2007b) in mind, it would seem that Ru may be a more effective reduction promoter than Cu when comparing reduction peak temperatures of Chun *et al.* (2014) vs. Fe/Al/K/Ru. This presumption is further reinforced by the TPR results on Fe/ZnO catalysts of Li *et al.* (2002), which shows reduction peak temperatures to be 50 – 100 °C lower for the Ru-promoted catalyst vs. the Cu-promoted catalyst.

4.2 FTS Catalyst Testing

4.2.1 CO-conversion and overall CH_4- and CO_2-selectivity

A plot of CO conversion, CO_2 and CH_4 selectivity at different GHSV and with time on stream (TOS) for Fe/Al/K and Fe/Al/K/Ru catalysts are presented in Figures 4.3 and 4.4 respectively. (Selected experimental data included in Tables A10 and A11 in Appendix A.)

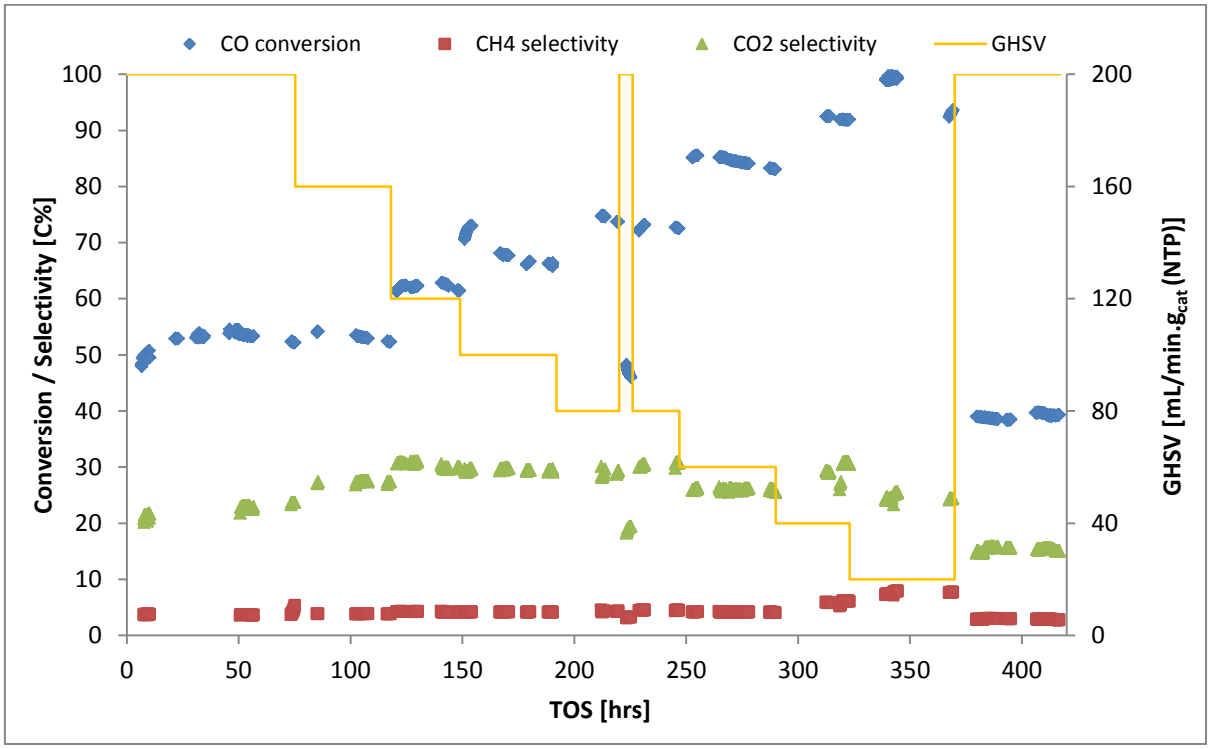

Figure 4.3: CO-conversion and overall CH_4- and CO_2-selctivities with TOS for Fe/Al/K

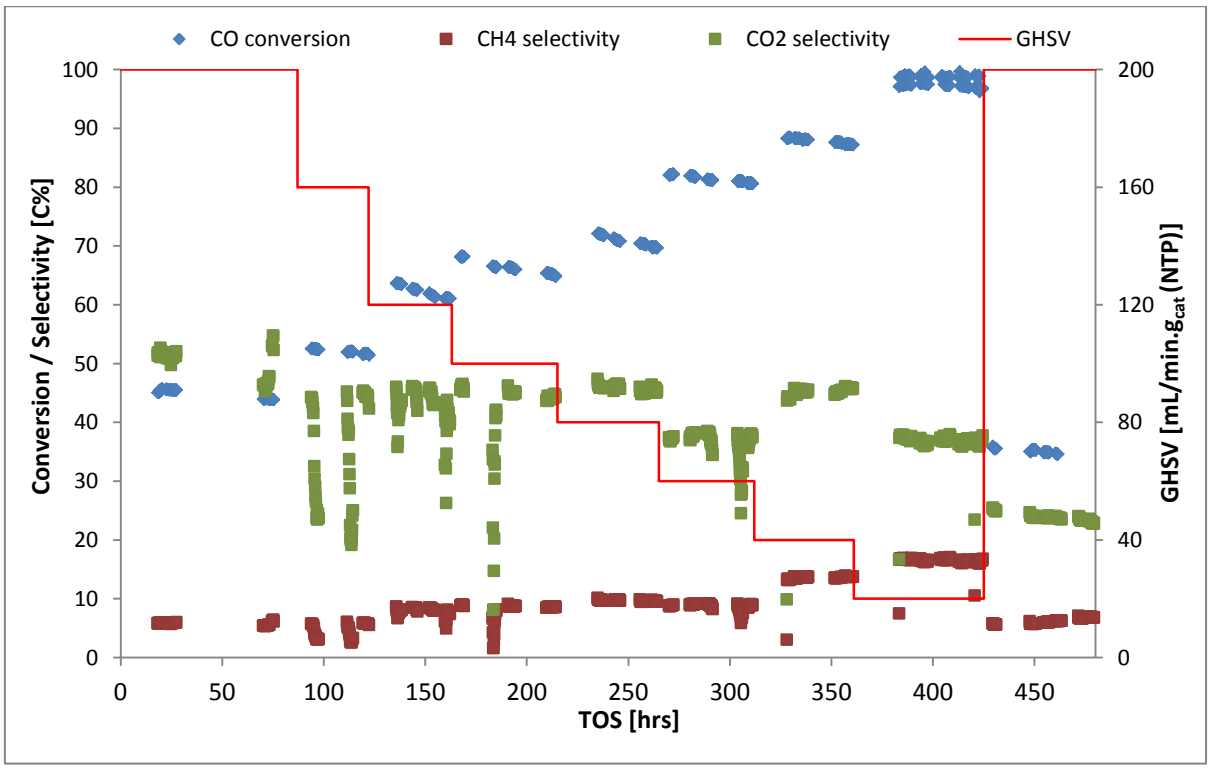

Figure 4.4: CO-conversion and overall CH_4- and CO_2-selctivities with TOS for Fe/Al/K/Ru

Both plots show an increasing CO-conversion with decreasing space velocity (increased residence time), as predicted by literature (Bukur *et al.*, 1990; Iglesia *et al.*, 1991; Kuipers *et al.*, 1996).

In Figure 4.3 it can be seen that for Fe/Al/K an initial steady-state CO-conversion of about 54 % was attained at a space velocity of 200 mL/min.g_{cat} (NTP) and a conversion of 39.6 % was recorded after returning to the initial conditions. This points to an apparent deactivation of about 26.6 % over the 415 hrs TOS.

Interruptions to the system were experienced on two occasions during the Fe/Al/K experiment, one being more severe than the other. After a 1 hour power outage at 220 hours TOS the reaction was reinitiated at the initial space velocity. After 6 hours at this space velocity a CO-conversion level of 48% was measured and the experiment continued at the previous space velocity of 80 mL/min.g_{cat} since apparent deactivation of the catalyst was in the range 5%. When sampling at 367 hours the system was not at steady state due to another interruption experienced by the system at 340 hours TOS, which went unnoticed until after the completion of the experiment.

The highest level of CO-conversion was attained at 99% and a space velocity of 20 mL/min.g_{cat}. Corresponding CO_2- and methane selectivities were 25% and 7.5%, respectively. A relatively stable overall CH_4-selectivity was observed at around 4 – 4.5%

rising to a maximum of 7 – 7.4% at the highest achieved conversion level of ± 98%. This is to be expected since decreasing space velocity and increasing conversion is known to increase CH_4-selectivity (Van der Laan & Beenackers, 1999; Cairns, 2008; Chonco, 2014).

For Fe/Al/K overall CO_2-selectivity seems to rise gradually from an initial value of about 20.7% and level off at around 30%. Though expected to increase with increasing conversion level, lower CO_2-selectivities of around 25 – 26% are observed at 84%, 92% and 99% conversion. The lowest value of 15.3% was observed at 39.6% conversion when returning to initial conditions.

In Figure 4.4 a lower initial steady-state conversion was achieved for Fe/Al/K/Ru at 44% and reached a maximum of close to 99% at the lowest space velocity, while upon returning to initial flow conditions a steady-state conversion of around about 35 % is obtained. This implies an apparent deactivation of about 21% over the 478 hrs TOS. In terms of stability, this is a better result than the 27% deactivation observed with Fe/Al/K over 415 hrs.

It should be noted that not only did Fe/Al/K/Ru undergo operation at FTS conditions for a longer total period of time, but due to the upset in the Fe/Al/K experiment at 340 hrs TOS the Ru-promoted catalyst spent more time at ultra-high CO-conversion conditions (around twice as long). Yet Fe/Al/K/Ru showed a markedly lower extent of apparent deactivation. This result would imply the Ru-promoted Fe-catalyst would be operable at very high levels of CO-conversion for significantly longer than Fe/Al/K. Taking into account the CO_2-selectivity of Fe/Al/K/Ru, this improved resistance to deactivation is in large part probably due to less exposure to water seeing as the catalyst seems to possess more water-gas-shift activity than the non-Ru-containing catalyst. Ru may also be playing a part in facilitating the recarburisation of magnetite crystallites as is proposed for Fe-Cu-systems by Chonco *et al.* (2013), thereby ensuring higher sustained levels of iron carbides and resulting in a catalyst with more stable activity.

Compared to the initial CO-conversion over Fe/Al/K at 54 %, the initial CO-conversion over Fe/Al/K/Ru at 44% is significantly lower. This could be partly explained by the slightly lower Fe-loading for the same mass of catalyst as well as additional Fe active site coverage by Ru. However, it should also be noted that though the Fe/Al/K initial CO-conversion was higher it also remained constant despite a decrease in space velocity, unlike Fe/Al/K/Ru attaining a steady-state conversion level of ± 51.8% which is similar to the Fe/Al/K conversion level at this same space velocity. Considering the very similar

levels of CO-conversions attained at the same space velocities, both catalysts would seem to be equally active for the most part and differ mainly in their product selectivity.

Selectivity to methane for Fe/Al/K/Ru follows a similar trend to Fe/Al/K, rising with decreasing space velocity. CH_4-selectivity is, however, observed to be nearly double that observed for Fe/Al/K. CH_4-selectivity attains minimum steady-state values during initial run-in and upon returning to initial conditions at 5 – 6% (44% and 34% CO-conversion, respectively) and maximum of 16% at 98% conversion.

The CH_4-selectivity of the Fe/Al/K/Ru catalyst is also much higher (almost double that observed for Fe/Al/K). This higher methane selectivity can be linked to the enhanced methane production attributed to "high temperature" and "low pressure" operation for Ru. It is also known that higher H_2/CO ratios increase methane selectivity and thus this result should not be too surprising considering the high WGS activity of the catalyst producing additional hydrogen in addition to the 2:1 H_2/CO ratio fed to the reactor.

At 25 – 28% CO-conversion Bahome *et al.* (2007) noted very similar methane selectivities over CNT supported 10Fe/0.25Ru and 10Fe/0.25Ru/0.2K catalysts. This would suggest the methanation activity to be mostly ascribed to the presence of Ru and probably its interaction with Fe, which is in keeping with the result of higher CH_4-selectivity over Fe/Al/K/Ru compared to Fe/Al/K. In their study FTS was carried out at 8 bar, 275 °C and H_2/CO = 2:1, so knowing Ru to be almost purely selective to CH_4 at 1 atm and 300 °C (Davis & Maitlis, 2013), it can probably be safely assumed that at the reaction conditions, if Ru is acting as both promoter and FT-catalyst, its FT-activity would produce significant amounts of methane. It is suspected that the higher CH_4-selectivity over Fe/Al/K/Ru is due to a combination of a chemical promotion effect of Ru as well as ruthenium's inherent FT-activity and product distribution at the operating conditions.

It is noted that a much higher CO_2-selectivity is observed for Fe/Al/K/Ru. Some variation in the data is observed, the cause of which is unclear. An overall trend is still visible, however, where CO_2-selectivity seems to be at a relatively stable value of around 44 – 47% with exception at 81% and 98% CO-conversion, where CO_2-selectivities around 38% are observed. The higher CO_2-selectivity may be partly explained by re-carburization of magnetite crystallites being enhanced by Ru, similarly to Cu as proposed by Chonco *et al.* (2013). However, enhanced re-carburisation of magnetite alone would not explain the significant increase in CO_2-selectivity. Since Ru shows no WGS activity on its own (Van der Laan & Beenackers, 1999), an increase in CO_2-selectivity at the same or similar CO-conversion levels must stem from a promotional effect of Ru enhancing WGS over Fe.

Non-structurally promoted, potassium and copper promoted Fe-catalysts tested by Özkara-Aydınoğlu *et al.* (2012) at 250 °C, 19 bar, $H_2/CO = 2:1$ and 50 mL/min.g_{cat} were able to achieve high CO-conversions ranging from 80 – 98%, thus attaining similar levels of CO-conversion as in this work. The highest conversion level of 98% was attained over a 100 Fe/7 Cu/3 K catalyst. All their catalysts had relatively high CO_2-selectivities of between 40% and 65%, the highest being over the catalysts containing 3wt% Cu. Similar high CO_2-selectivties of 30 – 45% were observed by Xu *et al.* (2003) over SiO_2-supported Fe/Pt catalysts, though not much higher than non-Pt-promoted Fe. This causes doubt as to whether noble metals promote WGS over Fe, but considering the similarities between lower WGS activity and CO_2-selectivities over Fe/K catalysts vs. Fe/Cu/K catalysts and the results presented for Fe/Al/K vs. Fe/Al/K/Ru, it seems likely that Ru plays a similar role to Cu during FTS with regard to WGS. Hayakawa *et al.* (2007) observed appreciable CO_2 formation (39 – 44%) over precipitated K-promoted Fe/SiO_2, understandably due to the low H_2/CO ratio of 1:1, but with low CH_4- and high C_{5+}-selectivity, thus performing better in terms of product quality than Fe/Al/K or Fe/Al/K/Ru.

4.2.2 CH_4- and C_{5+} Selectivity

Table 4.4 shows the methane- and C_{5+}-selectivities for the Fe/Al/K and Fe/Al/K/Ru catalysts on the basis of volatile organic compounds (VOC) at the sampling intervals.

Table 4.4: CH_4- and C_{5+}-selectivities (on VOC basis) at sampling intervals

Fe/Al/K									
TOS	**74**	**117**	**148**	**191**	**246**	**289**	**319**	**368**	**415**
$\mathbf{X_{CO}}$	52.31	52.35	61.47	66.05	72.64	83.15	91.93	93.18	39.15
$\mathbf{S'_{CH4}}$	5.22	5.2	5.9	5.8	6.5	5.5	7.44	10.11	3.26
$\mathbf{S_{C5+}}$	87.03	86.58	85.70	85.11	86.04	87.78	82.73	81.56	91.92
Fe/Al/K/Ru									
TOS	**72**	**121**	**161**	**213**	**263**	**310**	**360**	**424**	**478**
$\mathbf{X_{CO}}$	44.02	51.72	61.14	65.18	69.79	80.69	87.27	96.78	34.35
$\mathbf{S'_{CH4}}$	10.18	10.45	13.26	15.36	17.68	14.31	25.39	26.21	8.88
$\mathbf{S_{C5+}}$	77.29	76.15	74.92	70.52	66.97	71.86	52.03	57.00	81.09

Over the duration of the experiments it is clear that the Fe/Al/K catalyst has a consistently higher C_{5+}-selectivity and, conversely, a lower CH_4-selectivity, than Fe/Al/K/Ru. In keeping with the expectation an increased CH_4-selectivity is observed with increased CO-conversion and decreased space velocity. Though generally C_{5+}-

selectivity has a somewhat complex relationship with space velocity, it would generally be expected that C_{5+}-selectivity increase with decreasing space velocity as a higher chain growth probability would be expected to result from a higher residence time. Though not abundantly apparent in Table 4.4 (especially for Fe/Al/K), the data would suggest an inverse proportionality between CO-conversion and and C_{5+}-selectivity. Consequently the same can be said for C_{5+}-selectivity and space velocity. However, an inverse proportionality between CH_4- selectivity and C_{5+}-selectivity is quite apparent and expected.

Considering the known behaviour of Ru and known effects of Cu-promotion the increased methane selectivity is expected. However, it was hoped that the changes in selectivity would be less pronounced than what is observed to be more in line with what is observed with Cu. It is also clear from Figures 4.3 and 4.4 that Fe/Al/K/Ru possesses much higher WGS activity than Fe/Al/K considering the nearly 50% increase in the CO_2-selectivities at the same space velocities and highly similar conversion levels. In light of this it is highly undesirable that the selectivity to gaseous hydrocarbons should increase with such high CO_2-selectivities.

C_{5+} selectivities observed by Özkara-Aydınoğlu *et al.* (2012) were all below 60% (some below 40%), except for the 7:1 Cu/K ratio Fe-catalyst. CH_4-selectivities over their catalysts were considerably higher than observed for Fe/Al/K, but lower than for Fe/Al/K/Ru. Both catalysts thus performed better with respect to C_{5+}-selectivity in this work.

Contrary to what is normally reported for K-promoted iron, comparing the Fe/Ru and Fe/Ru/K catalyst of Bahome *et al.* (2007), tested at 275 °C and 8 bar, higher selectivity to lighter hydrocarbons is observed and almost no effect is seen with regard to CH_4-selectivity (at ±25% CO-conversion). Though most of the Fe/Ru catalysts study had C_{5+}-selectivities below 55%, the K-promoted Fe/Ru catalyst had a markedly lower C_{5+}-selectivity and selectivity to C_{12+} of close to zero. At higher CO-conversion (40 – 50%) the K-promoted catalyst had a markedly higher selectivity to C_{5+}, though still in the range of 55%, and a significantly lower CH_4-selectivity than the non-potassium promoted Fe/Ru.

At a similar conversion level of 70 – 80%, CH_4-selectivity and C_{5+}-selectivity of Fe/Al/K is similar to that reported by Wan *et al.* (2008) for their Fe/K catalyst. However, methane selectivity is much higher and C_{5+}-selectivity much lower over Fe/Al/K/Ru compared to their Cu- and K-promoted catalyst.

Observations by Iglesia *et al.* (1991) on FTS over Ru suggest an increasing molecular weight of product should be observed with decreasing space velocity. The opposite is observed with the Fe/Al/K/Ru catalyst looking at the lower- and decreasing C_{5+}-selectivity, probably due to the low loading of Ru. Bukur *et al.* (1990) found no corellation between the molecular weight distribution of the product and change in space velocity over Fe. This was, however, not the observation for Fe/Al/K nor Fe/Al/K/Ru since a clear shift to lower molecular weight products is seen.

Since ruthenium is used here as promoter, but is also a FT-catalyst in its own right, it is dificult to predict exactly the effect on selectivities when used in conjunction with precipitated Fe. Whether, here, Ru is acting as promoter, catalyst or both is not abundantly clear, but likely it is acting both as catalyst and promoter judging by the doubling of the CH_4-selectivity. In light of the loading used it is likely that the promotional effects of Ru will overshadow the catalytic effects.

Knowing Ru to show an increased methane selectivity with lower pressure and increased temperature (Pichler *et al.*, 1964; Everson *et al.*, 1978; Davis & Maitlis, 2013), it is expected that methane selectivity should be higher over Fe/Al/K/Ru than Fe/Al/K. In general also methane selectivity tends to increase with increasing conversion and this was seen over Fe/Al/K as well.

It is thought that methane selectivity was probably somewhat suppressed over Fe/Al/K/Ru during FTS at high conversions (though not necessarily noticeably), at least for Ru acting as FT-catalyst. Though it is known that Ru will have a significant selectivity to CH_4 at the reaction conditions (considered high temperature and low pressure for Ru), the presence of water has been found to increase selectivity to C_{5+} and lower CH_4-selectivity by Claeys & Van Steen (2002) in water co-feeding studies. Additionally, the Hibbitts *et al.* (2013) DFT study suggests water to act as co-catalyst and increase chain growth probability. Considering the results of Claeys & Van Steen (2002) where CH_4-selectivity reduced from 30C% to 20C% corresponding to water partial pressure increase from 0.2 bar to 4.5 bar (15 – 20 bar total pressure and 200 °C), it would not be unreasonable to assume that the catalytically active Ru should undergo the same type of CH_4-selectivity suppression as conversion levels increase. Therefore, the overall CH_4-selectivity of the catalyst should be somewhat suppressed by virtue of CH_4-selectivity suppression over Ru. However, with the low loading of Ru compared to Fe, and depending on how much of the Ru is catalytically active, it is not likely that the reduced selectivity would be observable given the already enhanced CH_4-selectivity of the catalyst, which would seem to stem from chemical promotion.

4.2.3 Olefin selectivity

Figures 4.5 and 4.6 show the carbon number specific olefin selectivities for the C_2, C_5 and C_9 product fractions for Fe/Al/K and Fe/Al/K/Ru, respectively.

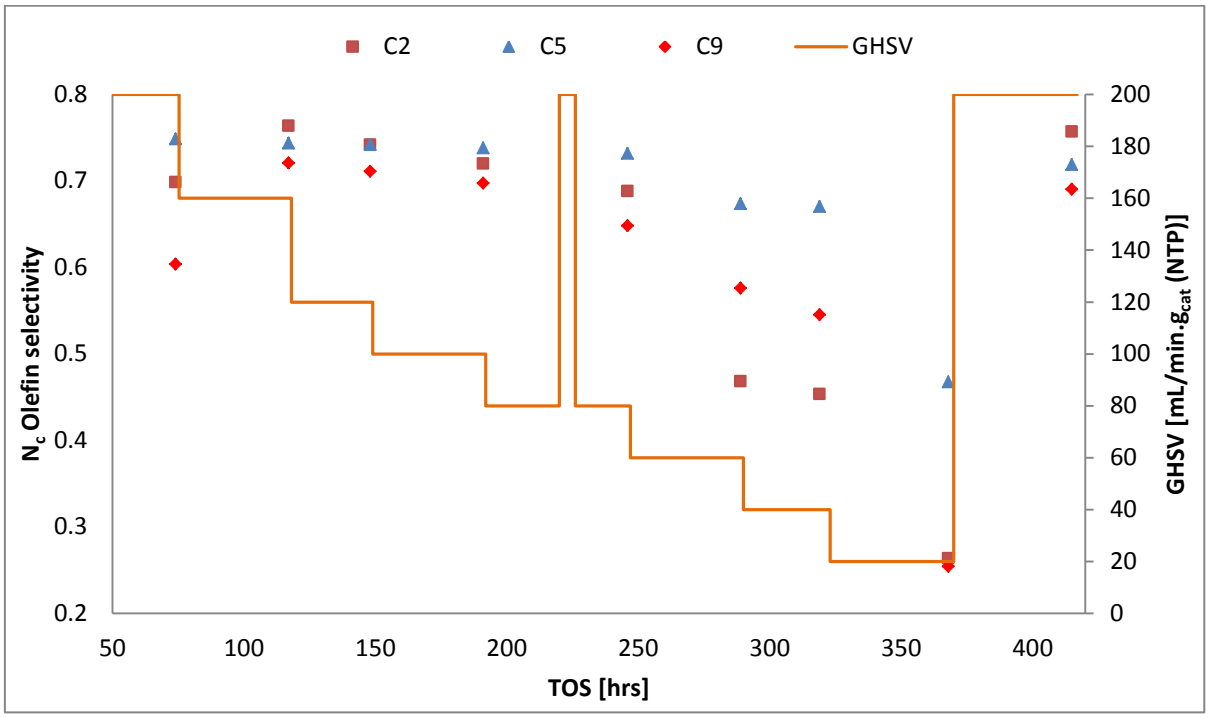

Figure 4.5: Fe/Al/K carbon number specific olefin selectivity for C_2, C_5 and C_9

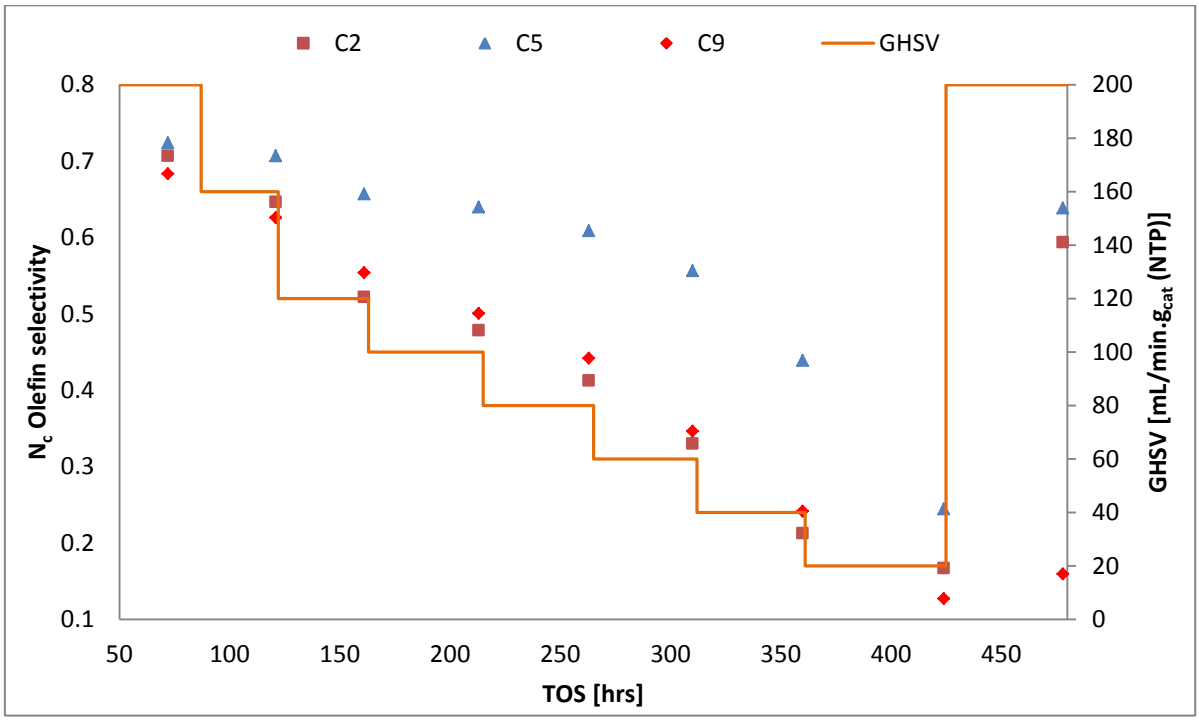

Figure 4.6: Fe/Al/K/Ru carbon number specific olefin selectivity for C_2, C_5 and C_9

The primary olefin to linear paraffin ratio for the two catalysts at similar approximate CO-conversion for the $C_2 – C_9$ products is shown in Table 4.5. (In Table 4.5 Fe/Al/K and Fe/Al/K/Ru have been abbreviated to Fe/K and Fe/K/Ru, respectively.)

Table 4.5: Primary olefin to linear paraffin ratios for $C_2 – C_9$ at similar CO-conversion

X_{CO}	52%		61%		69 - 73%		81 – 83%	
Cat.	**Fe/ K**	**Fe/ K/Ru**	**Fe/ K**	**Fe/ K/Ru**	**Fe /K**	**Fe/ K/Ru**	**Fe/ K**	**Fe /K/Ru**
C_2	3.23	1.83	2.87	1.09	2.21	0.88	0.88	0.49
C_3	3.78	3.20	3.88	2.62	3.79	2.88	2.88	1.89
C_4	3.30	2.80	3.31	2.32	3.17	2.54	2.54	1.65
C_5	2.90	2.41	2.87	1.91	2.73	2.06	2.06	1.25
C_6	2.84	2.36	2.78	1.80	2.18	1.85	1.85	1.08
C_7	2.64	2.12	2.61	1.55	2.04	1.53	1.53	0.83
C_8	2.57	1.98	2.51	1.39	1.99	1.40	1.40	0.67
C_9	2.58	1.67	2.46	1.24	1.84	1.36	1.36	0.53

The Fe/Al/K/Ru catalyst has a much less olefinic product, as can be seen from Table 4.5 and by comparison of Figures 4.5 and 4.6. It is also clear that olefin selectivity decreases with decreasing space velocity (increasing conversion) for both catalysts, as would be expected (Van der Laan & Beenackers, 1999; Cairns, 2008). Compared to other iron catalysts in literature it would seem that both catalysts are generally less selective to olefins. In contrast Özkara-Aydınoğlu *et al.* (2012) observed improved olefinicity over their catalysts with a Cu/K ratio of 7:3 and 3:1 with decreasing space velocity, with their 100 Fe/7 Cu/1 K and 100 Fe/3 Cu/ 3K showing the opposite trend up to C_{13}. Ignoring the trend observed by Özkara-Aydınoğlu *et al.* (2012), the product arising from Fe/Al/K and Fe/Al/K/Ru at similar CO-conversions is much less olefinic when compared to the olefin selectivities over all their catalysts, though similar process conditions and the same H_2/CO ratio was used.

Over a K-promoted precipitated Fe/SiO_2 catalyst Hayakawa *et al.* (2007) reported an overall olefin selectivity of around 75% at 80% CO-conversion, which higher than that observed for Fe/Al/K, though comparable at CO-conversion of 65% and below over Fe/Al/K. The olefin selectivity of Fe/Al/K/Ru falls short of this value at all levels of CO-conversion, being very significantly lower at comparable CO-conversion levels. Hou *et al.* (2008), over Fe/Cu/K/SiO_2, reported high olefin selectivities approaching 80% at 45% CO-conversion, outperforming both Fe/Al/K and Fe/Al/K/Ru.

Olefin selectivity for the $C_2 - C_4$ and $C_5 - C_{11}$ fraction over Fe/Al/K compared well with those reported by Bukur *et al.* (1990) for their potassium promoted Fe-catalysts at 250 °C, 15 bar and $H_2/CO = 1$. Selectivities were significantly lower for Fe/Al/K/Ru compared to their 3 Cu/0.5 K-promoted catalyst. Wan *et al.* (2008) reported highly similar values for $C_2 - C_4$ olefin selctivities for their Fe/K and Fe/Cu/K catalysts, with a significantly lower value for the $C_5 - C_{11}$ fraction over Fe/Cu/K. Their values are much higher than that obtained in this study, especially comparing the $C_5 - C_{11}$ fraction, at similar conversion for Fe/Al/K compared to their Fe/K. Comparing their Fe/Cu/K catalyst with Fe/Al/K/Ru, their catalyst produced a much more olefinic product across the board.

From the results in Figures 4.5 and 4.6 and Table 4.5 it appears that the addition of Ru is responsible for the reduced olifinicity, since process conditions remained the same when testing both catalysts. This may be due to a promoter effect or ruthenium's FT activity and product distribution at the reaction conditions, but likely is a combination of the two.

Considering the less olefinic product derived from Fe/Al/K/Ru vs. Fe/Al/K compared to the results of Bukur *et al.* (1990) and Wan *et al.* (2008) and Özkara-Aydınoğlu *et al.* (2012) over Fe/K and Fe/Cu/K catalysts, it is probable that Ru has an effect similar to- and probably stronger than Cu in influencing olefinicity. Keeping in mind the TPR results of Li *et al.* (2002), Ru seems a more effective reduction promoter than Cu. Considering this, Ru probably acts similarly to Cu, yet more strongly, in promoting H_2-adsorption and suppressing CO-adsorption. In so doing the CO-adsorption enhancement of K-promotion will be negated/undermined, leading to a greater extent of hydrogenation of primary olefins undergoing secondary reactions and chain termination by hydrogen addition should also be favoured.

As FT catalyst, at the operating temperature of 250 °C it is probable that Ru has significant CH_4-selectivity. Like Co it is known to produce a more paraffinic product compared to Fe. This would contribute to lower olefinicity itself, but at the Fe/Ru ratio used the catalytic activity and FT-product distribution over Ru alone is not likely to be the only contributor to the much lower observed olefinicity.

It would thus be more logical to assume Ru to act in both promotional and catalytic capacity in explaining the lower olefin selectivity, with promoter effects more probably being the major contributor.

5

Chapter 5: Conclusions and Recommendations

Catalysts prepared by combination of co-precipitation and incipient wetness impregnation techniques to have target compositions of 100 Fe/30 Al_2O_3/5 K and 100 Fe/30 Al_2O_3/5 K/3 Ru (abbreviated as Fe/Al/K and Fe/Al/K/Ru). The catalysts were characterised using XRD, SEM-EDX, ICP-OES, TPR and BET N_2-chemisorption.

XRD patterns of the catalysts confirmed the bulk phase of iron to be present as ferrihydrite. Aluminium, potassium and ruthenium compounds were not detected. This is thought to be due to high dispersion and low loadings, which causes the broad peak ferrihydrite pattern to obscure any structural information relating to the compounds. Elemental compositions as determined by SEM-EDX and ICP-OES were slightly off the target theoretical compositions, with Fe and Al loading being somewhat higher than expected. However, Fe/K and Fe/Ru ratios were fairly in line with the targets of 20:1 and 100:3 and the results deemed acceptable. High BET surface areas in line with the expectation for ferrihydrite were calculated. The surface areas were slightly lower than that reported for ferrihydrite, with the Ru promoted catalyst having a slightly smaller surface area than Fe/Al/K. TPR results showed the presence of Ru to improve the reducibility of the precipitated Fe-catalyst by a clear shift of the reduction peaks to temperatures that are 100 – 150 °C lower. Ru is thought to be a more potent reduction promoter than Cu when comparing the magnitude of peak shifts for Fe/Ru/K vs. Fe/K.

The Fe-based catalysts promoted with potassium and a combination of potassium and ruthenium were tested at industrially relevant LTFT conditions of 20 bar, 250 °C with a syngas composition of H_2/CO/Ar = 2:1:1. Both catalysts were capable of high CO-conversion levels in the region of 99% and showed the trend of increasing conversion with decreasing space velocity in addition to attaining very similar conversion levels at

the same space velocities. This would imply both catalysts to be equally active and differ mainly in terms of product selectivity.

The Fe/Al/K/Ru catalyst was determined to be more stable than Fe/Al/K based on the apparent deactivation of 21% over 478 hrs TOS vs. 27% over 415 hrs TOS. The catalyst was also much more selective to CH_4 and CO_2. The higher CO_2-selectivity is observed at identical process conditions and is thus ascribed to the chemical promotion with Ru. It is likely partly a result of increased re-carburisation of magnetite crystallites facilitated by Ru as has been suggested for Cu, but is not thought to be the only/major cause. Based on the higher CO_2-selectivity at identical process conditions Fe/Al/K/Ru is also thought to possess more WGS activity than Fe/Al/K. This would also offer an additional explanation as to its improved stability over the longer experimental run. It is thus thought that an enhanced re-carburisation of magnetite and increased WGS activity, resulting in lower H_2O partial pressure and a lesser extent of oxidation, is responsible for the observed increased stability of Fe/Al/K/Ru.

The expected trends in terms of CH_4- and C_{5+}-selectivity with decreasing space velocity were observed for both catalysts. Unfortunately the Fe/Al/K/Ru catalyst has a higher CH_4-selectivity as well as lower C_{5+}-selectivity, both being highly undesirable in light of increased CO_2-selectivity. The product quality of the more stable of the two catalysts is thus inferior.

In light of the product selectivities of the catalysts at similar conversion, in general both perform poorly against other reported Fe-catalysts. The most apparent of these parameters is the poorer olefin selectivity and higher methane selectivity.

In general C_{5+}-selectivities for Fe/Al/K were comparable to that reported in literature for K-promoted Fe, though generally reported CH_4-selectivities were similar or lower. High CH_4-selectivities were reported for Fe/Ru catalysts, but this was not surprising considering the process conditions used by the authors. Though Fe/Al/K/Ru had higher selectivity to C_{5+}, CH_4-selectivity was also far higher in addition a three times higher CO_2-selectivity. The high methane selectivity over Fe/Al/K/Ru is thought to arise partly from the inherent catalytic activity and product selectivites of Ru at “high temperature” and “low pressure”. In addition it is thought that Ru, by virtue of its efficacy as reduction promoter, has a similar, yet stronger, effect to Cu in promoting H_2 adsorption and supressing CO adsorption to shift product selectivity more toward lighter hydrocarbons.

Product olefinicity for both catalysts was determined to be, in general, lower than that reported in literature. Though higher than Fe/Al/K/Ru, olefin selectivities over Fe/Al/K still fell below values reported for K-promoted Fe at similar levels of conversion. Fe/Al/K/Ru also produces a significantly less olefinic product compared to Fe/Cu/K systems. The decrease in product olefinicity over Fe/Al/K/Ru is thought to stem mostly from ruthenium's more potent enhancing H_2 adsorption and increasing the probability of desorption via hydrogen addition.

In light of the results obtained for Fe/Al/K vs. Fe/Al/K/Ru, the latter was proven to be more stable even at longer TOS, also noting that the catalyst suffered less apparent deactivation while operating at ultra-high CO-conversion for twice as long as Fe/Al/K when taking into account the disturbance to the system at 340 hrs TOS. However, the methane selectivity is doubled, CO_2-selectivity increased by a third and C_{5+}-selectivity is 10 – 15% lower, except at conversions in excess of 90% where C_{5+}-selectivity shows an even more pronounced drop (nearly halves). Considering the additional cost of promoting with Ru, the increased catalyst stability at the expense of product quality does not make the use of Ru as chemical promoter a feasible at the conditions employed in the study. Based on the results of this work, at 250 °C and 20 bar, it does not seem likely that the increased TOS will negate the associated cost of promotion with Ru when taking into account poorer product quality and selectivity.

Better results may be seen when used at higher pressures (in the range of 25 bar or possibly higher) and lower temperatures (in the range of 220 °C or lower if acceptable activity for Fe can still be achieved) that fall more in line with what is suggested for Ru for the synthesis of high carbon number products. This should negate some of the negative impacts of the Ru product distribution at "high temperatures" such as its tendency to high methane selectivity, which is thought to play a part in the results obtained. The catalyst may prove more beneficial at lower H_2/CO ratios between 1 and 1.5 taking into account the enhanced WGS activity.

References

Abdus-Salam, N. & M'civer, F. A. 2012. Synthesis, Characterization and Application of 2-Line Ferrihydrite to Pb(II) Removal from Aqueous Solution. *Journal of Applied Science Environmental Management,* 16**,** 327-336.

Abrevaya, H., Targos, W. & Robota, H. M. J. Cohn," Development of Selective-Ruthenium Catalyst for Fischer-Tropsch Synthesis," U. S. Department of Energy Indirect Liquefaction Contractors' Review Meeting, December, 1986.

Anderson, K. G. & Ekerdt, J. G. 1985. Study of Fischer-Tropsch synthesis over FeSiO2: Effect of diethylamine on hydrocarbon and alcohol production. *Journal of Catalysis,* 95**,** 602-604.

Anderson, R. B. 1956. *Catalysts for the Fischer-Tropsch Synthesis,* New York, Van Nostrand Reinhold.

Anderson, R. B., Friedel, R. A. & Storch, H. H. 1951. Fischer-Tropsch Reaction Mechanism Involving Stepwise Growth of Carbon Chain. *The Journal of Chemical Physics,* 19**,** 313-319.

Atashi, H., Mansouri, M., Hosseini, S. H., Khorram, M.*, et al.* 2012. Intrinsic Kinetics of the Fischer-Tropsch Syntheis Over an Impregnated Cobalt-potassium Catalyst *Korean Journal of Chemical Engineering,* 29**,** 304-309.

Bahome, M. C., Jewell, L. L., Padayachy, K., Hildebrandt, D.*, et al.* 2007. Fe-Ru small particle bimetallic catalysts supported on carbon nanotubes for use in Fischer–Tröpsch synthesis. *Applied Catalysis A: General,* 328**,** 243-251.

Banditelli, P., Cuccuru, A. & Sodi, F. 1976. Decomposition studies of triruthenium dodecacarbonyl and triosmium dodecacarbonyl. *Thermochimica Acta,* 16**,** 89-93.

Bartholomew, C. H. & Bowman, R. M. 1985. Sulfur Poisoning of Cobalt and Iron Fischer-Tropsch Catalysts. *Applied Catalysis,* 15**,** 59-67.

Bartholomew, C. H. & Farrauto, R. J. 2011. *Fundamentals of Industrial Catalytic Processes*, Wiley.

Berry, F. J., Liwu, L., Chengyu, W., Renyuan, T., *et al.* 1985. An in situ Mossbauer investigation of the influence of metal-support and metal-metal interactions on the activity and selectivity of iron-ruthenium catalysts. *Journal of the Chemical Society, Faraday Transactions 1: Physical Chemistry in Condensed Phases,* 81**,** 2293-2305.

Biel, H. B. 2004. *The Effect of Water Partial Pressure on Low Temperature Iron Fischer-Tropsch Reaction Rate, Selectivity and Catalyst Structure.* Masters Thesis, University of Cape Town.

Bingen, M. 2002. PetroSA Masters Materials Problems Through the Power of Innovation. *Stainless Steel World (The Netherlands),* 14**,** 40-41.

Blekkan, E. A., Borg, O., Froseth, V. & Holmen, A. 2007. Fischer-Tropsch Synthesis on Cobalt Catalysts: The Effect of Water. *Catalysis.* The Royal Society of Chemistry.

Boss, C. B. & Fredeen, K. J. 1999. *Concepts, instrumentation and techniques in inductively coupled plasma optical emission spectrometry*, Perkin Elmer Norwalk.

Bukur, D. B., Patel, S. A. & Lang, X. 1990. Fixed bed and slurry reactor studies of Fischer-Tropsch synthesis on precipitated iron catalyst. *Applied Catalysis,* 61**,** 329-349.

Cairns, P. 2008. *Oxygenates in iron Fischer-Tropsch synthesis: is copper a selectivity promoter?* , University of Cape Town.

Callister, W. D. 2007. *Materials Science And Engineering: An Introduction*, John Wiley & Sons.

Chonco, Z. H. 2014. *Investigation of the promotional effect of Cu and Ag on iron-based Fischer-Tropsch catalysts using ferrites as model catalysts.* PhD, University of Cape Town.

Chonco, Z. H., Lodya, L., Claeys, M. & Van Steen, E. 2013. Copper Ferrites: A Model for Investigating the Role of Copper in the Dynamic Iron-based Fischer-Tropsch Catalyst. *Journal of Catalysis,* 308**,** 363-373.

Chorkendorff, I. & Niemantsverdriet, J. W. 2003. *Concepts of Modern Catalysis and Kinetics,* Weinheim, Wiley-VCH Verlag GmBH & Co. KGaA.

Chun, D. H., Park, J. C., Hong, S. Y., Lim, J. T., *et al.* 2014. Highly selective iron-based Fischer–Tropsch catalysts activated by CO2-containing syngas. *Journal of Catalysis,* 317**,** 135-143.

Claeys, M. & Van Steen, E. 2002. On the Effect of Water During Fischer–Tropsch Synthesis With a Ruthenium Catalyst. *Catalysis Today,* 71**,** 419-427.

Claeys, M. & Van Steen, E. 2004. Basic studies. *Studies in Surface Science and Catalysis,* 152**,** 601-680.

Cudennec, Y. & Lecerf, A. 2006. The Transformation of Ferrihydrite into Goethite or Hematite, Revisited. *Journal of Solid State Chemistry,* 179**,** 716-722.

Dalai, A. K. & Davis, B. H. 2008. Fischer–Tropsch Synthesis: A Review of Water Effects on the Performances of Unsupported and Supported Co Catalysts. *Applied Catalysis A: General,* 348**,** 1-15.

Dancuart, L. P. & Steynberg, A. P. 2007. Fischer-Tropsch Based GTL Technology: A New Process? *In:* Davis, B. H. & Occelli, M. L. (eds.) *Studies in Surface Science and Catalysis.* Elsevier.

Dasgupta, D. & Wiltowski, T. 2011. Enhancing Gas Phase Fischer–Tropsch Synthesis Catalyst Design. *Fuel,* 90**,** 174-181.

Davis, B. H. 2005. Fischer-Tropsch Synthesis: Overview of Reactor Development and Future Potentialities. *Topics in Catalysis,* 32**,** 143-168.

Davis, B. H. 2013. Preparation of Iron FT Catalysts. *Greener Fischer-Tropsch Processes for Fuels and Feedstocks.* Wiley-VCH Verlag GmbH & Co. KGaA.

Davis, B. H. & Maitlis, P. M. 2013. Other FT Catalysts. *Greener Fischer-Tropsch Processes for Fuels and Feedstocks.* Wiley-VCH Verlag GmbH & Co. KGaA.

De Beer, M., Claeys, M. & Van Steen, E. Preparation of Pt-Promoted Co/SiO2 Catalysts for CO Hydrogenation by Strong Electrostatic Adsorption (SEA). Advanced Materials Research, 2014a. Trans Tech Publ, 357-364.

De Beer, M., Kunene, A., Nabaho, D., Claeys, M., *et al.* 2014b. Technical and economic aspects of promotion of cobalt-based Fischer-Tropsch catalysts by noble metals-a review. *Journal of the Southern African Institute of Mining and Metallurgy,* 114**,** 157-165.

De Klerk, A., Li, Y.-W. & Zennaro, R. 2013. Fischer–Tropsch Technology. *Greener Fischer-Tropsch Processes for Fuels and Feedstocks.* Wiley-VCH Verlag GmbH & Co. KGaA.

De Smit, E. & Weckhuysen, B. M. 2008. The Renaissance of Iron-Based Fischer-Tropsch Synthesis: On the Multifaceted Catalyst Deactivation Behaviour. *Chemical Society Reviews,* 37**,** 2758-2781.

Derouane, E. G., Parmon, V., Lemos, F. & Ribeiro, F. R. 2006. *Sustainable Strategies for the Upgrading of Natural Gas: Fundamentals, Challenges, and Opportunities: Proceedings of the NATO Advanced Study Institute, held in Vilamoura, Portugal, July 6 - 18, 2003*, Springer Netherlands.

Dictor, R. A. & Bell, A. T. 1986. Fischer-Tropsch synthesis over reduced and unreduced iron oxide catalysts. *Journal of Catalysis,* 97**,** 121-136.

Donnelly, T. J. & Satterfield, C. N. 1989. Product distributions of the Fischer-Tropsch synthesis on precipitated iron catalysts. *Applied Catalysis,* 52**,** 93-114.

Drits, V., Sakharov, B., Salyn, A. & Manceau, A. 1993. Structural model for ferrihydrite. *Clay Minerals,* 28**,** 185-185.

Dry, M. E. 1981. The Fischer-Tropsch Synthesis. *In:* Anderson, J. R. & Boudard, M. (eds.) *Catalysis, Science and Technology*. Berlin: Springer Verlag.

Dry, M. E. 1990. The fischer-tropsch process - commercial aspects. *Catalysis Today,* 6**,** 183-206.

Dry, M. E. 1996. Practical and theoretical aspects of the catalytic Fischer-Tropsch process. *Applied Catalysis A: General,* 138**,** 319-344.

Dry, M. E. 2004. Present and future applications of the Fischer–Tropsch process. *Applied Catalysis A: General,* 276**,** 1-3.

Dung, E. J., Bombom, L. S. & Agusomu, T. D. 2008. The Effects of Gas Flaring on Crops in the Niger Delta, Nigeria. *GeoJournal,* 73**,** 297-305.

Eliason, S. A. & Bartholomew, C. H. 1999. Reaction and Deactivation Kinetics for Fischer–Tropsch Synthesis on Unpromoted and Potassium-promoted Iron Catalysts. *Applied Catalysis A: General,* 186**,** 229-243.

Everson, R. C., Woodburn, E. T. & Kirk, A. R. M. 1978. Fischer-Tropsch Reaction Studies With Supported Ruthenium Catalysts: I. Product Distributions at Moderate Pressures and Catalyst Deactivation. *Journal of Catalysis,* 53**,** 186-197.

Flory, P. J. 1936. Molecular Size Distribution in Linear Condensation Polymers1. *Journal of the American Chemical Society,* 58**,** 1877-1885.

Geus, J. W. 2007. 15 Production of Supported Catalysts by Impregnation and (Viscous) Drying. *Catalyst Preparation: Science and Engineering***,** 341.

Glebov, L. S. & Kliger, G. A. 1994. The molecular weight distribution of the products of the Fischer-Tropsch synthesis. *Russian Chemical Reviews,* 63**,** 185.

Gradassi, M. J. 1998. *Economics of gas to Liquids Manufacture,* Netherlands, Elsevier SCience Publishers.

Graham, U. M., Dozier, A., Khatri, R. A., Srinivasan, R.*, et al.* 2007. Eels-Stem Investigation of the Formation of Nano-Zones in Iron Catalysts for Fischer-Tropsch Synthesis. *In:* Davis, B. H. & Occelli, M. L. (eds.) *Studies in Surface Science and Catalysis*. Elsevier.

Grobler, T. 2008. *Two-dimensional Gas Chromatography: A Novel Technique for Iron Low Temperature Fischer-Tropsch Selectivity Studies*. Masters, University of Cape Town.

Hayakawa, H., Tanaka, H. & Fujimoto, K. 2006. Studies on Precipitated Iron Catalysts for Fischer–Tropsch Synthesis. *Applied Catalysis A: General,* 310**,** 24-30.

Hayakawa, H., Tanaka, H. & Fujimoto, K. 2007. Studies on Catalytic Performance of Precipitated Iron/Silica Catalysts for Fischer–Tropsch Synthesis. *Applied Catalysis A: General,* 328**,** 117-123.

Herington, E. F. G. 1946. Fischer-Tropsch synthesis considered as a polymerization reaction. *Chem. Ind. (London)***,** Medium: X; Size: Pages: 346-7.

Hibbitts, D. D., Loveless, B. T., Neurock, M. & Iglesia, E. 2013. Mechanistic role of water on the rate and selectivity of Fischer–Tropsch synthesis on ruthenium catalysts. *Angewandte Chemie International Edition,* 52**,** 12273-12278.

Höök, M., Fantazzini, D., Angelantoni, A. & Snowden, S. 2014. Hydrocarbon Liquefaction: Viability as a Peak Oil Mitigation Strategy. *Philosophical*

Transactions of the Royal Society A: Mathematical, Physical and Engineering Sciences, 372.

Hou, W., Wu, B., Yang, Y., Hao, Q., *et al.* 2008. Effect of SiO_2 Content on Iron-based Catalysts for Slurry Fischer–Tropsch Synthesis. *Fuel Processing Technology,* 89**,** 284-291.

Hou, X. & Jones, B. T. 2006. Inductively Coupled Plasma-Optical Emission Spectrometry. *Encyclopedia of Analytical Chemistry.* John Wiley & Sons, Ltd.

Iglesia, E., Reyes, S. C. & Madon, R. J. 1991. Transport-enhanced α-olefin Readsorption Pathways in Ru-catalyzed Hydrocarbon Synthesis. *Journal of Catalysis,* 129**,** 238-256.

Iglesia, E., Reyes, S. C., Madon, R. J. & Soled, S. L. 1993. Selectivity Control and Catalyst Design in the Fischer-Tropsch Synthesis: Sites, Pellets, and Reactors. *In:* D.D. Eley, H. P. & Paul, B. W. (eds.) *Advances in Catalysis.* Academic Press.

Iglesia, E., Soled, S. L. & Fiato, R. A. 1992. Fischer-Tropsch Synthesis on Cobalt and Ruthenium. Metal Dispersion and Support Effects on Reaction Rate and Selectivity. *Journal of Catalysis,* 137**,** 212-224.

Infomine. 2016. *6 Month Cobalt Prices and Price Charts - InvestmentMine* [Online]. Available: http://www.infomine.com/investment/metal-prices/cobalt/6-month [Accessed June 14 2016].

Itkulova, S. S., Zakumbaeva, G. D., Arzumanova, R. S. & Ovchinnikov, V. A. 2007. Production of Hard Hydrocarbons form Synthesis-gas Over Co-containing Supported Catalysts. *Fischer-Tropsch Synthesis, Catalysts and Catalysis***,** 75-85.

Jager, B. 2003. Development of Fischer Tropsch Reactors. *Prepared for Presentation at the AIChE 2003 Spring National Meeting.* New Orleans, LA.

Jager, B. & Espinoza, R. 1995. Advances in Low Temperature Fischer-Tropsch Synthesis. *Catalysis Today,* 23**,** 17-28.

Janney, D., Cowley, J. & Baseck, P. 2000. Transmission Electron Microscopy of Synthetic 2- and 6-line Ferrihydrite. *Clays and Clay Minerals,* 48**,** 111-119.

Jansen, E., Kyek, A., Schäfer, W. & Schwertmann, U. 2002. The Structure of Six-line Ferrihydrite. *Applied Physics A: Materials Science & Processing,* 74**,** 1004-1006.

Johnson, B. G., Bartholomew, C. H. & Goodman, D. W. 1991. The role of surface structure and dispersion in CO hydrogenation on cobalt. *Journal of Catalysis,* 128**,** 231-247.

Juncosa, E. C. 2008. *Adsorption Properties of Synthetic Iron Oxides: As(V) adsorption on Goethite (alpha-FeOOH).* Master's Thesis, Luleå University of Technology.

Kaiser, P. 2014. *Fischer-Tropsch-Synthese an Eisen- und Cobaltkatalysatoren mit kohlendioxidreichem Synthesegas: ein Beitrag zur Erzeugung flüssiger Kraftstoffe aus regenerativer elektrischer Energie und CO_2.* Phd, Universität Bayreuth.

Kaiser, R. 1969. *Chromatographie in der Gasphase,* Mannheim, Germany, Bibliographisches. In-stitut.

Kaminsky, M., Yoon, K. J., Geoffroy, G. L. & Vannice, M. A. 1985. Carbon-supported Fe · Ru catalysts prepared from stoichiometric mixed-metal carbonyl clusters. *Journal of Catalysis,* 91**,** 338-351.

King, D. L. 1978. A Fischer-Tropsch Study of Supported Ruthenium Catalysts. *Journal of Catalysis,* 51**,** 386-397.

Kuipers, E. W., Scheper, C., Wilson, J. H., Vinkenburg, I. H.*, et al.* 1996. Non-ASF Product Distributions Due to Secondary Reactions during Fischer–Tropsch Synthesis. *Journal of Catalysis,* 158**,** 288-300.

Kuipers, E. W., Vinkenburg, I. H. & Oosterbeek, H. 1995. Chain Length Dependence of α-Olefin Readsorption in Fischer-Tropsch Synthesis. *Journal of Catalysis,* 152**,** 137-146.

Kunene, A., Claeys, M. & Van Steen, E. 2014. Pt/Au Alloys as Reduction Promoters for Co/TiO2 Fischer-Tropsch Catalysts. *Advanced Materials Research*.

Laberty, C. & Navrotsky, A. 1998. Energetics of stable and metastable low-temperature iron oxides and oxyhydroxides. *Geochimica et Cosmochimica Acta,* 62**,** 2905-2913.

Larson, E. D. & Tingjin, R. 2003. Synthetic Fuel Production by Indirect Coal Liquefaction. *Energy for Sustainable Development,* 7**,** 79-102.

Leckel, D. 2009. Diesel Production from Fischer−Tropsch: The Past, the Present, and New Concepts. *Energy & Fuels,* 23**,** 2342-2358.

Lekhal, A., Glasser, B. J. & Khinast, J. G. 2007. 16 Drying of Supported Catalysts. *Catalyst Preparation: Science and Engineering*, 375.

Li, S., Krishnamoorthy, S., Li, A., Meitzner, G. D., *et al.* 2002. Promoted Iron-based Catalysts for the Fischer–Tropsch Synthesis: Design, Synthesis, Site Densities, and Catalytic Properties. *Journal of Catalysis,* 206**,** 202-217.

Liu, Y., Teng, B.-T., Guo, X.-H., Li, Y., *et al.* 2007. Effect of reaction conditions on the catalytic performance of Fe-Mn catalyst for Fischer-Tropsch synthesis. *Journal of Molecular Catalysis A: Chemical,* 272**,** 182-190.

Lok, M. 2009. Coprecipitation. *Synthesis of solid catalysts*, 135-151.

Maitlis, P. M. 2013. What is Fischer–Tropsch? *In:* Maitlis, P. M. & De Klerk, A. (eds.) *Greener Fischer-Tropsch Processes for Fuels and Feedstocks.* Weinheim: Wiley-VCH Verlag GmbH & Co. KGaA.

Maitlis, P. M., Long, H. C., Quyoum, R., Turner, M. L., *et al.* 1996. Heterogeneous catalysis of C-C bond formation: black art or organometallic science? *Chemical Communications*, 1-8.

Majzlan, J., Navrotsky, A. & Schwertmann, U. 2004. Thermodynamics of Iron Oxides: Part III. Enthalpies of Formation and Stability of Ferrihydrite (~$Fe(OH)_3$), Schwertmannite (~$FeO(OH)_{3/4}(SO_4)_{1/8}$), and ε–$Fe_2O_3$. *Geochimica et Cosmochimica Acta,* 68**,** 1049-1059.

Matthey, J. 2016. *Price Tables - PMM* [Online]. Available: http://www.platinum.matthey.com/prices/tables [Accessed 14 June 2016 2016].

Nijs, H. H. & Jacobs, P. A. 1980. New Evidence for the Mechanism of the Fischer-Tropsch Synthesis of Hydrocarbons. *Journal of Catalysis,* 66**,** 401-411.

Nwankwo, C. & Ogagarue, D. 2011. Effects of Gas Flaring on Surface and Ground Waters in Delta State, Nigeria. *Journal of Geology and Mining Research,* 3**,** 131-136.

Okereke, O. C. 2016. Exploring utilisation options of local energy resources in Nigeria in compliance with the Paris Climate Agreement.

Özkara-Aydınoğlu, Ş., Ataç, Ö., Gül, Ö. F., Kınayyiğit, Ş., *et al.* 2012. α-olefin Selectivity of Fe–Cu–K Catalysts in Fischer–Tropsch Synthesis: Effects of Catalyst

Composition and Process Conditions. *Chemical Engineering Journal,* 181–182**,** 581-589.

Pan, Y., Brown, A. & Brydson, R. 2006. Electron Beam Damage Studies on 6-Line Ferrihydrite. *Journal of Physics: Conference Series,* 26**,** 46-49.

Pichler, H. & Schulz, H. 1970. Neuere Erkenntnisse auf dem Gebiet der Synthese von Kohlenwasserstoffen aus CO und H2. *Chemie Ingenieur Technik,* 42**,** 1162-1174.

Pichler, V. H., Firnhaber, B., Kioussis, D. & Dawallu, A. 1964. Polymethylen aus kohlenoxyd und wasserstoff. *Die Makromolekulare Chemie,* 70**,** 12-22.

Quandl. 2016a. *COM | Iron Ore 62% Fe CFR China, CME* [Online]. Quandl. Available: https://www.quandl.com/data/COM/FE_TJN [Accessed June 14 2016].

Quandl. 2016b. *ODA | Iron Ore Price* [Online]. Quandl. Available: https://www.quandl.com/data/ODA/PIORECR_USD [Accessed June 14 2016].

Riedel, T., Claeys, M., Schulz, H., Schaub, G.*, et al.* 1999. Comparative study of Fischer–Tropsch synthesis with H2/CO and H2/CO2 syngas using Fe- and Co-based catalysts. *Applied Catalysis A: General,* 186**,** 201-213.

Roginski, S. Proceedings. 3rd Congress on Catalysis 1965 Amsterdam. Wiley, New York.

Ross, G. S., Hudgins, R. & Silveston, P. 1987. The fischer—tropsch synthesis over a ruthenium catalyst under composition cycling. *The Canadian Journal of Chemical Engineering,* 65**,** 958-965.

Rothenberg, G. 2000. Catalysis. *Kirk-Othmer Encyclopedia of Chemical Technology*. John Wiley & Sons, Inc.

SASOL 2014. A New Era for SASOL: Annual Integrated Report 30 June 2014. SASOL.

Satterfield, C. N., Hanlon, R. T., Tung, S. E., Zou, Z. M., *et al.* 1986. Effect of Water on the Iron-catalyzed Fischer-Tropsch Synthesis. *Industrial & Engineering Chemistry Product Research and Development,* 25**,** 407-414.

Schulz, C. 1935. Ueber die beziehungen zwischen reakionsgschwinddigkeit and zusammenstzung des reaktionprodukts bei makropolymerisations-vorgangen. *Z. Phys. Chem. B,* 30**,** 379-398.

Schulz, H. 1999. Short History and Present Trends of Fischer–Tropsch Synthesis. *Applied Catalysis A: General,* 186**,** 3-12.

Schulz, H. & Claeys, M. 1999. Kinetic modelling of Fischer–Tropsch product distributions. *Applied Catalysis A: General,* 186**,** 91-107.

Schulz, H., Nie, Z. & Ousmanov, F. 2002. Construction of the Fischer–Tropsch regime with cobalt catalysts. *Catalysis Today,* 71**,** 351-360.

Schüth, F., Hesse, M. & Unger, K. K. 2008. Precipitation and Coprecipitation. *In:* Ertl, G., Knözinger, H., Schüth, F. & Weitkamp, J. (eds.) *Handbook of Heterogeneous Catalysis*. Wiley-VCH Verlag GmbH & Co. KGaA.

Sehabiague, L., Lemoine, R., Behkish, A., Heintz, Y. J.*, et al.* 2008. Modeling and Optimization of a Large-scale Slurry Bubble Column Reactor for Producing 10,000 bbl/day of Fischer–Tropsch Liquid Hydrocarbons. *Journal of the Chinese Institute of Chemical Engineers,* 39**,** 169-179.

Shroff, M. D., Kalakkad, D. S., Coulter, K. E., Kohler, S. D.*, et al.* 1995. Activation of Precipitated Iron Fischer-Tropsch Synthesis Catalysts. *Journal of Catalysis,* 156**,** 185-207.

Sing, K. 2001. The use of nitrogen adsorption for the characterisation of porous materials. *Colloids and Surfaces A: Physicochemical and Engineering Aspects,* 187**,** 3-9.

Spivey, J., Han, Y. & Dooley, K. 2015. *Catalysis*, Royal Society of Chemistry.

Sternberg, H. & Wender, I. 1959. International Conference on Coordination Chemistry, London 1959. *Chem. Soc.(London) Spec. Publ,* 13**,** 35.

Steynberg, A. & Dry, M. 2004. *Fischer-Tropsch Technology*, Elsevier Science.

Steynberg, A. P. & Nel, H. G. 2004. Clean Coal Conversion Options Using Fischer–Tropsch Technology. *Fuel,* 83**,** 765-770.

Storch, H., Golmbic, N. & Anderson, R. B. 1951. *The Fischer-Tropsch and related Synthesis,* New York, John Wiley and Sons.

Stranges, A. N. 2007. A History of the Fischer-Tropsch Synthesis in Germany 1926–45. *In:* Davis, B. H. & Occelli, M. L. (eds.) *Studies in Surface Science and Catalysis.* Elsevier.

Subiranas, A. M. 2008. *Combining Fischer-Tropsch Synthesis (FTS) and Hydrocarbon Reactions in One Reactor.* Phd, Universität Karlruhe.

Tang, H.-q. & Li, J.-l. 2011. Performance of Silica-nanotube-supported Ruthenium Catalysts for Fischer-Tropsch Synthesis. *Journal of Fuel Chemistry and Technology,* 39**,** 615-620.

Thomas, J. M. & Thomas, W. J. 2015. *Principles and Practice of Heterogeneous Catalysis*, Wiley.

Towe, K. M. & Bradley, W. F. 1967. Mineralogical constitution of colloidal "hydrous ferric oxides". *Journal of Colloid and Interface Science,* 24**,** 384-392.

van der Kraan, A. M., Nonnekens, R. C. H., Stoop, F. & Niemantsverdriet, J. W. 1986. Characterezation of FeRu/TiO2 and Fe/TiO2 catalysts after reduction and fischer-tropsch synthesis by Mo˝ssbauer spectroscopy. *Applied Catalysis,* 27**,** 285-298.

Van der Laan, G. P. 1999. *Kinetics, selectivity and scale up of the Fischer-Tropsch synthesis.* Doctor of Philosophy, Groningen.

Van der Laan, G. P. & Beenackers, A. A. C. M. 1999. Kinetics and Selectivity of the Fischer–Tropsch Synthesis: A Literature Review. *Catalysis Reviews,* 41**,** 255-318.

Van Dijk, H. A. J. 2001. *The Fischer-Tropsch Synthesis: A mechanistic study using transient isotopic tracing.* PhD, Technische Universiteit Eindhoven.

Van Steen, E. & Claeys, M. 2008. Fischer-Tropsch Catalysts for the Biomass-to-Liquid (BTL)-Process. *Chemical Engineering & Technology,* 31**,** 655-666.

Visconti, C. G., Tronconi, E., Lietti, L., Zennaro, R.*, et al.* 2007. Development of a complete kinetic model for the Fischer–Tropsch synthesis over Co/Al2O3 catalysts. *Chemical Engineering Science,* 62**,** 5338-5343.

Wan, H., Wu, B., Li, T., Tao, Z.*, et al.* 2007a. Effects of SiO_2 and Al_2O_3 on Performances of Iron-Based Catalysts for Slurry Fischer–Tropsch Synthesis. *Journal of Fuel Chemistry and Technology,* 35**,** 589-594.

Wan, H., Wu, B., Zhang, C., Xiang, H., *et al.* 2008. Promotional Effects of Cu and K on Precipitated Iron-Based Catalysts for Fischer–Tropsch Synthesis. *Journal of Molecular Catalysis A: Chemical,* 283**,** 33-42.

Wan, H., Wu, B., Zhang, C., Xiang, H., *et al.* 2007b. Study on Fe–Al_2O_3 Interaction Over precipitated Iron Catalyst for Fischer–Tropsch Synthesis. *Catalysis Communications,* 8**,** 1538-1545.

Williams, R. H. & Larson, E. D. 2003. A Comparison of Direct and Indirect Liquefaction Technologies for Making Fluid Fuels from Coal. *Energy for Sustainable Development,* 7**,** 103-129.

Wojciechowski, B. W. 1988. The Kinetics of the Fischer-Tropsch Synthesis. *Catalysis Reviews,* 30**,** 629-702.

Wood, D. A., Nwaoha, C. & Towler, B. F. 2012. Gas-to-Liquids (GTL): A Review of an Industry Offering Several Routes for Monetizing Natural Gas. *Journal of Natural Gas Science and Engineering,* 9**,** 196-208.

Xu, J., Bartholomew, C., Sudweeks, J. & Eggett, D. 2003. Design, Synthesis, and Catalytic Properties of Silica-Supported, Pt-Promoted Iron Fischer–Tropsch Catalysts. *Topics in Catalysis,* 26**,** 55-71.

Yang, J., Ma, W., Chen, D., Holmen, A., *et al.* 2014. Fischer–Tropsch synthesis: A review of the effect of CO conversion on methane selectivity. *Applied Catalysis A: General,* 470**,** 250-260.

Zennaro, R., Ricci, M., Bua, L., Querci, C., *et al.* 2013. Syngas: The Basis of Fischer–Tropsch. *Greener Fischer-Tropsch Processes for Fuels and Feedstocks.* Wiley-VCH Verlag GmbH & Co. KGaA.

Zimmerman, W., Bukur, D. & Ledakowicz, S. 1992. Kinetic model of fischer-tropsch synthesis selectivity in the slurry phase. *Chemical Engineering Science,* 47**,** 2707-2712.

A

Appendix A

A1: Pressure testing

Table A1: Pressure testing results (Fe/Al/K)

Initial reactor pressure	29.61 bar
Pressure after 24 h	29.26 bar
Pressure drop	0.35 bar
Rate of pressure drop (assumed linear)	≈ 0.0146 bar/h

Table A2: Pressure testing results (Fe/Al/K/Ru)

Initial reactor pressure	29.72 bar
Pressure after 24 h	29.28 bar
Pressure drop	0.44 bar
Rate of pressure drop (assumed linear)	≈ 0.0183 bar/h

A2: GC-FID

Table A3: GC-FID specifications

Model:	Varian CP-3800
Detector	Flame Ionisation Detector
Detector temperature	200 °C
Column	25 m x 0.15 mm Capillary Column CP-SIL 5CB (2 μm film thickness)
Column Pressure	1.72 bar
Carrier Gas	H_2, 30 mL/min (STP)
Makeup Gas	N_2, 25 mL/min (STP)
Coolant	CO_2

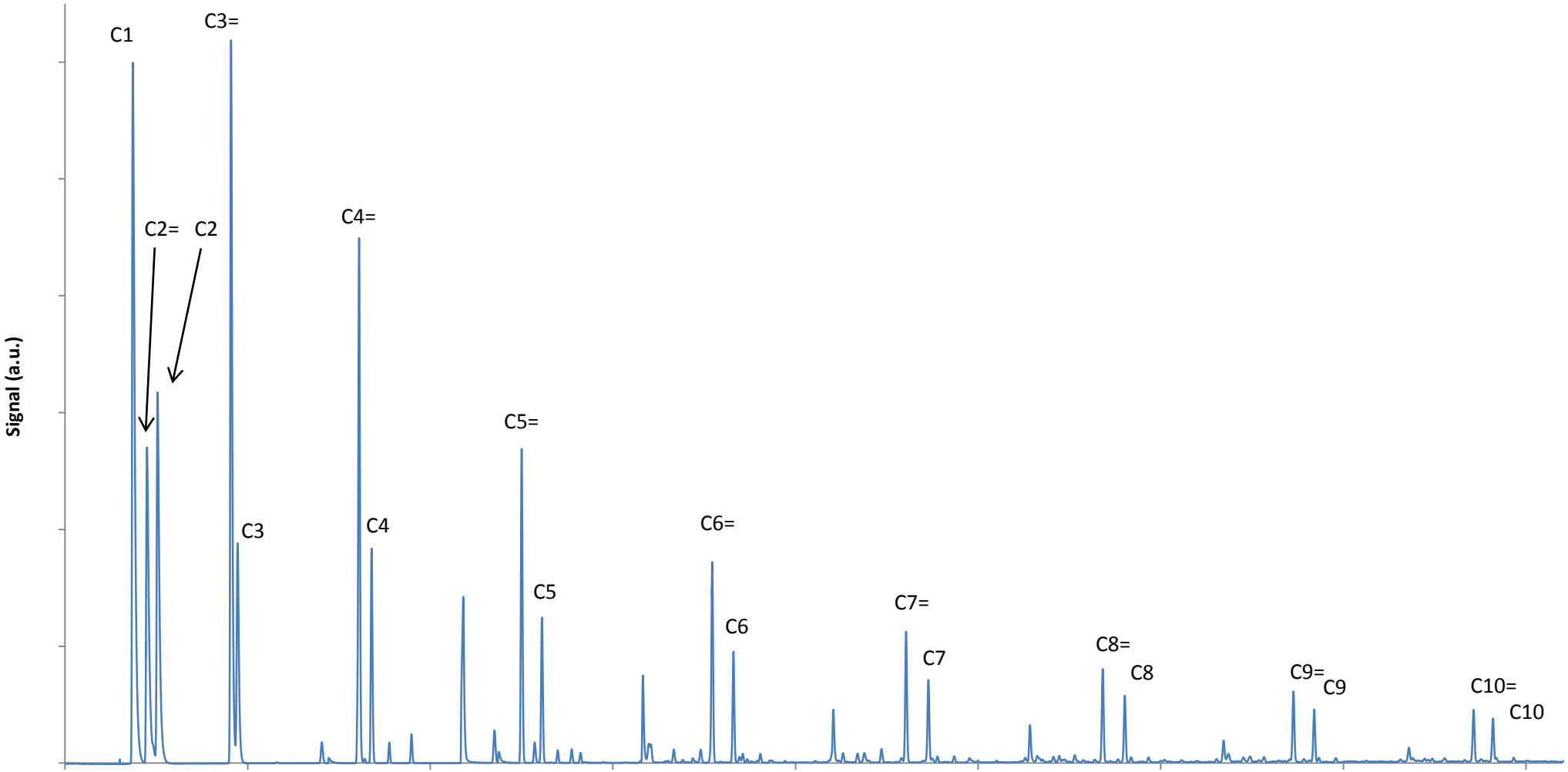

Figure A1: Typical GC-FID chromatogram with major FTS products identified

A3: GC-TCD

Table A4: GC-TCD specifications

Model:	Varian CP-4900 Micro Gas Chromatograph
Channel 1	
Detector	Thermal Conductivity Detector
Column	Molsieve 5 Å Plot Column, 20 m
Carrier gas	H_2
Temperature	80 °C
Pressure	150 kPa
Gases Detected	Ar, CH_4, CO
Channel 2	
Detector	Thermal Conductivity Detector
Column	PORA PLOT Q Column, 10 m
Carrier gas	He
Temperature	60 °C
Pressure	100 kPa
Gases Detected	CO_2
Channel 3	
Detector	Thermal Conductivity Detector
Column	Molecular Sieve 5 PLOT 10 m
Carrier gas	Ar
Temperature	80 °C
Pressure	150 kPa
Gases Detected	H_2

Table A5: GC-TCD response factor determination for Channel 1 gases

	Argon		Nitrogen			Methane			Carbon monoxide		
	t_{ret}	Area	t_{ret}	Area	$R_{f,TCD}$	t_{ret}	Area	$R_{f,TCD}$	t_{ret}	Area	$R_{f,TCD}$
	0.87	25971.30	1.24	13865.10	1.037	1.71	42591.70	1.090	2.59	52815.80	1.022
	0.87	25969.70	1.24	13575.60	1.015	1.71	41263.40	1.056	2.59	52686.20	1.019
	0.87	25855.00	1.24	13502.20	1.014	1.71	41477.10	1.066	2.59	66269.40	1.288
	0.87	25894.20	1.24	13498.00	1.012	1.71	41588.20	1.067	2.59	52982.50	1.028
	0.87	26042.20	1.24	13572.20	1.012	1.70	41727.40	1.065	2.59	53328.90	1.029
	0.87	25881.10	1.24	13499.30	1.013	1.71	41343.70	1.061	2.60	52646.00	1.022
	0.87	25931.20	1.24	13515.00	1.012	1.71	41601.70	1.066	2.60	52864.90	1.024
	0.87	25889.50	1.24	13493.80	1.012	1.71	41849.80	1.074	2.59	53085.90	1.030
	0.87	26020.40	1.24	13558.40	1.012	1.71	42086.50	1.075	2.59	54719.20	1.057
	0.87	26063.70	1.24	13557.00	1.010	1.71	41815.30	1.066	2.59	53034.90	1.022
Average	0.87	25951.83	1.24	13563.66	***1.015***	1.71	41734.48	***1.069***	2.59	54443.37	***1.054***
Standard deviation (%)	0.00	0.27	0.00	0.78	***0.73***	0.18	0.88	***0.82***	0.15	7.31	***7.45***

Table A6: GC-TCD response factor determination for Channel 2 gases

	ALL OTHERS		Methane			Carbon dioxide		
	t_{ret}	Area	t_{ret}	Area	$R_{f,TCD}$	t_{ret}	Area	$R_{f,TCD}$
	0.34	129368.90	0.37	44880.20	1.148	0.42	38372.10	1.523
	0.34	135686.60	0.37	47289.40	1.210	0.42	41033.40	1.628
	0.34	137650.50	0.37	47992.80	1.233	0.42	41836.80	1.668
	0.34	137713.20	0.37	48028.80	1.232	0.42	41906.20	1.668
	0.34	135951.10	0.37	47441.40	1.210	0.42	41444.50	1.640
	0.34	137911.20	0.37	48093.70	1.235	0.42	41997.70	1.672
	0.34	137386.20	0.37	47920.20	1.228	0.42	41838.00	1.663
	0.34	137994.20	0.36	48119.60	1.235	0.42	42009.60	1.672
	0.34	136023.20	0.36	47466.40	1.212	0.42	41472.20	1.643
	0.34	137638.70	0.37	48002.60	1.222	0.42	41939.00	1.658
Average	0.34	136332.38	***0.37***	47523.51	***1.217***	0.42	41384.95	***1.644***
Standard deviation (%)	0.00	1.91	***1.15***	2.06	***2.15***	0.00	2.67	***2.74***

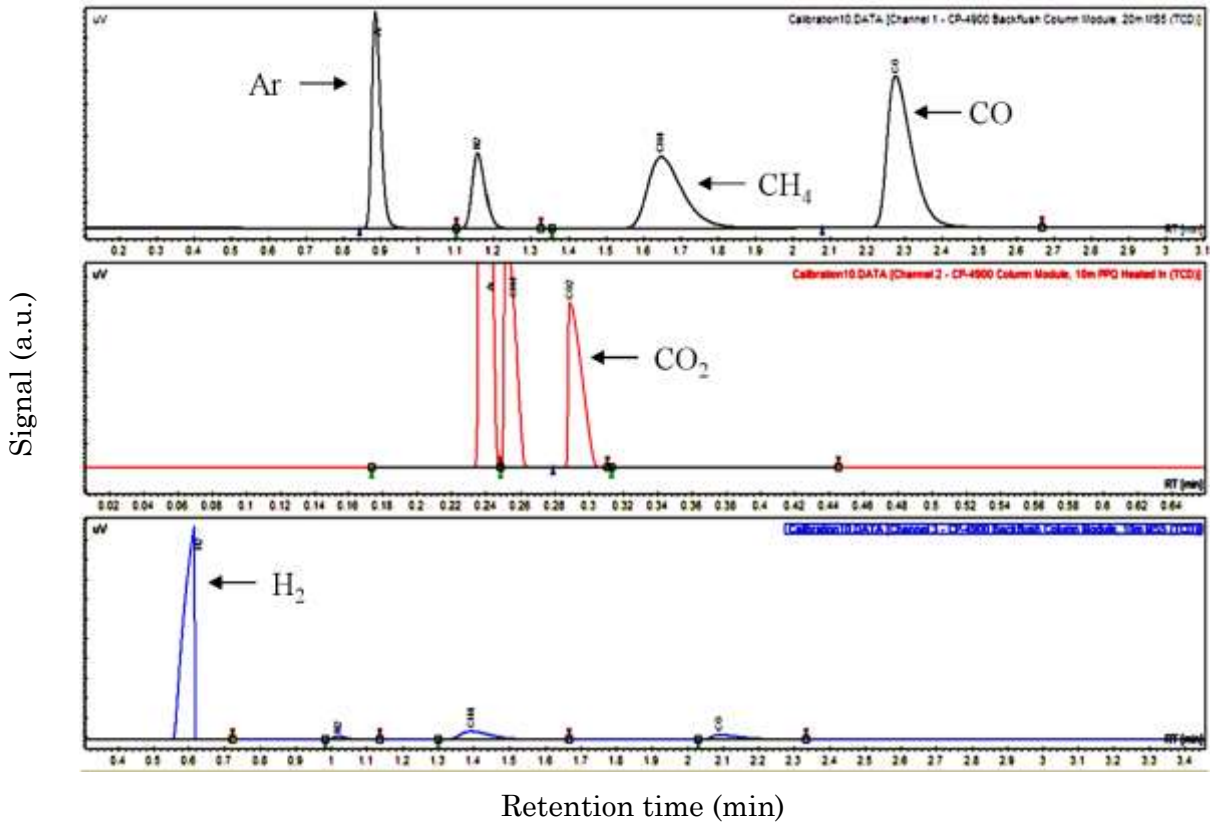

Figure A2: Typical GC-TCD chromatogram (Chonco, 2014)

A4: MFC calibration

Table A7: Carbon monoxide MFC calibration data

MFC setting (%)	Measured volume (mL)	Time (s)	Flow rate (mL/s @ NTP)	Average flow rate (mL/min @ NTP)
2.8	10	22.48	0.44	26.61
		22.44	0.45	
		22.52	0.44	
		22.60	0.44	
		22.60	0.44	
		22.24	0.45	
		22.64	0.44	
		22.13	0.45	
		22.68	0.44	
		22.68	0.44	
5.5	10	10.87	0.92	54.77
		10.89	0.92	
		11.00	0.91	
		10.87	0.92	
		10.89	0.92	
		10.96	0.91	
		11.05	0.90	
		10.94	0.91	
		10.89	0.92	
		11.00	0.91	
8.3	10	7.34	1.36	81.80
		7.43	1.35	

		7.34	1.36	
		7.36	1.36	
		7.34	1.36	
		7.38	1.36	
		7.31	1.37	
		7.27	1.38	
		7.29	1.37	
		7.41	1.35	
11	10	6.31	1.58	98.13
		6.24	1.60	
		5.98	1.67	
		6.05	1.65	
		6.20	1.61	
		6.08	1.64	
		6.26	1.60	
		6.12	1.63	
		5.98	1.67	
		6.23	1.61	
13.8	10	4.78	2.09	124.93
		4.86	2.06	
		4.91	2.04	
		4.90	2.04	
		4.86	2.06	
		4.81	2.08	
		4.82	2.07	
		4.75	2.11	
		4.70	2.13	
		4.75	2.11	
16.5	20	8.01	2.50	149.16
		7.88	2.54	
		8.15	2.45	
		7.90	2.53	
		8.21	2.44	
		7.96	2.51	
		8.14	2.46	
		8.00	2.50	
		8.08	2.48	
		8.18	2.44	
22	20	5.90	3.39	199.72
		5.85	3.42	
		6.02	3.32	
		6.06	3.30	
		6.36	3.14	
		6.01	3.33	
		5.94	3.37	
		6.02	3.32	
		5.95	3.36	
		6.02	3.32	

25.8	20	4.90 4.89 5.02 4.81 4.90 4.93 4.94 4.98 4.86 4.92	4.08 4.09 3.98 4.16 4.08 4.06 4.05 4.02 4.12 4.07	244.52
34.8	30	5.36 5.34 5.43 5.34 5.37 5.56 5.53 5.41 5.29 5.41	5.60 5.62 5.52 5.62 5.59 5.40 5.42 5.55 5.67 5.55	333.16

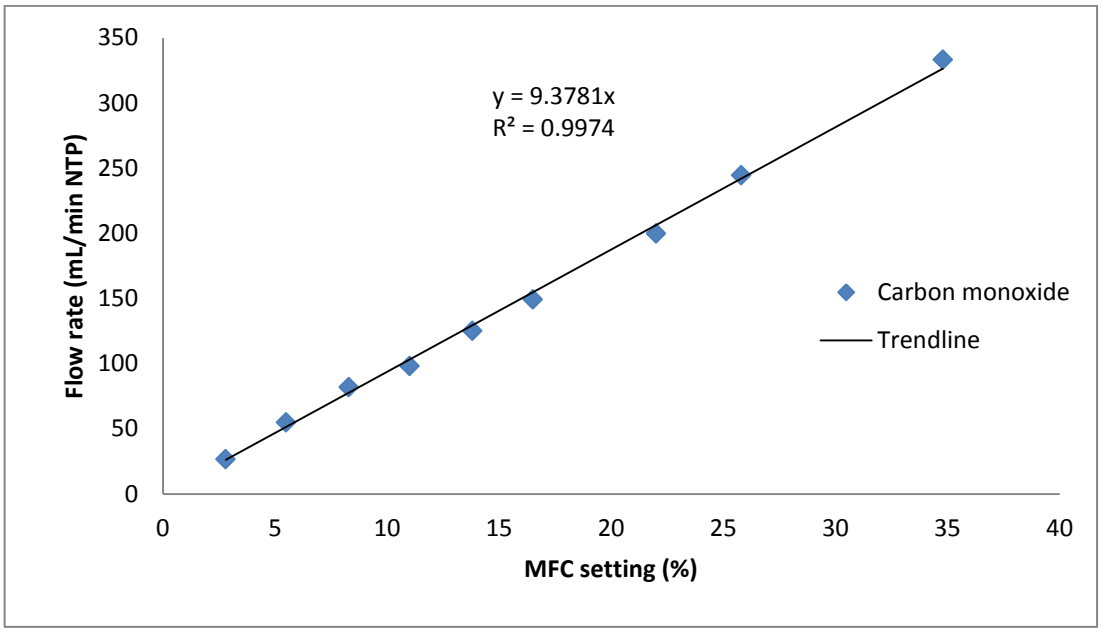

Figure A3: MFC calibration curve for CO

Table A8: Hydrogen MFC calibration data

MFC setting (%)	Measured volume (mL)	Time (s)	Flow rate (mL/s @ NTP)	Average flow rate (mL/min @ NTP)
5	10	14.95	0.67	40.01
		14.93	0.67	
		15.07	0.66	
		15.02	0.67	
		14.95	0.67	
		15.20	0.66	
		15.03	0.67	
		14.96	0.67	
		14.88	0.67	
		14.87	0.67	
15	20	10.53	1.90	116.37
		10.30	1.94	
		10.42	1.92	
		10.27	1.95	
		10.35	1.93	
		10.30	1.94	
		10.27	1.95	
		10.23	1.96	
		10.38	1.93	
		10.18	1.96	
25	20	6.17	3.24	192.97
		6.18	3.24	
		6.31	3.17	
		6.14	3.26	
		6.13	3.26	
		6.32	3.16	
		6.20	3.23	
		6.26	3.19	
		6.27	3.19	
		6.19	3.23	
35	20	4.34	4.61	272.54
		4.37	4.58	
		4.46	4.48	
		4.41	4.54	
		4.35	4.60	
		4.45	4.49	
		4.37	4.58	
		4.38	4.57	
		4.37	4.58	
		4.43	4.51	
45	30	5.22	5.75	346.32
		5.15	5.83	
		5.17	5.80	
		5.21	5.76	
		5.20	5.77	
		5.24	5.73	
		5.11	5.87	
		5.20	5.77	
		5.17	5.80	
		5.36	5.60	

59.3	20	2.69 2.73 2.60 2.68 2.86 2.51 2.66 2.59 2.66 2.64	7.43 7.33 7.69 7.46 6.99 7.97 7.52 7.72 7.52 7.58	450.21
79	100	9.96 9.98 9.92 10.04 10.13 9.83 10.09 9.95 9.93 9.85	10.04 10.02 10.08 9.96 9.87 10.17 9.91 10.05 10.07 10.15	602.13

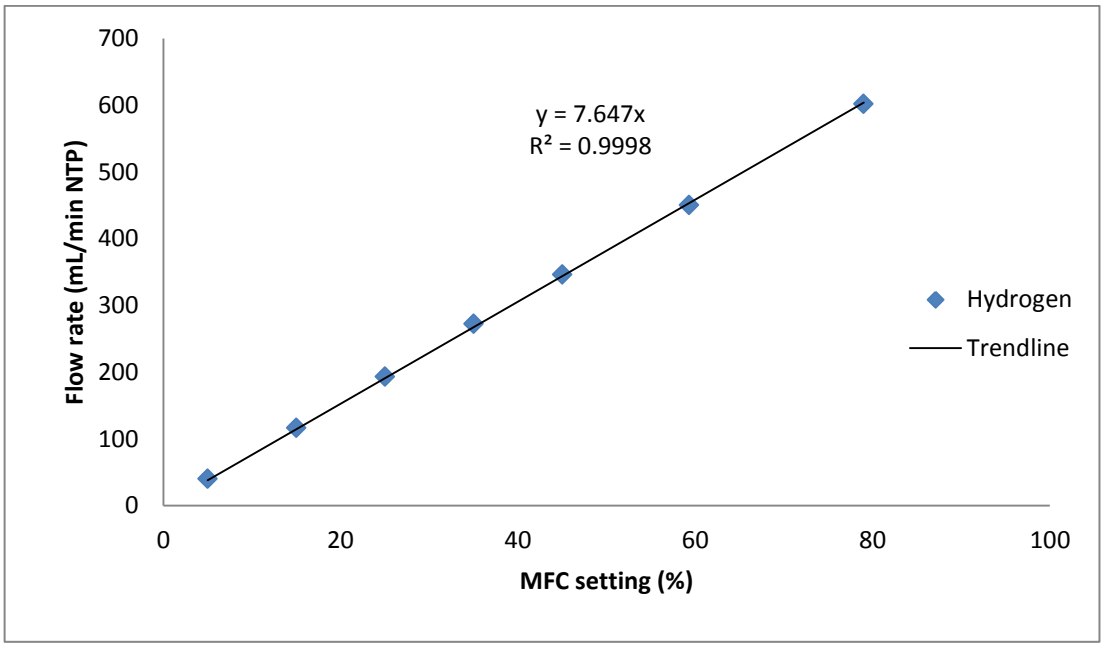

Figure A4: MFC calibration curve for H_2

Table A9: Argon MFC calibration data

MFC setting (%)	Measured volume (mL)	Time (s)	Flow rate (mL/s @ NTP)	Average flow rate (mL/min @ NTP)
6.4	10	22.02	0.45	26.79
		22.03	0.45	
		22.02	0.45	
		22.77	0.44	
		22.28	0.45	
		22.04	0.45	
		22.77	0.44	
		22.13	0.45	
		22.64	0.44	
		22.87	0.44	
12.8	10	10.64	0.94	55.74
		10.55	0.95	
		10.70	0.93	
		10.84	0.92	
		10.89	0.92	
		10.78	0.93	
		10.68	0.94	
		10.95	0.91	
		10.73	0.93	
		10.78	0.93	
19.1	10	8.44	1.18	70.67
		8.48	1.18	
		8.53	1.17	
		8.53	1.17	
		8.44	1.18	
		8.46	1.18	
		8.41	1.19	
		8.62	1.16	
		8.53	1.17	
		8.47	1.18	
25.5	20	11.88	1.68	101.04
		12.13	1.65	
		11.74	1.70	
		11.90	1.68	
		13.23	1.51	
		10.66	1.87	
		11.91	1.68	
		11.88	1.68	
		11.88	1.68	
		11.85	1.68	
31.9	20	9.47	2.11	125.59
		9.43	2.12	
		9.51	2.10	
		9.60	2.08	
		9.69	2.06	
		9.56	2.09	
		9.51	2.10	
		9.51	2.10	
		9.58	2.09	
		9.71	2.06	

38.8	20	8.00 7.90 7.85 7.93 8.03 5.79 7.94 8.03 7.87 8.05	2.50 2.53 2.55 2.52 2.49 3.45 2.52 2.49 2.54 2.48	155.75
51	20	5.96 5.89 5.72 5.78 5.96 5.84 5.73 5.74 5.80 5.93	3.36 3.40 3.49 3.46 3.36 3.42 3.49 3.48 3.45 3.37	205.88
63.8	20	4.60 4.76 4.59 4.64 4.75 4.60 4.59 4.66 4.67 4.89	4.35 4.20 4.36 4.31 4.21 4.35 4.36 4.29 4.28 4.09	256.36
90	20	3.33 3.30 3.46 3.16 3.23 3.33 3.20 3.37 3.22 3.24 3.30	6.01 6.06 5.78 6.33 6.19 6.01 6.25 5.93 6.21 6.17 6.06	365.47

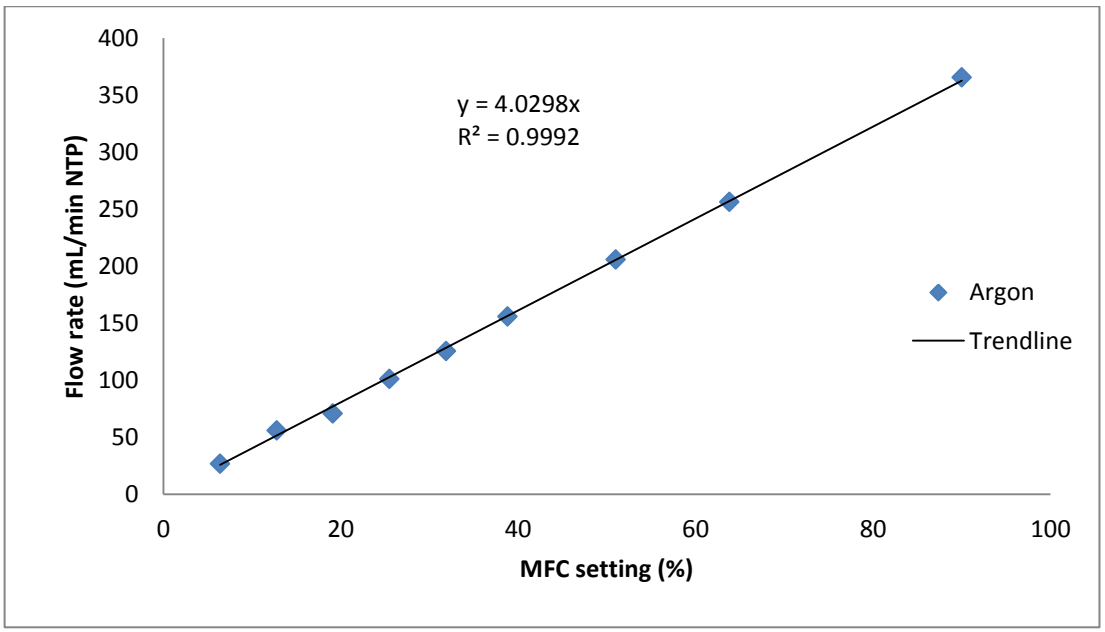

Figure A5: MFC calibration curve for Ar

A5: FTS selected experimental data

Table A10: Conversion and selectivity data at sampling intervals for Fe/Al/K

TOS (h)	74	117	148	191	246	289	319	368	415
X_{CO} (%)	52.31	52.35	61.47	66.05	72.64	83.15	91.93	93.18	39.15
S_{CH_4} (%)	3.99	3.8	4.1	4.1	4.5	4.1	5.41	7.65	2.77
S'_{CH_4} (%)	5.22	5.2	5.9	5.8	6.5	5.5	7.44	10.11	3.26
$S_{C_{5+}}$ (%)	87.03	86.58	85.70	85.11	86.04	87.78	82.73	81.56	91.92
S_{CO_2} (%)	23.65	27.36	29.93	29.38	30.80	25.95	27.26	24.34	15.14

Table A11: Conversion and selectivity data at sampling intervals for Fe/Al/K/Ru

TOS (h)	72	121	161	213	263	310	360	424	478
X_{CO} (%)	44.02	51.72	61.14	65.18	69.79	80.69	87.27	96.78	34.35
S_{CH_4} (%)	5.45	5.79	7.73	8.57	9.62	8.93	13.75	16.49	6.83
S'_{CH_4} (%)	10.18	10.45	13.26	15.36	17.68	14.31	25.39	26.21	8.88
$S_{C_{5+}}$ (%)	77.29	76.15	74.92	70.52	66.97	71.86	52.03	57.00	81.09
S_{CO_2} (%)	46.50	44.55	41.68	44.23	45.57	37.56	45.83	37.06	23.07

Table A12: Carbon number specific olefin selectivity (mol%) for Fe/Al/K up to C_{13}

TOS (h)	**74**	**117**	**148**	**191**	**246**	**289**	**319**	**368**	**415**
X_{CO} (%)	**52.31**	**52.35**	**61.47**	**66.05**	**72.64**	**83.15**	**91.93**	**93.18**	**39.15**
C_2	0.70	0.76	0.74	0.72	0.69	0.47	0.45	0.26	0.76
C_3	0.73	0.79	0.80	0.79	0.79	0.74	0.74	0.60	0.75
C_4	0.77	0.77	0.77	0.77	0.76	0.72	0.72	0.55	0.75
C_5	0.75	0.74	0.74	0.74	0.73	0.67	0.67	0.47	0.72
C_6	0.69	0.74	0.74	0.73	0.69	0.65	0.64	0.41	0.71
C_7	0.58	0.73	0.72	0.72	0.67	0.60	0.58	0.34	0.70
C_8	0.55	0.72	0.72	0.71	0.67	0.58	0.55	0.28	0.70
C_9	0.60	0.72	0.71	0.70	0.65	0.58	0.55	0.25	0.69

Table A13: Carbon number specific olefin selectivity (mol%) for Fe/Al/K/Ru up to C_{13}

TOS (h)	**72**	**121**	**161**	**213**	**263**	**310**	**360**	**424**	**478**
X_{CO} (%)	**44.02**	**51.72**	**61.14**	**65.18**	**69.79**	**80.69**	**87.27**	**96.78**	**34.35**
C_2	0.71	0.65	0.52	0.48	0.41	0.33	0.21	0.17	0.59
C_3	0.78	0.76	0.72	0.71	0.70	0.65	0.57	0.38	0.72
C_4	0.75	0.74	0.70	0.69	0.67	0.62	0.53	0.36	0.70
C_5	0.72	0.71	0.66	0.64	0.61	0.56	0.44	0.24	0.64
C_6	0.72	0.70	0.64	0.62	0.61	0.52	0.39	0.22	0.59
C_7	0.70	0.68	0.61	0.58	0.54	0.45	0.32	0.16	0.44
C_8	0.70	0.66	0.58	0.55	0.51	0.40	0.28	0.14	0.26
C_9	0.68	0.63	0.55	0.50	0.44	0.35	0.24	0.13	0.16

Table A14: Primary olefin to linear paraffin ratio for Fe/Al/K up to C_9

TOS (h)	**74**	**117**	**148**	**191**	**246**	**289**	**319**	**368**	**415**
X_{CO} (%)	**52.31**	**52.35**	**61.47**	**66.05**	**72.64**	**83.15**	**91.93**	**93.18**	**39.15**
C_2	2.31	3.23	2.87	2.57	2.21	0.88	0.83	0.36	3.12
C_3	2.67	3.78	3.88	3.70	3.79	2.88	2.92	1.53	3.01
C_4	3.37	3.30	3.31	3.26	3.17	2.54	2.54	1.24	2.96
C_5	2.98	2.90	2.87	2.82	2.73	2.06	2.03	0.88	2.55
C_6	2.21	2.84	2.78	2.72	2.18	1.85	1.77	0.70	2.50
C_7	1.36	2.64	2.61	2.53	2.04	1.53	1.38	0.51	2.36
C_8	1.23	2.57	2.51	2.42	1.99	1.40	1.23	0.38	2.31
C_9	1.52	2.58	2.46	2.30	1.84	1.36	1.20	0.34	2.23

Table A15: Primary olefin to linear paraffin ratio for Fe/Al/K/Ru up to C_9

TOS (h)	**72**	**121**	**161**	**213**	**263**	**310**	**360**	**424**	**478**
X_{CO} (%)	**44.02**	**51.72**	**61.14**	**65.18**	**69.79**	**80.69**	**87.27**	**96.78**	**34.35**
C_2	2.41	1.83	1.09	0.92	0.70	0.49	0.27	0.20	1.46
C_3	3.45	3.20	2.62	2.46	2.28	1.89	1.30	0.62	2.58
C_4	3.02	2.80	2.32	2.18	2.00	1.65	1.14	0.55	2.35
C_5	2.62	2.41	1.91	1.78	1.55	1.25	0.78	0.32	1.77
C_6	2.56	2.36	1.80	1.64	1.57	1.08	0.65	0.28	1.42
C_7	2.37	2.12	1.55	1.39	1.15	0.83	0.47	0.19	0.80
C_8	2.30	1.98	1.39	1.21	1.02	0.67	0.38	0.16	0.36
C_9	2.15	1.67	1.24	1.00	0.79	0.53	0.32	0.15	0.19